X-612-67-150

NASA TM X-55740

OGO-A MAGNETIC FIELD OBSERVATIONS

BY

J. P. HEPPNER

M. SUGIURA

T. L. SKILLMAN

B. G. LEDLEY

M. CAMPBELL

MARCH 1967

NASA

GODDARD SPACE FLIGHT CENTER

GREENBELT, MARYLAND

OGO-A Magnetic Field Observations

by

J. P. Heppner
M. Sugiura*
T. L. Skillman
B. G. Ledley
M. Campbell**

NASA Goddard Space Flight Center
Greenbelt, Maryland

March 1967

*On leave of absence to University of Washington, Seattle, Washington
**Now at Cornell University, Ithaca, New York

Abstract

This paper summarizes the new findings which have come from the initial study of the OGO-A fluxgate magnetometer measurements between 4 and 24.5 R_e. These include the following: (a) A model magnetic field profile of the cross-sectional structure of the bow shock is derived in terms of the sharpness of the interface, the rise time, and the total time interval occupied by a field pile-up at the shock. Using a simple model to derive the velocity of shock movements these times are converted to three thickness dimensions roughly of the order < 20, 70, and 250 km, which emphasizes the need for strict definition of the meaning of "thickness" in collisionless shock theories. (b) Superimposed on the average shock structure, (a) above, two classes of field oscillations are frequently observed: coherent circularly polarized waves with frequencies typically between 0.5 and 1.5 cps in the satellite reference frame, and higher frequency fluctuations, > 7 cps, which are unresolved by the measurements and whose identity is not known. The coherent oscillation is identified as being in the whistler mode, exists in the form of wave packets, and usually shows a sharp upper frequency cut-off in power spectra analysis. (c) A series of bow shock crossings during the main phase of the April 18, 1965 magnetic storm occur at an abnormally large distance from the earth principally as a consequence of the strong, 20-27$^{\gamma}$, interplanetary field which lowers the Alfvén Mach number to 1.5. The transition region magnetic field adjacent to the shock interface is exceptionally stable in contrast to a number of theoretical predictions and the

typical shocks observed at high Mach numbers. (d) The magnetopause in the sunward hemisphere is most typically observed as a smooth transition over a dimension comparable to the ion Larmor radius. (e) The correlation of negative bay onsets in the auroral belt with OGO-A observations on the night-side of the earth supports more general morphological arguments that the onset originates within the closed magnetosphere or auroral ionosphere and is not dependent on being triggered by a sudden change in the solar wind plasma or field. The view is advanced that the onset results from short-circuiting effects in the ionosphere. (f) At middle latitudes between 5 and 10 R_e near the midnight time sector the total field intensity is found to be considerably stronger than predicted by existing field models. This is believed to be caused by high plasma pressures near the equator at similar distances in the same time sector. (g) Near the magnetopause within the local time sector 4^h30^m to 6^h30^m and geomagnetic latitudes $\pm$ 15° the magnetospheric field intensity is generally found to be $\leq B_t$, the field intensity in the adjacent transition region. This condition and the behavior of the field gradient within the magnetosphere leads to the conclusion that a $\beta \geq 1$ condition must persist over this sector of the outer magnetosphere beyond 11 R_e. The consequences of the magnetopause being a boundary between two high β regions are noted in terms of boundary instability, plasma entry, and the possible existence of secondary shocks in the transition region. A similar, but not identical, condition may exist in the evening twilight local time sector.

1. Introduction

The Eccentric Orbit Geophysical Observatory satellite, OGO-A (also called EGO-1), was instrumented with a 3-axis, dual range, fluxgate magnetometer for vector field measurements over the ranges 0 to 30^{γ} and 0 to 500^{γ} and a 4-cell rubidium vapor magnetometer for scalar field measurements over the range 3^{γ} to 14000^{γ} with programmed bias fields incorporated for vector measurements in weak fields. OGO spacecraft are designed to have 3-axis stabilization [for a comprehensive description of OGO satellites see Ludwig, 1963]. Also, as designed, the magnetometer sensors are located on a boom which extends 22 ft. from the spacecraft body. In the case of OGO-A two boom appendages failed to deploy and this in turn contributed to failure of the stabilization system. One of the booms which failed to deploy held the magnetometers. The net result was that: (a) the spacecraft assumed a spin stable configuration rather than complete 3-axis stabilization, (b) the optical pumping, Rb-vapor, magnetometer was left against the spacecraft body in a high gradient field where it could not operate, and (c) the 3-axis fluxgate magnetometer was left in a position several feet from the spacecraft body in a region of moderate spacecraft fields for this proximity. The resultant configuration is illustrated in Figure 1.

Despite the unfavorable configuration, noted above, a great amount of good quality data has been obtained during 20 of the first 28 months since launch on September 5, 1964 and data transmission is to be resumed again in March 1967. The following favorable factors are of particular significance to the obtaining of quality data despite the deployment failure: (a) the spacecraft's spin axis is highly stable and aligned to within 3 degrees of

the Z axis (see Figure 1), (b) the fluxgate sensor axes are co-linear with the spacecraft body axes in the undeployed state which in turn means that measurements along the X and Y axes can be made independent of the spacecraft's field, (c) the spacecraft's magnetic field, as determined by the X and Y mean values per spin, and measurements in weak interplanetary fields, has remained remarkably stable, (d) the different biases imposed by the spacecraft field on each axis combined with the use of two sensitivities and scale ranges per axis provides various combinations of readings for cross checking calibration curves and evaluation of zero drift as distinct from changes in spacecraft field, and (e) the inertial orientation of the spin axis is roughly perpendicular to meridian planes of the earth at great distances which, as explained later, permits simple interpretation of field direction for a number of problems even though analyzed aspect data giving an inertial direction reference in the XY plane is in general not available at this date.

In this paper results and preliminary interpretations are presented bearing on specific phenomena and field behavior in selected regions between distances of 4 and 24.4 R_e (R_e = 6378 km) throughout 360° of sun-earth-probe angle (i.e., 24 hours of local time) but using primarily data reduced for the eight months of September-December 1964 and March-June 1965. The specific phenomena and spatial features discussed are those that can be tackled without being misled by limitations in the data at this date, which are principally: (a) lack of an exact inertial reference direction in the XY plane of the spacecraft for most, but not all, orbits, (b) a possible uncertainty of $\pm$ 3$^{\gamma}$ in the average spacecraft field along the

Z-axis, and (c) short period changes in the spacecraft field which are readily identified in weak fields and found to have magnitudes $\leq 2.5^{\gamma}$. Thus, for this paper we are not able to transform the data accurately from spacecraft coordinates to other systems and topics dependent on exact knowledge of the field direction cannot be treated. Similarly, we are ignoring any problem where an error of several gammas in the Z-axis would effect interpretation. There are, however, sections of data where the precision of the Z-axis measurements is better than 3^{γ}.

The data presented and discussed are restricted to findings related to the following topics: average and abnormal positions of the magnetopause and bow shock, the detailed cross-sectional structure of the magnetopause, the detailed cross-sectional structure of the bow shock, the generation of coherent waves and high frequency fluctuations at the bow shock, correlations between auroral zone negative bay onsets and sudden changes in the low latitude nighttime magnetosphere, the existence of unusually intense and stable magnetic fields at middle latitudes in the nighttime magnetosphere, the finding of a persistent low latitude field behavior inside the magnetopause near the dawn meridian which implies a high β within this region and the existence of magnetopause instability, and the comparison of the high β field behavior near the dawn meridian with that near the dusk meridian. This restriction of topics particularly emphasizes new findings from OGO-A as opposed to a more general presentation of the data which would include many observations that primarily confirm previous results from a number of satellites. A number of the results reported here were orally presented by the authors at the Inter-Union Symposium on Solar-Terrestrial Physics in Belgrade, Yugoslavia in August 1966.

2. Orbit and Satellite Orientation

OGO-A was launched September 5, 1964 into an orbit of 31° inclination, 282 km perigee height, and 155780 km apogee (= 24.4 R_e), geocentric. A unique characteristic of this orbit is that the period is almost exactly 64 hours such that there are 3 orbits per 8 days. This means that the satellite is located identically relative to a point on the earth's surface every 8 days except that it is displaced 8 degrees in longitude because of the earth's orbital motion about the sun. The particular significance of this for magnetic field measurements is that each of the 3 successive orbits has distinctly different geomagnetic coordinates but each set repeats every 8 days with an 8° displacement in longitude. The 8° displacement is sufficiently small to permit detailed comparison of measurements under different magnetic conditions at essentially repeat locations. Thus a rather ideal combination of magnetic latitude coverage and repeat measurements is achieved.

Figure 2 (September 7-15, 1964) illustrates a sequence of three orbits as projected to a geomagnetic meridian plane. Other properties of the orbit are that with time the inclination increased, perigee distance increased, and apogee distance decreased. At the end of the first years operation perigee and apogee increased and decreased, respectively, by 1 R_e and the inclination increased to 46° thus giving field measurements at magnetic latitudes as great as 58°. A sequence of three orbits after one years operation is also illustrated in Figure 2.

Figure 3 illustrates the projection of an early orbit onto the equatorial plane of the earth. Initially apogee was located at 21^h 22.3^m

local time with crossing of the midnight meridian near 6 R_e, geocentric distance. With time the line of apsides moves essentially one degree per day, clockwise in the projection of Figure 3.

Determination of the inertial orientation of the spin axis was initially a problem in that the spacecraft horizon scanning system was not functional. Using theoretical magnetic field models the fluxgate data were used to determine a best fit both by matching magnitudes simultaneously in the Z direction and in the XY plane of the spacecraft near 4 R_e and by observing a sudden flip in the sign of the saturation of the Z sensor at perigee. This yielded values of 44° right ascension, and -10° declination. Subsequent independent evaluations [Wiggins, E. T., 1965] involving use of error signals from the solar arrays to determine solar aspect gave values of right ascension = 45°, declination = -12° and right ascension = 44°, declination = -8°. Other determinations have yielded similar values. Thus an initial spin axis orientation of 44° R.A. and -10° Dec. was adopted for the magnetic field data reduction with the uncertainty believed to be within $\pm$ 1° in right ascension, and $\pm$ 2° in declination. The probable change in orientation as a function of time appears to be roughly -1° per year in right ascension and 2° per year in declination. As this is also roughly the uncertainty, the change is not proven but has been used in the data reduction without encountering conflicting results.

The magnetic field measurements also demonstrate very clearly that the spin axis is displaced from the Z axis of the spacecraft by 3° when it is assumed that the XYZ axes of the magnetometer are exactly co-linear

with the XYZ axes of the spacecraft. This appears as a modulation of the Z sensor when the field in the XY plane becomes strong. The fact that the 3^{o} coning angle has been independently verified further substantiates the colinearity of the fluxgate and spacecraft axes. Inasmuch as errors introduced by neglecting the 3^{o} angle for averages over a spin period are proportional to (1-cos 3^{o}) and thus less than 1^{γ} in fields as strong as 500^{γ}, the difference in coordinates is ignored in Figure 1.

As indicated in Figure 3 the spin axis is approximately perpendicular to meridian planes of the earth at large distances. Thus the sign of Z for various special problems specifies the gross direction of the field. Illustrative examples are: for apogee measurements near 18^{h} or 06^{h} L.T. the sign distinguishes between solar or anti-solar directed fields, and with apogee near noon the distinction is between eastward or westward directed fields. The more general problem of having complete aspect such that coordinates other than those of the payload can be used is theoretically possible inasmuch as solar sensors on the spacecraft give a reference direction in the XY plane. In practice the personnel performing the reduction of solar aspect data have found this to be extremely difficult as a consequence of infrequent sampling of the solar sensors. The task has been performed for sections of various orbits and verified relative to model magnetic fields. However, as these are not orbits of particular interest for this paper, the presentation here is in terms of field magnitudes in the XY plane and along the Z axis of the spacecraft.

3. Fluxgate Magnetometer and Data System Characteristics

The 3-axis fluxgate magnetometer was designed to be compatible with the OGO system 8 bit/word analog to digital conversion in a manner which would provide high sensitivity in weak fields and a useful sensitivity over a much larger range. The Schonstedt Engineering Co. accomplished this by building a two range instrument with separate outputs for each range on each axis. The calibration curves for the Y-axis sensor of the magnetometer flown, shown in Figure 4, are typical. Each 0-5 volt output is digitized by the spacecraft converter to provide a resolution of 1 part in 255. The corresponding field resolution is shown in Table 1.

A basic data frame in the OGO-A spacecraft is made up of 128 words of 9 bits each for a total of 1152 bits/frame. Data are collected at three optional rates 1000 bits/sec, 8000 bits/sec, and 64000 bits/sec. If tape recorded in the satellite it is always collected at 1000 bits/sec; if transmitted in real time any of the 3 modes may be used. Thus a given word in the sequence of 128 is sampled 0.868, 6.94, or 55.55 times per second. The fluxgate magnetometers use 9 of the 128 words per frame. Two sets of three words, separated by one-half a frame for equal spacing, are used for the sensitive scale and one set of three words is used for the insensitive scale. Thus in the 1 kilobit (1000 bits/sec) mode each sensitive output of each axis is sampled 1.736 times per second and each insensitive output 0.868 times per second. In the other two modes this sampling is multiplied by 8 and 64. In Table 1 these sampling rates have been converted to show the number of samples for each 12 second spin period of OGO-A.

The high data rates of the OGO system would be of little use if the magnetometer response was slow. Thus an additional feature of the OGO fluxgates is the achievement of fast response, or broad band, operation while maintaining a noise level smaller than the incremental resolution of the data system. Response curves for the magnetometers flown are shown in Figure 5.

In-flight calibration of the fluxgates zero levels was normally expected from the rubidium vapor magnetometer. Lack of rubidium magnetometer data for this purpose is of course without consequence in the spin stable configuration for the X and Y axes as described in the next section. As an additional check on sensitivity the fluxgate system includes circuits for applying a regulated current to a solenoidal coil surrounding each sensor. This current, which produces a 10^{γ} field, was programmed to switch-on for 3 seconds each 5 minutes. A spacecraft command enables one to activate or de-activate the programmed calibration such that the calibration interval can be eliminated when it is not providing new information.

4. Flight Data Characteristics

As noted previously, with the lack of a direction reference in the XY plane of the spacecraft the data for most topics in this paper are in the form magnitude in the XY plane of the spacecraft, B_{XY}, and magnitude and direction (or sign) along the Z axis of the spacecraft, B_Z. Figure 6 illustrates how these quantities are obtained in the presence of a spacecraft field (Note: in the undeployed state the -Y and -Z instrument

axes are reversed and coincide with the +Y and +Z spacecraft axes. As this is merely a sign designation in data reduction it is ignored here and all reference to field direction, unless otherwise noted, is in terms of spacecraft axes). Readings from the X and Y sensors are redundant for direct amplitude readings when the field is stable for periods long compared to the 12 second spin period. In practice, however, the large bias of the X-axis spacecraft field (near - 57^{γ} as shown in Figure 7) places the X readings on the insensitive scale in very weak fields and for these fields the Y sensitive readings are used exclusively for B_{XY}. For slightly stronger B_{XY} fields (e.g., 25 to 80^{γ}) the troughs of the spin sine waves of either X or Y or both X and Y, depending on field strength, saturate on the sensitive scale and 0.25^{γ} resolution is achieved by reading values at the peaks of the sine waves relative to spacecraft fields determined in previous periods. Alternatively, one may sacrifice resolution and use the insensitive scale. The practice followed in routine data reduction of a long pass of data has been to always use the most sensitive values but it is apparent that if there are variations in the spacecraft field when B_{XY} is in the range 25 to 80^{γ} these variations will limit the accuracy to approximately 0.25^{γ} plus any short term spacecraft field variations that are not large enough to be detected as variations on the insensitive scale. In B_{XY} fields $>80^{\gamma}$ only the insensitive scale applies and X and Y are redundantly used by averaging in routine data reduction.

B_{XY}, as explained above, is measured independent of the spacecraft field contribution. The accuracy of measuring B_Z (Figure 6) is, however,

directly dependent on knowing the spacecraft's field along the Z sensor axis. The most reliable determination of this contribution is obtained when the satellite is in interplanetary fields. Essentially this is equivalent to assuming that the interplanetary field along the Z axis will average to zero over a number of days, weeks, or months. By this means the value of -54^{γ} for the Z-axis spacecraft field was determined soon after the satellite encountered the interplanetary region. Six months, November-December 1964 and March-June 1965, of interplanetary data was subsequently examined without finding persistent deviations that would indicate that the Z spacecraft field value had shifted outside the $\pm 3.5^{\gamma}$ width of the field increments at this point on the Z calibration curve. In view of the deviations in the Y spacecraft field at the end of May 1965 and the X spacecraft field between May 15 and June 18, 1965, as shown in Figure 7, this is somewhat surprising but it is also consistent with finding that the insensitive Z axis does not show short period spacecraft field changes as discussed below. Consistent behavior of the B_Z measurements relative to theoretical fields within the magnetosphere lends credence to the belief that the -54^{γ} value is valid to a similar accuracy during these months in much stronger field environments.

The above discussion is concerned primarily with average and long period characteristics of the spacecraft field. On time scales of hours, minutes, or seconds detailed discussion of spacecraft field changes is more complex but is relatively easily summarized. The complexity results from the fact that the sources of short period changes are not all understood and the frequency of occurrence of short period changes is not the same

over a number of months or within a series of successive orbits or in some cases from hour to hour. There are also many hours when short period changes are apparently absent. The variety of conditions is reasonably attributed to changes in spacecraft configuration in the sense of power distribution, which experiments are turned on or off and whether or not these experiments have programmed cycles, and how these parameters relate to the spacecraft data mode being used. Substantiation of this belief comes from observations: (1) that the maximum short period change detected in X or Y is always less than 3^{γ} which is consistent with finding maximum changes near 2^{γ} in controlled tests of switching experiments on and off in flight, and (2) this is also approximately the scatter of values obtained between points taken from averaging samples on successive orbits, as indicated in Figure 7. The consequences for data presented here are of three types: (1) impulsive changes in level must be removed if they appear during periods when power spectra are being determined, (2) whether or not the B_Z measurements are affected, and (3) the effect on B_{XY} in the range 25 to 80^{γ}. On the second point, the data clearly show that the short period changes in the Z axis spacecraft field must be smaller than the resolution of the insensitive scale. This is particularly evident through the lack of change in the Z readings concurrent with identifiable spacecraft changes in the X or Y readings. We have not, however, performed statistical studies to establish exactly how large the Z axis changes could be without being readily identified and hence must allow for possible uncertainties of this type with magnitudes possibly approaching 2^{γ}. On the third point, it is evident that small short period changes in X or Y can escape detection

when X and Y are saturated on the sensitive scale for an appreciable fraction of a spin period. In these cases they can give errors equivalent to their magnitude (i.e., $< 3^{\gamma}$) because this is less than the resolution of the insensitive scale. These errors, $< 3^{\gamma}$, will of course also appear in fields $> 80^{\gamma}$.

5. Locations of the Magnetopause and Bow Shock

Crossings of the magnetosphere boundary by Explorer's-10, 12, and 14 [Heppner et al., 1963; Bonetti et al., 1963; Cahill and Amazeen, 1963; Freeman et al., 1963; Frank and Van Allen, 1964] and the bow shock front as well as the magnetosphere boundary by Explorer 18 [Ness et al., 1964; Bridge et al., 1965; Wolfe et al., 1966], Explorer 21 [Fairfield and Ness, 1966], and Vela's 2A and 2B [Gosling et al., 1967a] have provided extensive information on boundary locations for different latitudes, local time zones, dates and times. This information has been commonly used to check the degree of agreement with models developed through analogy to hypersonic flow about a blunt body such as that of Spreiter and Jones [1963] and by some investigators [e.g., Patel and Dessler, 1966; Gosling et al., 1967a; Holzer, et al., 1966] to show dependence, or lack of dependence, of geomagnetic activity on solar wind velocity. The previously published boundary location data will soon be statistically dwarfed by more recent data from IMP-C and OGO's A and B. This is illustrated by the number of crossings from OGO-A shown in Figure 8 and the rough estimate that these points probably represent less than 70 percent of the available boundary points from OGO-A's first 16 months in orbit. The most general conclusion that one reaches from this increase in statistics is that the boundary locations must be a

function of a number of variables and consequently it becomes meaningless to select any two quantities such as Kp and solar wind velocity and expect them to correlate as a function of these locations.

Initial looks at OGO-A magnetic field data [Heppner, 1965; Holzer, et al., 1966] showed that multiple crossings of the bow shock front in the sunward hemisphere were much more prevalent in the OGO measurements than in the measurements reported from previous satellites. This is probably, in part, a consequence of the orbit which gives OGO-A a lower radial velocity at shock front distances than satellites such as IMP-A. The line segments, solid for bow shock and dashed for magnetopause, in Figure 8 represent orbit segments over which two or more boundary crossings were observed. The attached number gives either the exact number of crossings observed or, where the 'greater than' sign is shown, the minimum number. The > sign in general signifies one of the following situations: (a) cases where a number of successive crossings occurred with time separations too small to suggest substantial relative movement of the satellite and the boundary, and (b) cases where there was a short time gap in the data during which at least one crossing would have had to occur.

In Figure 8, and Figures 9 and 10, boundary crossings have been projected onto the solar ecliptic plane [see Heppner et al., 1963 for the definition of solar-ecliptic coordinates] by spherically rotating the radial distances in earth centered solar-ecliptic meridian planes. To possibly eliminate one variable influencing the distribution of boundary crossings, the plotted locations have been corrected for variations in the geomagnetic latitude of the sub-solar point using the same procedure applied

to IMP-A by Ness et al. [1964], i.e., an expansion factor $K=(1 + 3 \sin^2\chi_{ss})^{\frac{1}{6}}$ is applied for sub-solar geomagnetic latitudes χ_{ss}. Inspection of plots, like Figure 8, made with and without this correction has not demonstrated that the correction reduces the scatter of crossing locations. We interpret this simply to mean that the boundary locations are more dependent on other variables than upon the variation in the magnetic latitude of the sub-solar point.

Spherical rotation of the crossing points cannot be an ideal technique for two dimensional representation of crossings in the night hemisphere in that it obviously leads to an unreal tail closure for crossings at high latitude for the middle of the night sector. However, for the crossings of Figure 8, where the density of points is insignificant for the local time sector $00^h \pm 3.5^h$, it is not obvious that the representation from 3.5^h to 20.5^h is greatly affected by spherical rotation. Use of cylindrical projection for the night hours has for example been tried without significantly reducing the scatter. The lack of latitude dependence for the available statistics as illustrated by Figure 9 is interpreted to mean: that for geomagnetic latitudes $< 35^o$ and local time 3.5^h to 20.5^h spherical rotation is justified relative to the variations in boundary location attributable to causes other than this geometrical consideration.

The solar wind velocity must be an important parameter influencing the boundary locations. However, stemming from the correlation of solar wind velocity and Kp found by Snyder et al. [1963] there has been disagreement over use of Kp as an indicator of solar wind velocity to normalize boundary locations. For example, Patel and Dessler [1966] using Explorer 12 particle data [Freemen, 1964] and IMP-A plasma data [Wolfe et al., 1966] found that

"no strong correlation is evident between the size of the magnetosphere, as determined from magnetopause crossings, and geomagnetic activity indexes". However, Holzer et al. [1966] using preliminary OGO-A data noted that the magnetopause was closer to the earth with increased Kp and Gosling et al. [1967a] using Vela-2 data concluded that the average positions of the magnetopause and shock correlate quite well with Kp.

Figure 10 gives the 3 hour Kp indices for the crossings of Figure 8. Purely from inspection it is apparent that there may be a slight tendency for boundaries to be closer to the earth when Kp increases but there is not a strong general correlation of Kp and boundary locations. There are, instead, specific cases and sub-sets of data which when examined in detail could lead one to believe either of two extremes: (1) that the cavity dimensions decrease with increasing Kp, or (2) that the cavity dimensions increase with Kp. As examples of this paradox note in support of (1) above: (a) that the two closest magnetopause crossings occur during Kp = 3+ and 3- and (b) that the shock crossing with maximum displacement toward the earth from the model position occurs during Kp = 4- (shown as a short line with 3 crossings near Y_{se} = 17, X_{se} = -2 and discussed in Section 13). In support of (2) above: (a) the most outstanding example occurs near Y_{se} = -22, X_{se} = 7 where the shock crossings at maximum distance occur during Kp = 6+ to 8- (also see data in Figure 11), and (b) although maximum distance magnetopause crossings in the afternoon daylight hemisphere are at Kp = 0 to 1 the maximum, single forenoon crossing in the daylight hemisphere is at Kp = 4-.

This apparent paradox, and the futility of expecting boundaries to be normalized by using Kp as a measure of solar wind velocity is not

surprising when it is recognized: (1) that Kp is primarily a measure of auroral electrojet effects as seen at an average geomagnetic latitude of 56° (for discussion, see Sugiura and Heppner, 1965), (2) that large changes can take place within the 3-hour interval represented by a single Kp value, and (3) that plasma pressures within the magnetosphere are from recent results, discussed in Sections 12 and 13 below, inferred to be greater than previously expected and also probably more variable with time and local time and latitude. Thus, better agreement between theoretical cavity models and measured boundary location cannot be expected until internal plasma pressures are included in the models or in attempts at normalizing the boundary locations. This also leads to a number of secondary conclusions. For example, unless there is a direct relationship without significant time delays between the internal plasma pressure and the solar wind pressure the cavity will contract and expand in response to their relative magnitudes. It also appears probable that the magnetopause surface will develop bumps in response to longitudinal (i.e., local time) and latitudinal gradients of the internal plasma pressure. Such bumps can in turn lead to: (1) generation of secondary shocks within the transition region stemming from the magnetopause at local times remote from the sub-solar region, and
(2) local curvatures of the magnetopause surface that would be considered unstable for interchange instabilities. These possibilities are discussed further in Section 12.

The total problem of boundary locations is undoubtedly even more complex than suggested by the above comments. In particular, the strength

and variability of the transition region magnetic field could have an influence on the magnetopause location comparable to that of the internal plasma pressure. Statistical comparisons of transition field intensities with simultaneous interplanetary field intensities have not been made but a proportionality is generally indicated. Several specific cases are illustrated in Sections 7 and 9. In general, this suggests that the magnetopause location should depend also on the interplanetary magnetic field intensity. Judging from the scatter of points obtained by Wilcox, et al. [1967] in plotting Kp vs. interplanetary field intensities it does not appear that a Kp normalization would significantly take field intensity dependence into account. Some dependence of boundary locations on the direction of the interplanetary field is also probable. Walter's [1964], in particular, has predicted that large asymmetries (e.g., up to 25^{o}) in the magnetosphere boundary relative to the sun-earth line will occur as a function of the interplanetary field direction. Statistically, the OGO crossings, Figure 8, would limit the asymmetry of the type proposed by Walters [1964] to values certainly $< 10^{o}$, and perhaps $< 5^{o}$, unless the effect is counter balanced by other influences. A counter-balancing effect which would obscure such an asymmetry in the magnetopause could result from plasma pressures in the outer magnetosphere being greater in the early morning sector (e.g., up to 07^{h} local time) than in the late evening sector (e.g., after 17^{h}). An asymmetric magnetospheric inflation of this type does not appear to be prohibited by the available data and could explain why the shock stand-off distance in Figure 8 appears to be smaller in the sector prior to 07^{h} LT than in the sector after 17^{h}. For

Walters [1964] prediction, however, a decrease in stand-off distance does not appear in the morning sector and it becomes doubtful that this lends any support to his asymmetry argument. An asymmetrical inflation effect is, however, a real possibility that is discussed in Section 12.

6. Abnormal Bow Shock Location on April 18, 1965

Figure 11 (right-side, after 06^h) shows the magnetic field data at the time of the abnormal shock location near $Y_{se} = -22$, $X_{se} = 7$ (see Figure 8) noted in the previous section. By taking an extreme case such as represented by the April 17-18, 1965 storm one can hope to isolate some of the factors influencing the boundary variability. For example, an inflation effect is suggested by the correlation of the crossings at $08^h09^m25^s$ and $08^h59^m42^s$ with the period of maximum main phase field depression. However, more complete consideration using the simultaneous plasma measurements from OGO-A and Vela-2 satellites shows that the abnormal bow shock position is primarily the result of an exceptionally strong interplanetary magnetic field occurring simultaneous with an inflated magnetosphere. To discuss these effects we assume that the displacement, approximately 5 R_e, from a statistically normal position is functionally dependent on $f_1(M_R) + f_2\ [W(p_{ri}, B_{ri})] + f_3(nm\underline{v}^2)_{ip} + f_4(\underline{B})_{ip}$ where M_R is the magnetic moment of a magnetospheric ring current, $W(p_{ri}, B_{ri})$ represents the energy density in asymmetric inflated regions of the outer magnetosphere, $(nm\underline{v}^2)_{ip}$ represents the solar wind energy density, and $(\underline{B})_{ip}$ is the interplanetary magnetic field. To a first approximation the bow shock location can be considered as depending on the magnetopause location and the bow shock stand-off distance. The factors influencing the magnetopause dimensions will be examined first.

Model calculations [e.g., Mead, 1964] of the geocentric distance to the magnetopause are usually based on the magnitude of $(M_e^2/nmv^2)^{\frac{1}{6}}$ where M_e is the magnetic moment of the earth's main field and $2nmv^2$ is the solar wind pressure at the boundary. If there is a significant ring current field as definitely indicated on April 18th, Figure 11, its magnetic moment, M_R, must be added to M_e in the boundary problem. From values of the low latitude D_{st} ($\simeq -137^{\gamma}$ between 8^h and 9^h UT) surface disturbance and the measurements of Explorer 26 [Cahill, 1966] placing the maximum field depression near 3 R_e for this storm, we can safely assume $M_R < M_e$ and most likely $M_R \leq 0.5\ M_e$. If, in fact, we accepted Cahill's [1966] interpretation that at this time the ring current had not really developed and the field depression was coming primarily from an asymmetric inflation on the evening side of the earth near 3 R_e, the term M_R would be very small. However, this interpretation neglects the influence of associated ionospheric currents and has to be questioned. Simple scaling of model boundaries at the location of the April 18th shocks illustrates that the 5 R_e displacement could be explained by making $M_R = M_e$ if all other parameters remain at average levels. This, however, is not realistic as indicated above and the fact that the plasma flux, nev, observed on OGO-A by the MIT plasma probe [Vasyliunas, personal communication] and Vela-2 [Gosling, et al., 1967b] during the general period of interest was 2 or 3 times the average level. Although the relative contributions of n and v have not been determined for the OGO-A plasma measurements and there are gaps in the time coverage of Vela-2, the general behavior suggests that the increased flux comes partially from an increase in v but that the changes in number density, n, are more significant in increasing

the flux, nev. Thus, if $M_R \leq 0.5\ M_e$ it is unlikely that the geocentric distance to the sub-solar magnetopause is increased and it seems more probable that it might be slightly less than it is under average conditions.

In looking for effects that might increase the dimensions of the magnetosphere in the morning sector the other possibility is that there is regional inflation, $W(p_{ri}, B_{ri})$ above. Here we are not concerned with the 3 R_e asymmetric inflation noted by Cahill [1966] in the evening sector but instead with the high β inflation of the outermost magnetosphere near the dawn meridian which is a general condition suggested by the observations discussed later in Section 12. Unfortunately we do not know of any measurements in this region at the appropriate time so this possibility becomes as explanation only if all other possibilities are found to be inadequate.

The unusually strong, 20 to 27$^{\gamma}$, interplanetary field during this period (right-side of Figure 11) suggests that the Alfvén Mach number. $M_A = (4\ \pi nmv^2)^{\frac{1}{2}}/B$, could be abnormally low and thus greatly increase the stand-off distance between the magnetopause and the bow shock. Fortunately a Vela-2 satellite [Gosling, et al., 1967b] was located in the interplanetary medium outside the bow shock during the periods of interest and simultaneous measurements are available at appropriate times for estimating the Mach number for the period within the transition region prior to 09^h UT, Figure 11. These measurements clearly indicate that an increase in stand-off distance because of a low M_A is probably the primary, but not the only, reason for the abnormal location. The following are examples of the behavior of M_A for either simultaneous times or periods within reasonable time proximity for making estimates

subject to uncertainties imposed by data gaps. (a) Near 16^h UT, April 17 (not shown in Figure 11) simultaneous interplanetary measurements give an $M_A \simeq 5.3$. (b) Between 20^h and 24^h UT, April 17 (left-side of Figure 11) when in the interplanetary medium the field was about 14^γ. Vela-2 measurements are available prior to roughly 20^h30^m and if we assume the field was also 14^γ at that time, an $M_A \simeq 2.2$ is indicated. It is to be noted that the shock crossings during this period are located close to the shock positions observed under average conditions. (c) between 06^h08^m and 06^h30^m UT April 18, simultaneous interplanetary measurements give an $M_A \simeq 1.8$. (d) The interplanetary field intensity during the 5 minutes preceding the shock crossing at $08^h09^m25^s$ UT was 27^γ. Using this field value with the Vela-2 measurements available prior to 08^h54^m, when OGO-A was in the transition region, gives an $M_A \simeq 1.5$. The fact that the transition region field level did not change significantly between the shock crossing and 08^h54^m suggests that the use of 27^γ is valid for this entire interval. (e) As discussed further in the next section the solar wind flux after 08^h54^m increased greatly and OGO-A re-entered the interplanetary field at $08^h59^m42^s$. The simultaneous measurements between 09^h01^m and 09^h05^m give values for $M_A \simeq 4.2$ to 4.8. (f) Between 10^h00^m and 10^h20^m UT simultaneous measurements give an $M_A \simeq 2.9$. (g) After about 10^h20^m UT Vela-2 measurements are not again available until near 14^h UT thus accurate comparisons are not possible for the shock crossings near 10^h55^m UT, Figure 11. However, the MIT plasma probe on OGO-A shows a slightly decreasing flux with time after 10^h20^m which extends until after 11^h UT. Thus, it is reasonable to assume an $M_A < 2.9$ during this interval.

Spreiter and Jones [1963] have given theoretical curves for the stand-off ratio, d/r_o (where r_o is geocentric distance to the magnetopause at the sub-solar point and d is the distance between the bow shock and the magnetopause), at the sub-solar point as a function of M_A. Using these curves and assuming that r_o is close to an average value (i.e., $\simeq$ 10 R_e), it is apparent from simple scaling that d/r_o has to be increased to values ≥ 0.6 to approach the 5 R_e additional displacement of the bow shock observed on April 18. This means an $M_A \leq 2$. The condition $M_A \leq 2$ is very clearly met during the period between 08^h and 09^h, Figure 11, when the shock had to be located at a greater distance than OGO-A. The bow shock did not however reach the Vela-2 satellite at 17.1 R_e near the sun-earth line [Gosling, et al., 1967b]. If the bow shock had a model shape, such as shown in Figure 8, this means that it was located very close (i.e., within about 1 R_e) to both OGO-A and Vela-2 although on opposite sides, or alternatively, either (a) the flow direction of the solar wind was from a more easterly direction (facing the sun) than normal, or (b) the magnetopause was exceptionally inflated to larger dimensions in the morning sector. Although the Vela-2 measurements [Gosling et al., 1967b] show flow directions between 0^o and 5^o west of the sun prior to 08^h56^m UT the possibility of a flow direction influence cannot be ignored inasmuch as shocks were not observed by OGO-A between 06^h08^m and 06^h30^m when M_A was as low as 1.8 but when Vela-2 was showing a flow from 8^o west of the sun. This west of the sun flow was also observed after 20^h UT, April 17 when from the previous discussion an $M_A \simeq 2.2$ is indicated and the bow shock is near the position where it is normally encountered.

A factor that is ignored in the above discussion is the direction of $(\underline{B})_{ip}$. Consideration of this influence is necessarily vague in light of existing theory but comparison of the time interval prior to 23^h25^m April 17 and the apogee time interval after 06^h08^m, April 18 (Figure 11) indicates that a possible direction influence cannot be ruled out. Lacking aspect information in the XY plane of the spacecraft, we can only examine the behavior of Z. Rotation of the orbit shown in Figure 3 to the appropriate local time illustrates that Z is essentially a measure of the field in the direction tangent to the theoretical bow shock curves illustrated in Figure 8. Prior to 23^h25^m, April 17 (Figure 11), when the shock had an average location, B_Z was consistently negative during interplanetary intervals which means there was a significant component in the antisolar direction. In contrast, after 06^h08^m UT, April 18 (Figure 11) B_Z was consistently slightly positive and became gradually more positive until the first abnormal shock appeared at $08^h09^m25^s$. The tangent direction in the X_{se}, Y_{se} plane in this case is into the sunward hemisphere. The transition region field in all cases maintains the same sign for B_Z as the interplanetary field in adjacent time intervals. It should be noted that the possible existence of an effect attributable to the direction of the interplanetary field does not need to be of the type proposed by Walters [1964]. Instead, an effect could be indirect; for example, the field direction may influence the entry of particles into the outer magnetosphere and thus change the degree of inflation and, in turn, the dimensions of the magnetopause in the inflated region.

In total from the above discussion, we conclude: (a) that a low Alfvén Mach number resulting from an exceptionally strong interplanetary field is the principal cause of the abnormal bow shock location, (b) that the abnormal location also depends on there being sufficient magnetospheric inflation to counterbalance most of the additional magnetospheric compression during the main phase of the storm, and (c) that there may be secondary influences resulting from changes in the flow direction of the solar wind, the direction of the interplanetary magnetic field, and regional inflation of the outer magnetosphere in the morning sector.

7. Other Characteristics of the April 18, 1965 Bow Shock

In addition to the abnormal location, the four bow shock crossings on April 18, 1965, Figure 11, are somewhat uncommon in several other respects. First, the strong magnetic field within the transition region between shock crossings is exceptionally stable. In fact, using only magnetic field data one could not be sure that the field within these intervals is a transition region field. The positive identification of the transition region intervals between shocks comes from the plasma behavior [Vasyliunas, personal communication]. Second, the shock crossings are exceptionally sharp. In 3 of the 4 crossings the crossing takes place in less than the time interval between two data samples of the insensitive data scales; that is, less than 1.16 seconds. The fourth occurs within 12 seconds. Field oscillations, as described in the next section, are not observed near or at any of the four crossings.

These characteristics appear to be in almost complete contrast with theoretical expectations regarding the shock structure [see, e.g., a recent review by Kennel and Sagdeev, 1966] and also differ from the shocks

most typically observed by OGO-A, described in Section 9. Tentatively, at least until other shocks with these characteristics can be studied with simultaneous plasma measurements, there is some justification in assuming that these characteristics are a consequence of the low Mach number. A comparison with the low Mach number predictions of Auer, et al. [1962] [also see Spreiter and Jones 1963], illustrates the contrast. For $M_A \lesssim 2$ Auer, et al. [1962] predict that the field behind the shock will consist of a train of hydromagnetic pulses that have grown in amplitude with distance from the magnetopause. In contrast, the observed transition region field, Figure 11 after $08^h09^m25^s$, is exceptionally stable. They also predict that the ratio of field intensities across the shock is given for $M_A > 1$ by $3M_A^2/(M_A^2+2)$. In contrast for the observed $M_A \simeq 1.5$ the observed ratio is 2.3 as opposed to 1.6 which one would expect for the prediction.

Comparison of the sharpness of the shock with either theory or the model shocks of Section 9 is less definite in that one must allow for the possibility that the shock was moving with a high speed, at the time of the crossings. The association of the shocks at $08^h09^m25^s$ and $08^h59^m42^s$ with sudden impulses at the earth's surface would be indicative of rapid motion. However, from other arguments presented in the previous section the bow shock was probably close to the crossing location throughout the period after 06^h08^m UT and a large change in shock location may not have taken place. Similarly, the shocks near 10^h55^m UT are not correlated with either abrupt changes in the solar wind flux or sudden impulses at the earth's surface and the first of these is as sharp as the previous shocks while the second, although not as sharp, is similar in the sense of not

being associated with field oscillations. Thus, it is also possible that the field jump at the shock occurs over a shorter dimension than a typical bow shock.

Another interesting aspect of these shocks appears when the times of occurrence of the shocks at $08^h09^m25^s$ and $08^h59^m42^s$ are compared with the times of occurrence of two nearly coincident, but earlier, world-wide impulses at the earth's surface. The range of begin and end times for each of these impulses as scaled from a number of stations is shown in Figure 11. Although not as clear in Figure 11 as on original records these impulses are identified at all low latitude stations examined. In terms of the usually accepted explanation they would be attributed, respectively, to a sudden decrease in solar wind pressure before the 07^h58^m to 08^h02^m onset interval and a sudden increase in solar wind pressure before the 08^h53^m to 08^h58^m onset interval. This appears to be confirmed by the plasma probe measurements in that Vasyliunas [personal communication] finds a relative decrease in solar wind flux beginning near 07^h50^m and a relative increase in the transition region flux beginning near 08^h54^m. The Vela-2 satellite [Gosling, et al., 1967b] also sees a jump in plasma flux beginning between 08^h54^m and 08^h56^m.

The importance of correlating the surface impulses with the times of bow shock crossings is that it not only presents an opportunity to test the well-known premise that the shock response occurs after the solar wind change has encountered the magnetospheric obstruction to the flow, but also, that it presents the opportunity to estimate the velocity with which a magnetopause change is communicated upstream to the shock

location. For this estimate we are concerned primarily with the time interval between the surface impulse and the time of shock movement. From the time the impulse first appears at the earth's surface we can estimate the earliest time at which the solar wind change had an effect on the magnetopause. We cannot, for example, as accurately use the time at which the flux change appeared at the satellite because this involves greater uncertainties related to the geometry of the solar wind change in sweeping over the earth's cavity, the abruptness of the change, etc. [see, e.g., Nishida, 1966 for a tabulation of factors involved in explaining this time difference]. The minimum transit time for hydromagnetic propagation from the magnetopause to the earth's surface is in excess of one minute from the calculations of Dessler, et al. [1960], Sugiura [1965] and the time differences deduced from Explorer 12 [Nishida and Cahill, 1964]. Thus, the impulse which began at the earth's surface at 07^h58^m would have appeared no later than 07^h57^m at the magnetopause location of first contact. Communication from this point to the shock location being considered thus had to take more than 12 minutes. The same reasoning applied to the shock crossing at $08^h59^m42^s$ gives a minimum time of 8 minutes. Using either a blast wave model, planar front approaching perpendicular to the sun-earth line, or a filamentary model with the solar stream sweeping from the afternoon to the forenoon side of the earth, highly unlikely assumptions are required to get a time difference of more than 5 minutes between arrival times of a solar wind change over the daylight hemisphere of the magnetopause. Assuming that up to 5 minutes of the time differences noted above could be accounted for in this way, one is left with minimum time intervals for the upstream propagation of 7 and

3 minutes, respectively, for the two bow shock movements. Considering that these minimum time intervals could easily be between 1 and 5 minutes too short as a consequence of the assumptions made, one can conclude that the times are consistent with upstream propagation at Alfvén wave velocities of the order 100 to 200 km/sec.

8. Structure of the Magnetosphere Boundary

Figure 12 shows an example of multiple crossings of both the magnetosphere boundary and the shock front. In the Figure all the data points for the sensitive Y component are plotted on a condensed time scale; the data were taken on the outbound pass on November 24 to 25, 1964. The time scale is so condensed that the quasi-sinusoidal curves due to the spin modulation become virtually near-vertical lines, and the data points are densely packed between two envelopes. The vertical width of the clustered points is twice the magnitude of the magnetic field in the plane normal to the spin axis. This method of machine plotting has proved to be useful for demonstrating in condensed form the existence of discontinuities such as the magnetosphere boundary and the shock front. Different degrees of darkness in the record are mainly due to different bit rates of the data and of course partly due to different magnitudes of the field (i.e., the vertical spread). Crossings of the magnetosphere boundary and the shock front are indicated in Figure 12 by arrows below the record, and the region which the satellite was in is specified by one of the symbols M, T, or I; these stand for the magnetosphere, the transition region, and interplanetary space, respectively. Telemetry data rates are also indicated below the graph in Kilobits (Kbt). The three crossings of the magnetosphere

boundary at 10^h58^m, 11^h10^m, and 11^h29^m on November 24 are discussed in some detail below (Figures 15, 16 and 17). Although there are gaps in the record shown in Figure 12 due to missing data, four sections can be readily identified as periods during which the satellite was in interplanetary space. The local time for the position of the satellite was about 16^h at 0^h UT on November 25. The distance of the satellite was near 15 R_e at the times of the three crossings of the magnetosphere, and was 21.4 R_e at the time of the first crossing of the shock and 23.7 R_e for the last shock crossing shown in Figure 12.

Figure 13 shows the variations of the horizontal component H observed on the ground at Tucson and Honolulu to illustrate gross relations, during a very quiet period, between magnetic variations observed at the earth's surface and movements of the magnetosphere boundary and the bow shock as detected by traversals of the shock by the satellite. The second crossing in Figure 13 from interplanetary space to the transition region that took place at $20^h55^m26^s$ must be due to an outward movement of the bow shock possibly as a result of a response of the shock to a decrease in the solar wind pressure. It is of interest to explore the possibility that this expansion of the bow shock is related to the small negative impulse observed at the earth's surface at about 21^h00^m. The magnetic field in the transition region near the shock was about 20^γ. If we take the average field for the entire transition region to be of this magnitude and the average density and the temperature to be 10 ions/cm^3 and $10^{5o}K$

respectively, then the speed of magnetoacoustic wave is roughly 130 km/sec. If the position of the magnetosphere boundary at the time of the shock crossing is assumed to be the same as that at the last crossings of the boundary (Figure 17), the thickness of the transition region as measured radially is about 39,000 Km. Thus the transit time of a magnetoacoustic wave, if propagated radially, is in the neighborhood of 5 minutes. The transit time for a hydromagnetic wave from the magnetosphere boundary to the earth is expected to be about 1.5 to 2 minutes. Thus the time lapse of about 4.5 minutes is less than the time required for a perturbation to be transmitted radially inward from the position of the shock crossing to the earth. The estimate of the speed of magnetoacoustic wave in the transition region is more likely to be on the higher side than on the lower. It is noted here however that one might expect two entirely different effects of a solar wind discontinuity on the bow shock. One is a direct response of the shock to an encounter with the discontinuity, as suggested by the above example, and the other a more major change due to a movement of the magnetosphere boundary responding to the change in the solar wind pressure when the latter arrives at the boundary. The perturbation associated with the latter case should therefore propagate from the magnetosphere boundary outward. A good example of such propagation is discussed in Section 7. For the former case, after its encounter with the bow shock the solar wind discontinuity would proceed through the transition region toward the magnetosphere boundary. The speed for this propagation would

generally be greater than the hydromagnetic wave speed, and this could explain the short time difference between the shock crossing and the impulse observed at the ground. However, it is also possible that there is no direct association between the shock crossing in question and the impulse observed at the ground, and this may indeed be the case.

The slight increase of the magnetic field between 3^h and 4^h at the ground (which may not be clearly discernible in the reproduction of the record in Figure 13 but are definitely seen in the original magnetograms from many observatories distributed over the world) appears to have some connection with a contraction of the magnetosphere as indicated by the last two crossings in Figure 12. Of these two crossings the first may or may not have been due to an inward motion of the shock, since the satellite was moving outward, but the second must have been due to an overtaking of the satellite by the shock during an outward motion of the shock. The arrival of the perturbation at the ground is earlier than this overtaking by about 6 minutes. This is roughly consistent with the example in Section 7 in which a perturbation associated with a sudden motion of the magnetosphere boundary is propagated both inward to the earth and outward to the shock.

Figure 14 gives plots of the sensitive Y component (in the plane normal to the spin axis) together with 1-minute averages of the insensitive Z component (parallel to the spin axis) and the standard deviation for Z for the same intervals, for the outbound pass on

December 18, 1964. The magnetosphere boundary was crossed at about 13.6 R_e and near 13^h local time. The sudden change in the Z component indicates a large change in the direction of the magnetic field at the boundary. The rugged envelopes in the Y plots and the rapid large fluctuations in the standard deviation in Z show the well-known irregular character of the transition region. The satellite crossed the shock front at 13^h54^m UT at the distance of 17.4 R_e, but was again in the transition region for about 11 minutes and finally went into a steady interplanetary field at 14^h11^m.

We now examine the three crossings of the magnetopause on November 24 (Figure 12) in more detail. Figures 15, 16, and 17 show these crossings on an expanded scale. In these Figures the magnitude of the field in the plane normal to the spin axis as determined from smooth envelopes of the spin modulated quasi-sinusoidal curve for the Y component is given at the top; the average of the Z component over the spin period is shown in the middle; and the scalar total field determined from these two components is given at the bottom. Together with the first and the last curves the magnitude of the theoretical reference field B_o and twice this value are indicated by a full line and broken lines respectively. Figure 15 shows the first outward crossing of the magnetopshere boundary at about 10^h58^m UT. Somewhat irregular behavior before the boundary crossing is a commonly observed feature. The field strength just inside the boundary is approximately twice the reference field; this has been observed repeatedly [e.g., Cahill and Amazeen, 1963; Ness et al., 1964]. The transition from

the regular magnetic field in the magnetosphere to the irregular fields outside the boundary is smooth. This is in contrast to the more irregular features in the transition at the bow shock discussed later. In Figure 15 the time required for the satellite to pass through the magnetosphere boundary is approximately 1 minute. The second crossing from the transition region to the magnetosphere due to an expansion of the magnetosphere is shown in Figure 16; in this crossing the time spent by the satellite in the boundary layer is 50 seconds to 1 minute. About 19 minutes later the satellite crossed the boundary outward, but the boundary expanded and took over the satellite and then the satellite finally entered the transition re-tion; these successive crossings are shown in Figure 17. The time lengths involved in the crossings in Figure 17 are about 30 seconds, 20 seconds, and 80 seconds. A change in the Z component is indicated in the boundary crossings in Figures 16 and 17; in the case shown in Figure 15 the field change is essentially in the plane normal to the spin axis.

To determine the thickness of the magnetosphere boundary the velocity of its movement must be estimated. For this purpose it is important to recognize that a single crossing of the magnetosphere boundary is observed on many orbits. In these cases the velocity of the boundary, if it was in motion at all, must have been in general considerably less than that of the satellite, and at most, of the same order of magnitude as the latter. Even when two or three crossings are observed as on the orbit shown in Figures 15, 16, and 17, the time required for the satellite to cross the boundary is not substantially

different from that in the cases of single crossings. This suggests that the average velocity of the boundary is likely to be less than 100 km/min, which is the approximate velocity of the satellite at the distance of the magnetosphere boundary. Of course, the boundary may have velocities exceeding this value when a major change in the position of the boundary takes place. On the basis of analyses of selected cases and inspection of the original records the time required for traversing the boundary is about 1 minute. Thus the thickness of the boundary is estimated to be about 100 km with 200 km as a likely upper limit. Since it is intrinsically impossible to determine unambiguously the velocity of the boundary from one satellite, the above argument is necessarily qualitative. However it is unlikely that the above estimate is in error by a factor greater than 2.

Taking B to be 25$^{\gamma}$ and the ion velocity to be 300 km/sec the Larmor radius of the ion is 120 km. Thus our estimate of the thickness of the boundary is of the order of the ion Larmor radius. This is consistent with the view that the electrostatic field, which would be created by the difference in momenta between the ions and electrons if these particles had zero temperature, is short-circuited by the thermalized electrons in the transition region. A theoretical model for such an interface between a plasma and a magnetic field has been given, with certain simplifying assumptions, by Morozov and Solov'ev [1961] and Sigov and Tverskoy [1963]. If the motions of the ions and electrons were unidirectional and with no thermal energy, the thickness would have a scale length equal to the characteristic Larmor radius of the electrons defined by c/ω_{pe}, where c is

the velocity of light and ω_{pe} the electron plasma frequency [Ferraro, 1952; Shabansky, 1961]. Taking the electron density n to be 1 to 10 cm^{-3}, c/ω_{pe} ($\approx 5.3 \times 10^5\ n^{-\frac{1}{2}}$ cm) is 5.3 to 1.7 km. Thus it seems certain that the electrostatic field plays, if it does at all, only a minor role in the normal magnetosphere boundary. The magnetic field in the transition region is generally not completely turbulent. In most cases the field is ordered such that the spin modulation in a component normal to the spin axis is the dominant variation with other variations having the appearance of being superimposed. This is not to say that there are not times or regions where the field is completely irregular. When such an irregular condition prevails just outside the magnetosphere, we might expect the thickness of the boundary to be several times the ion Larmor radius. As Morozov and Solov'ev [1961] showed theoretically, there may be an electron sheath just inside the boundary layer itself, and the thickness of the electron sheath would be of the order of the Debye length. It would be worthwhile to look for such a sheath when time resolution in the plasma measurements is improved in the future.

9. Structure of the bow shock

The movements of the bow shock appear to be more frequent and with greater speed than those of the magnetosphere boundary. The study of the structure of the shock is more difficult than that of the magnetosphere boundary because variations in the field associated with the shock frequently, but not always, occur on a time scale that is less than or comparable to the spin period. There are cases in which the scalar field variation through the shock can be deduced, as

was done for the magnetosphere boundary, with a reasonable certainty. Two such examples are shown in Figures 18 and 19, which are taken from the shock crossings in Figures 12 and 14 respectively.

In Figure 18 the curve on the top is drawn through points representing 1-second averages of the sensitive Y component which is normal to the spin axis, and hence the quasi-sinusoidal nature is due to the spin modulation. The lower of the next two curves gives values of the -Z component (along the spin axis) averaged over the spin period and the upper curve shows the standard deviation in this component over the same period. The fourth curve is the magnitude of the field in the XY plane as determined from smoothed envelopes of the top curve. The bottom graph gives the total scalar field deduced from the two components, normal and parallel to the spin axis; in so doing the values for the -Z component were interpolated from the third curve. The time required in traversing the shock is very much shorter than that for the magnetosphere-boundary crossing; the major change occurs within 30 seconds, and the initial rapid rise is nearly completed in about 10 seconds.

Figure 19 is a simplified presentation of similar plots for the first of the three shock crossings shown in Figure 14. The rise in B from the interplanetary field to the peak takes place in 15 seconds. In both Figures 18 and 19, after passing a peak, B decreases somewhat and then reaches what appears to be a new average level. The peak value of B at the shock is about 5 times the value for the interplanetary field in both examples. However, this degree of 'piling-up' of the field is likely to be dependent on the solar wind conditions

at the time and also the crossing location relative to the stagnation region. The new level of B behind the shock is about 3 times the value for the interplanetary field in both Figures 18 and 19. The time interval from the onset of the rise to the time when B reaches the new level is roughly 60 seconds in Figure 18 and 30 seconds in Figure 19.

In addition to detailed, but smoothed, plots of selected crossings, such as shown in Figures 18 and 19, all of the shock crossings shown in Figure 8 have been examined in raw data plots. When this is done it is apparent that a large fraction, probably one-half or more, have a similar average total field profile. When these are examined in further detail it is also apparent that a model profile of the average field during these "most typical" shock crossings can be constructed. This model is shown in Figure 20. It is characterized by the following three times, or time intervals: (1) t_o, the time at which the average field level deviates from the interplanetary level; this break is usually identifiable within two seconds, (2) the time interval $|t_o - t_1|$ over which the field intensity rapidly changes level; this is usually a well defined characteristic of the shock, and (3) the time interval $|t_o - t_2|$ between the break at t_o and the time t_2 when the field reaches a new average level. The interval $|t_o - t_2|$ is the most poorly defined characteristic both because of the difficulty in accurately picking the time t_2 and the fact that a "bump" in field intensity does not always occur on the transition region side of the sharp change in field level. As indicated in Figure 20, by means of a dashed line and question mark, a

slight decrease in field intensity is sometimes observed on the interplanetary field side of the principal field change. It is doubtful that this slight decrease should be called a typical characteristic but it is seen often enough that its existence cannot be ignored in a model presentation. An example of a slight decrease of this type appears in Figure 19.

The model profile of Figure 20 is necessarily given in terms of time intervals rather than length. To convert the time intervals to length, for example, to estimate shock thickness, the relative velocity of the satellite and the shock movement must also be known. As discussed below velocities can be estimated for simple models.

There are cases in which the crossing of the total shock structure is completed in a time considerably less than one spin period (i.e., 12 seconds), suggesting rapid movements of the shock on such occasions. Sometimes the shock is crossed in one pass well over 20 times (Figure 8). As may be expected from this feature, movements of the shock as detected by multiple crossings are not, in general obviously related to any conspicuous changes observed at the earth's surface. There are cases, however, when such a correspondence is seen as in the examples shown above and in Section 7. Thus it is more difficult to assess the average speed for the shock than for the magnetosphere boundary. The speed of fast hydromagnetic waves under the normal conditions of the solar wind is in the vicinity of 70 km/sec; this speed is of course not adequate to transmit 'information' upstream with a moving bow shock. As has been pointed out by Fishman et. al. [1960], the group velocity for fast hydromagnetic waves can

be greater than the phase velocity, and can reach the streaming speed of the solar wind. Since, in addition to currents, waves (e.g., fast hydromagnetic waves as in the collisionless shock model proposed by Fishman et al. [1960] and Camac et al. [1962], or ion waves as in the model proposed by Tidman [1966a, 1966b] may be a substantial constituent of the shock, it seems reasonable to assume the presence of fluctuations in the position of any specific segment of the shock even if the overall shape and position of the whole bow shock remain nearly stationary. Since the overall position is likely to fluctuate statistically due to irregularities in the solar wind, there is additional reason to suppose that there is considerable small amplitude motion in the shock when its fine structure is investigated as in the case of satellite measurements with high time resolution. In our view, therefore, the multiple crossings often observed are usually due to relatively small changes in the position of the shock. If this is so, the average speed of a surface element of the shock may be expected to be a small fraction of the streaming speed of the solar wind. Then it appears reasonable to estimate the velocity of the shock by assuming that the shock oscillates back and forth about a mean position.

To estimate an approximate average velocity of the shock movements we take a sawtooth model as shown in Figure 21. In this Figure the zigzag line represents the fluctuating position of the shock and the near-straight line the position of the satellite, both as functions of time which is taken along the horizontal axis. We

estimate the average speed of the shock from the amplitude, A, (defined by one-half of the range of the sawteeth) and the number of cycles, n, that the shock has completed between the first and the last crossings; the value of n is not necessarily integral. However, neither A nor n can be determined exactly from the observed crossings, and hence we approximate A and n in the following manner. Let the total number of crossings observed be denoted by s the times of crossings by t_1, t_2, ..., t_s, and the radial distances at which these crossings took place by r_1, r_2 ...., r_s. We define the <u>apparent</u> amplitude A' by $(r_s-r_1)/2$, and the apparent number of cycles n' by $(s-1)/2$; and we assume that A' and n' respectively approximate A and n. Then an approximate speed V_s of the shock is given by

$$V_s = 4n'A'/(t_s-t_1).$$

By approximating A and n by A' and n' respectively, we tend to underestimate A and overestimate n; thus these errors tend to cancel each other. In this crude approximation it suffices to consider changes in the radial distance of the shock and the radial velocity of the satellite. Cases in which the satellite was within 1 R_E of its apogee were excluded from the present study, because in such cases the satellite velocity is so small that the method adopted here cannot be applied. Statistically speaking, it might be thought that the larger the value of n' the greater the reliability of the result. Thus the relevant statistical results are given in Table 2 for the cases with $n' \geq 3$ and for those with $n' < 3$ separately, and also for

all the cases. The overall average value of the shock velocity is 6.5 km/sec, and the minimum and maximum values are 1.8 km/sec and 28.2 km/sec., respectively. The average velocity for the group of large number of crossings ($n' \geq 3$) is more than twice that for the group of small number of crossings ($n' < 3$), and the average value of the apparent amplitude for the former group is about twice that for the latter group. These differences are statistically significant, but the crude model does not warrant more detailed statistical analysis.

The samples are distributed over two local time zones 5^h to 10^h and 13^h to 21^h. Data were not available near noon, because the spacecraft is inoperative during the January-February low power period when apogee is toward the sun. Within the local time zones indicated above there were no recognizable systematic changes in the above shock velocity with local time.

From the above statistics, and weighting the statistics toward cases of $n' \geq 3$, we conclude that the average velocity of the shock is about 8 km/sec and that the average apparent amplitude of the fluctuations of the shock position is about 3000 km, or approximately 0.45 R_E. A similar study has been reported, without specific details by Holzer et al. [1966]. Their estimates of the average velocity and the amplitude are 10 km/sec and 1.5 R_E, respectively. In our study orbits or major sections of an orbit were not used for the analysis if the succession of crossings was such that the type of model used obviously could not be applicable. For example,

an isolated crossing displaced several hours from a series of crossings occurring over much shorter time intervals is omitted in the analysis. Similarly two groups of successive crossings along the same orbit but separated by a number of hours were treated as two samples rather than one. This neglecting of long intervals of time is equivalent to assuming that the mean position of the shock has undergone a major change as opposed to the small amplitude changes inherent to the model. This may be the reason for the appreciable difference between the amplitude found here and the much larger value given by Holzer, et al. (1966).

Using the model profile of Figure 20 and the velocity estimates of Table 2, probable values for the shock thickness can be calculated. However, the usual expression "shock thickness" becomes ambiguous relative to the model shock of Figure 20 unless one can state which of the three quantities $t_o \pm 2$ sec, $t_o - t_1$ or $t_o - t_2$ defines the thickness. The quantity $t_o \pm 2$ sec. representing the sharpness of the shock onset could, for example, be the most meaningful quantity for some theories although it would usually not be considered a "thickness" dimension. If we take the rise time of the sharp field increase to be the length of the shock, then the average value of this length is 50 - 100 km. In the solar wind the characteristic Larmor radius of the ion (defined for the ion speed equal to the Alfvén speed) is approximately 70 km when the density is taken to be 10 ions/cm^3. If the density increase across the shock is assumed to be a factor of 2 (Wolfe et al., 1965), the characteristic ion Larmor radius is approximately 50 km behind the shock. The scale length of the sharp rise in the shock is thus comparable, within a factor of 2,

to these characteristic lengths. However, there is no a priori reason to take only the sharp rise as the "thickness" of the shock. If waves play an important role in the shock and if the 'bump' we have shown is related to such waves, the bump could be an important part of the structure of the shock. Extreme caution is needed when one speaks of a shock thickness, and it is suggested that a definition be given whenever a "thickness" or "scale length" is discussed in connection with a shock.

It is noted that the magnetic field behind the shock is usually not completely turbulent. The spin modulation is in most cases clearly seen in the component (Y) normal to the spin axis. There are cases when the field is so irregular that the spin modulation is no longer visible, but this is seldom the case. Thus the magnetic field behind the shock has an ordered background on which irregular fields of varying degrees of randomness are superimposed. This is in accordance with the conclusion drawn from the plasma measurements in the transition region that the ion motions in this region are not completely random and that the ions follow an orderly flow pattern around the magnetosphere boundary [Wolfe et al., 1965].

One of the important characteristics of the magnetic field behavior found at and near the bow shock is the frequent presence of waves with frequencies near 1 cps, the frequency being defined with respect to a frame of reference stationary relative to the satellite. Figure 22 shows an example of waves near 1 cps observed at and near the shock. The record, covering approximately 2 minutes from $0^h1^m0^s$

on November 25, 1964, is for the sixth shock crossing in Figure 12 from interplanetary space to the transition region and is one of the cases used previously to show gross characteristics of the shock (Figure 18). The sensitive Y and insensitive Z components are plotted on an expanded time scale. The satellite entered the shock at $0^h2^m11^s$. Beginning with this time several cycles of oscillation at a frequency of approximately 1 cps are clearly indicated. If we give a more precise description of the oscillation, a wave with a frequency of very nearly 1 cps completed four cycles of oscillation with a diminishing amplitude, and was followed by another wave of slightly lower frequency which continued for three or four cycles; the latter wave was further followed by a series of less regular waves. The amplitudes of these waves become small after about 20 seconds from the beginning of the shock traversal, and thereafter variations are more irregular and do not have an appearance of waves. The maximum amplitude (i.e., one-half of the range) is about 4^γ in the regular waves. It is remarked again that the magnetic field at least in the X-Y plane is not turbulent behind the shock in this case and that the sinusoidal spin modulation of the Y component of the field dominates over the irregular variations superimposed on it.

An interesting feature to be observed in Figure 22 is that coherent waves of small amplitudes and of frequencies near 1 cps are also observed in the interplanetary magnetic field prior to the shock crossing. The maximum amplitude (or one-half of the maximum range) of these waves is about 1.2^γ, and most of the outstanding waves have

amplitudes of about 1^{γ}. Regular waves are not seen before about 50 seconds prior to the encounter with the shock, although there are indications of waves with amplitudes of 0.5^{γ} or less and with frequencies of 1.2 to 1.4 cps as far back as 3 or 4 minutes before the shock crossing, but these small amplitude waves occur much less frequently than those observed within 50 seconds of the shock. There appears to be a tendency that the frequency becomes slightly lower as the satellite approaches the shock and that the average frequency for the waves observed before the shock crossing is slightly higher than that for the waves seen after the beginning of the shock traversal. It is important to note that regular waves with frequency near 1 cps usually complete 3 or 4 cycles of oscillation before being damped out and seldom maintain clear wave forms more than 6 or 7 cycles. This applies to waves observed on the solar wind side of the shock or behind it. Another characteristic of the waves near 1 cps is that they are found to be circularly (or elliptically) polarized when their amplitude is sufficiently large for the oscillation to appear coherently on the insensitive X and Z scales. When the oscillation amplitude is small (e.g., < 2 or 3^{γ}), such as it usually is when within the interplanetary field, the polarization is not revealed. It appears logical, however, to assume that the same polarization characteristic is present.

Waves near 1 cps such as those described above are frequently observed at and near the shock, but they are not the only type of waves found in association with the shock. A period of 2 minutes from

$16^h14^m03^s$ to $16^h16^m03^s$ UT on March 24, 1965 is shown in Figure 23 as an example in which fluctuations with frequencies higher than the Nyquist frequency, which is 7 cps for the 8 kbt data, are observed at the shock. Inasmuch as this is a case in which the shock front touched but did not completely cross the satellite location, such that momentarily there was nearly zero relative velocity, it is difficult to assign an exact time to the beginning of the shock, but it must be near $16^h14^m20^s$. Starting about this time high frequency fluctuations were observed and persisted for more than 1 minute. At about $16^h15^m47^s$, approximately 1^m27^s after the first encounter with the shock, the satellite re-entered the interplanetary magnetic field. The high frequency fluctuations continuously existed throughout the interval within the shock front and persisted for about 40 seconds afterward. For a period of 5 seconds or so beginning a few seconds after the shock re-entered the interplanetary field, the amplitudes of high frequency fluctuations were small, and their power was not very much above the instrumental noise level, but the fast fluctuations returned immediately and continued to exist for about 40 seconds. After this time similar fast fluctuations were observed only for a few seconds beginning 1^m27^s after re-entering the interplanetary field; however, their amplitudes were very small. It is noted that though the interplanetary magnetic field contained considerable high frequency fluctuations after the shock encounter, similar fluctuations were not observed before the encounter when the satellite was in the interplanetary field; this indicates that the

presence of high frequency fluctuations is a relatively rapidly changing feature. During the time when the satellite was in the shock irregular variations of large amplitude were also present at frequencies below the Nyquist frequency and the high frequency fluctuations were superimposed on these variations. Typically, when the power specturm density is computed for such a period it is found that noise covers the entire frequency range from the spin frequency (or a little above this frequency) to the Nyquist frequency; the power spectrum above this latter frequency is of course folded back. The scatter of the data points in Figure 23 indicates that the range of the high frequency fluctuations is 5 to 10^{γ} in the shock front and is 1 to 5^{γ} in the solar wind. These magnitudes may be considered as typical values for high frequency fluctuations associated with the shock. There are cases when such fluctuations have larger magnitudes than the above values in the shocked region, but in front of the shock they appear to be within the range given above.

The appearance of the fluctuations superimposed on the magnetic field profile in the vicinity of the shock varies from one case to another. However, it is possible to classify a large variety of behaviors into a relatively small number of types. The classification adopted here is based on: whether or not a wave phenomenon is observed at the shock, and if it is, what type of waves are the most dominant feature. Figure 24 presents three essential types: (i) a shock without regular waves, marked (a); (ii) a shock with regular waves with frequency near 1 cps, with the waves being mainly associated

with the sharp rise as in (b), or packets of waves spreading out on both sides of the shock as in (b'); and (iii) a shock with high frequency fluctuations (f > 3 cps) existing at the sharp rise of the field as in (c) or extending to a longer time interval on both sides of the shock as in (c'). Not all the cases of shock crossing fall in one of these classes or sub-classes, and many examples show combinations of more than one type. Nevertheless the above classification can be applied to the majority of cases and it is thought that such a classification will be useful as a guide for statistical and theoretical studies of the bow shock in future studies. An example of one of the common combinations of these types of fluctuations is shown in Figure 25. In this case the rapid fluctuations, f > 3 cps, appear at the shock and in the interplanetary field near the shock, whereas the coherent oscillations near 1 cps appear at the shock and on the transition region side of the shock in several groups of 3 to 6 cycles.

Regardless of whether or not waves are observed in the vicinity of the shock a sudden change in the power spectrum density is a notable feature in a traversal of the shock. When waves are observed this aspect becomes a subject of considerable interest. Figure 26 shows an example demonstrating differences in the power spectrum densities on both sides of a shock for the sensitive Y-component. The curve marked A gives the estimate of the power spectrum density on the solar-wind side of the shock, and the curve marked B that for the shocked region. The two time intervals, each of 144

seconds in length, are consecutive with a dividing line coincident with the onset of the sharp rise in the magnetic field at the shock. The number of degrees of freedom for the analysis is 10. The spectral speak at the low frequency end in both A and B is due to the spin modulation, and estimates of the effects of the first four positive side lobes are indicated by the numerals 1 to 4 for each of the two curves. Although the spin modulation can be eliminated by use of a numerical filter (and this method has been employed), we prefer to leave the spin effect in the power spectrum density estimates for the present purpose, since a sudden change in the field causes a ringing of the filter.

Referring to the curve A, a remarkable sharp dropoff of the power spectrum density at about 1.3 cps is the most outstanding feature of the power spectrum for the region in front of the shock. The waves observed in this region are within a well-defined band between 0.5 to 1.5 cps in the example shown here. The average level of the power spectrum density above 1.5 cps, which is about $10^{-2\gamma^2}$/cps, is the noise level for a steady quiet field. The spectral peaks at this low level in this frequency region are likely to be due to artificial noises from the spacecraft. The sharp cutoff on the high frequency end of the band in which waves are confined varies to some extent from one case to another, but it is roughly within a range from 0.5 to 2.5 cps with 0.7 to 1.5 cps being most common.

For the time interval of 144 seconds including the crossing of the shock and the region immediately behind it the power density is increased throughout the range from a little above the spin

frequency to the Nyquist frequency of the present analysis which is approximately 3.5 cps. The power-density increase in and behind the shock for frequencies above the cutoff frequency observed on the upstream side of the shock is generally by a factor of 5 to 10, and for the lower frequencies the power-density increase is usually by one or two orders of magnitude. The Nyquist frequency in the analysis can be raised to approximately 7 cps by using all the data points, but it is found that unless the higher frequency fluctuations are present, not much more information is gained in general by this refinement over the results obtained by using every point as in the analysis for Figure 26. Thus, because many power spectra have been taken with a Nyquist frequency of 3.5 cps, and also because 3 cps is roughly the limit of visual wave resolution in examining raw data plots, we have referred to the rapid, unresolved, fluctuations as having $f > 3$ cps, rather than $f > 7$ cps, in Figure 24 and various places in the text. It is however probable that it is generally correct to refer to these fluctuations as having frequencies > 7 cps.

Power spectra computed for the sensitive Y component for a series of intervals of 144 seconds in close succession during multiple crossings is shown in Figure 27. The sequence runs from left to right and from top to bottom, and the beginning time for each of the 11 intervals is indicated. During the first two intervals the satellite was in the interplanetary field; there were irregular variations for about 30 seconds ending approximately at $22^h13^m10^s$, which was probably a period during which the satellite was in close

proximity to the shock, or alternatively, it could represent an interval of perturbations in the solar wind. The magnetic field was steady during the first interval, but there were small amplitude waves lasting almost continuously but not necessarily coherently. There is some indication of frequency cutoff at about 1.7 cps in the first interval. The interplanetary field was very quiet during the second interval. There was a large sudden change in the magnetic field at about $22^h23^m37^s$, the impulsive change lasting for about 12 seconds. There were irregular waves of frequencies of 0.5 to 1 cps before this event. These waves increased their amplitude during and after this large change and the magnetic field became irregular. At about $22^h25^m18^s$ a major change took place and high frequency noise was observed for 45 or 50 seconds following the change. The third interval in Figure 27 immediately follows this large change. It is not completely clear whether the satellite was in the shocked region during the large variation or whether these changes could be caused by a large perturbation in the interplanetary magnetic field. A sudden increase in the power spectrum density in the third interval in Figure 27 is evident. During the fourth interval the satellite was definitely in the interplanetary field. The presence of waves with frequencies near 1 cps is indicated. The fifth interval, beginning at $22^h34^m02^s$, includes crossings of the shock. Prior to the sixth interval the satellite re-entered the interplanetary field and the graphs for the subsequent three intervals demonstrate a cutoff of wave energy in the vicinity of 1.5 cps. The remaining three periods show remnants of waves with frequency below 2 cps.

So far we have shown quasi-periodic waves associated with the bow shock or possibly in some cases, although unlikely, with large perturbations in the magnetic field in the solar wind. Large amplitude quasi-periodic waves are also sometimes observed in the transition region in association with sudden large variations there. Because of frequent and rapid motions of the shock relative to the satellite the possibility that all these waves originate in the bow shock or that the large changes in the field represent brief periods during which the satellite was in the shocked region cannot be ruled out. There are, however, cases in which waves are associated with well-defined sudden changes that do not appear likely to be the bow shock itself. Figure 28 shows an example of a quasi-sinusoidal wave of about 1.5 seconds in period observed together with a sudden change in what appears to be a quiet interplanetary magnetic field. This could represent a steepening of a finite amplitude hydromagnetic wave. Figure 29 shows an example of quasi-sinusoidal waves associated with irregular variations in the transition region. Such waves may have very large amplitudes as in the example shown.

The frequencies mentioned above are all measured in a frame of reference stationary to the satellite. To interpret the waves observed it is necessary to transform the frequencies to those measured in a reference frame stationary with respect to the plasma. For simplicity we consider an idealized case of a one-dimensional Doppler shift. The frequency f' with respect to a frame of reference

K' fixed to the satellite is related to the frequency f in a frame of reference K stationary in the solar wind plasma as follows:

$$f' = |(1 \mp v_s/v_{ph})f|$$

where v_s and v_{ph} are the velocity of the satellite and the phase velocity of the wave both relative to K; the upper and lower signs correspond, respectively, to the direction of wave propagation being toward the sun (i.e., like that of the satellite motion) or away from the sun. It should be noted that since the satellite velocity relative to the earth is only about 1 km/sec at distances of our present interest, v_s is virtually the velocity of the earth in K and hence is numerically approximately the solar wind velocity.

An obvious possibility is that the waves near 1 cps observed in the vicinity of the shock could be standing waves associated with the shock, and that these waves move together with the shock past the satellite giving an apparent frequency of 1 cps [Tidman, 1966b]. However, we reject this possibility on the ground that these waves are usually observed as wave packets and that each wave packet has a characteristic amplitude behavior. This lack of amplitude continuity between adjacent wave packets is considered as an important factor in ruling out the standing wave interpretation. Thus we believe that the waves observed near the shock are generated in some way in the shock and propagate in the plasma. It is noted that for the waves under discussion, propagation is in the whistler mode.

We first discuss the waves observed in the interplanetary field ahead of the shock. Since the average velocity of the shock, relative to the earth, about 8 km/sec, is much less than the solar wind velocity, the waves observed on the solar side of the shock must be propagating upstream. Thus for the waves observed in this region the minus sign is applicable in the Doppler equation. For the plasma conditions appropriate for interplanetary space we now look for waves satisfying two conditions: (i) that waves propagate upstream with group velocities nearly equal to the solar wind velocity and (ii) that waves have frequencies in the vicinity of 1 cps in the satellite reference system K'. The condition regarding the group velocity is similar to that considered in the theoretical collision-free shock model of Fishman et al. [1960]. In order to provide quantitative discussions, group and phase velocities have been calculated using the dispersion equation for a two-component cold plasma [e.g., Stix, 1962]. The exact expression for the refractive index was used in the computation of group and phase velocities, and an expression obtained by the Appleton-Hartree approximation was used as a check. The relevant plasma parameters were selected so that they represent typical conditions in the solar wind and behind the shock surface.

In their shock model Fishman et al. [1960] required that waves have a group velocity <u>perpendicular</u> to the magnetic field comparable to the flow velocity ahead of the shock because the unperturbed magnetic field is assumed to be parallel to the plane of the shock and perpendicular to the plasma velocity. In the case of the

solar wind the magnetic field typically makes an angle of about 45^{o} from the plasma velocity due to the rotation of the sun, and hence under ordinary conditions the component of the magnetic field normal to the shock is probably greater than the component parallel to the shock. Therefore, denoting the angle between the wave normal and the magnetic field by θ, we are concerned with propagation with $\theta \sim 45^{o}$. However this value of θ should be considered merely as an illustrative example, and in the subsequent numerical discussions θ is taken to be 0^{o} to 45^{o}. It is found that the general argument is rather insensitive to the choice of θ. Generally speaking, the condition (i) above, namely that the group velocity be nearly equal to the solar wind velocity is satisfied in two frequency regions, one just above the ion cyclotron frequency and the other just below the electron cyclotron frequency. Between these regions the group velocity is considerably greater than the solar wind velocity. Here we confine our attention to the lower of the two frequency regions. In the solar wind with the ion density n= 5 cm^{-3} and B = 5^{γ}, if we limit the group velocity to be less than about 360 km/sec then frequency f has to be 0.4 to 0.7 cps for $\theta = 0^{o}$, and 0.3 to 0.9 cps for $\theta = 45^{o}$. For these conditions the group velocity is a minimum near 0.5 cps for both $\theta = 0^{o}$ and 45^{o}, and has values of 348 km/sec and 332 km/sec, respectively. Taking the solar wind velocity to be 300 km/sec, frequency f' in the satellite frame of reference K' for these frequencies is 0.6 to 0.7 cps for $\theta = 0^{o}$, and 0.7 to 0.9 cps for $\theta = 45^{o}$. These frequencies, in particular, those for $\theta = 45^{o}$ are approximately the

frequencies frequently observed. As the ion density n decreases the group and phase velocities both increase; for n = 1 cm^{-3} and B = 5^{γ}, the group velocity is again a minimum near f = 0.5 cps, and with the solar wind velocity of 300 km/sec, f' is about 0.1 cps which is well below the observed frequencies. For these values of n and B there does not appear to be any frequency range for which f falls in the vicinity of 1 cps. Thus in the solar wind the above two conditions are met only when the plasma density and the magnetic field are within relatively narrow ranges.

Discussion of the waves observed in and behind the shock is more complicated than that for the waves in the interplanetary field, because such a straight forward propagation condition as used above cannot be directly applied. First of all, the waves are generated in the region of the shock where the magnetic field rises very sharply. In this region the main problem concerns the generation of waves rather than their propagation, and discussion of the mechanism(s) of the wave generation is not attempted in the present paper. However, waves are observed behind this region which could be considered as waves propagating away from the region of generation. As has been shown earlier in this section the power spectra computed for a short time interval (144 seconds) taken immediately on the downstream side of the shock show that power density is increased in all frequencies extending to above the Nyquist frequency (Figure 26). Thus unlike on the solar side of the shock the wave propagation need not be limited to the upstream direction. It would be more natural to assume

that waves propagate in all directions from the points of generation. Thus in the Doppler formula both signs are likely to be applicable. Although how the electron density and plasma velocity vary behind the front surface of the shock is not precisely known, the magnetic field usually attains a new steady level behind the shock as has been illustrated by Figure 20. In some cases coherent waves near 1 cps are observed after this steady magnetic field level is reached as in model (b') in Figure 24. Hence it is worthwhile to investigate what conditions prevail in this region regarding wave propagation. It is noted here that since the plasma flow now contains considerable randomness, the following argument should not be taken literally. Taking n to be 10 cm^{-3} and B to be 15γ, the group velocity is a minimum near f = 1.5 cps in the reference frame K stationary in the plasma, and its value is roughly 700 km/sec for $\theta = 0^{o}$. The phase velocity at this frequency is 284 km/sec to 102 km/sec as θ varies from 0^{o} to 90^{o}. Taking the plasma velocity to be 150 km/sec, that is, one-half of the solar wind velocity, f' corresponding to f = 1.5 cps is 0.7 or 2.3 cps depending on whether the minus or the plus sign is taken in the Doppler formula. These are quite reasonable values compared with the observed frequencies. As a matter of fact, from the Doppler shift consideration alone, such a favorable circumstance is met for a considerable range of values of f. For f = 0.5 to 2.0 cps, f' varies from 0.9 to 5.0 cps including both signs in the Doppler formula.

Thus we can construct a reasonable picture concerning the coherent waves observed near 1 cps (in the satellite frame of reference),

if we suppose that waves of frequencies in the general vicinity of 0.5 to 2 cps are generated by some mechanism in the region of the shock where the sharp field increase takes place. These waves are within the general range of frequencies for the waves considered in the shock model proposed by Fishman et al. [1960] and Carmac et al. [1962]. However we do not necessarily imply that the waves observed are the same waves as in their model. The fact that coherent waves are not always observed seems to suggest that although the generation of such waves is a frequently occurring phenomenon, waves are probably not a permanent structure of the shock. We have mentioned above that waves with frequencies just below the electron cyclotron frequency could also satisfy the condition that the group velocity be nearly equal to the solar wind velocity and we have indicated in the past, in verbal presentation, that the observed waves near 1 cps might be such waves. However, from the standpoint of Doppler shift this frequency region is found to be less favorable than the frequency range considered here. Without plasma data the discussions given here are necessarily qualitative. However, when data on the plasma density and velocity become available some of the points considered above can be discussed on a more solid basis.

We have so far confined our discussion only to coherent waves, and have not attempted to reach an explanation for the occurrences of high frequency, $f > 7$ cps, fluctuations. Since the frequencies of these fluctuations are above the Nyquist frequency of our measurement, the power specturm of these fluctuations cannot be

determined; nor do we know whether these fluctuations are coherent waves or incoherent noise. However a few remarks should be made regarding these high frequency fluctuations. First, when these fluctuations occur they are observed continuously. This contrasts to the occurrences of wave packets in the case of coherent waves near 1 cps. Secondly, the high frequency fluctuations appear distinct from the lower frequency coherent waves in that gradations between these two categories are not evident.

10. Correlations with Auroral Zone Negative Bay Onsets

On the night side of the earth beyond the 500^{γ} saturation level and extending into the geomagnetic tail, the field behavior along middle latitude outbound passes is distinctly different than along in-bound low latitude passes. There are also distinct differences between successive low latitude passes as a function of latitude and distance. Under average conditions it is found that each of these regions of different behavior for temporal variations is also characterized by different ranges of ΔB = B (measured) -B (computed for earth's main field). Thus discussion is facilitated by designating these regions as shown in Figure 30. Lines bounding designated regions are not intended to be statistically exact (e.g., the location of the lowest latitude boundary on the "Quiet" tail region is primarily dictated by the orbital latitude for the months in which outbound passes occurred at night). The "reference field" used throughout this paper is the earth's main field calculated from Jensen and Cain coefficients [1962].

In this section we will consider primarily the inbound data at low latitudes (i.e., the disturbed tail region $\Delta B > 0$ and the disturbed equatorial region $\Delta B < 0$ in Figure 30) and direct our attention to rapid changes which correlate with the sudden onset of negative bays in the auroral belt at the earth's surface. The sudden onset of a negative bay at its point of origin in the auroral belt coincides with: (a) "auroral break-up," which is the time when the lowest latitude auroral arcs breaks into active rayed forms, (b) the reversal of the west to east ionospheric current previously associated with the lowest latitude arcs, (c) a large increase, following the onset, in the east to west current crossing the meridian of onset [Heppner, 1954], and (d) a reversal in the east-west direction of auroral motions [Davis, 1962]. In total (See, e.g., Sugiura and Heppner, 1965), it marks the occurrence of a major perturbation in the ionospheric electric fields driving the electrojet currents and one would expect correlated changes of either a cause or effect nature to appear in the distant magnetosphere along field lines intersecting the ionospheric area that is affected.

The first example of correlation encountered in the data analysis is illustrated in Figure 31. The satellite is inbound in the $\Delta B > 0$ low latitude tail region during moderately disturbed conditions and the intensity of the tail field is greater than under quieter conditions in accord with previous measurements [e.g., Behannon and Ness, 1966]. At 19^h22^m UT a negative bay begins relatively abruptly at Kiruna, indicating that it is near the onset location. The satellite

is also near this meridian. Following 19^h30^m UT a small decrease in B_{XY} begins and at 19^h37^m UT an abrupt decrease is noted in B_{XY} which is essentially the field in the earth's meridian plane. Following this bay the tail field regains its high level. At 21^h25^m UT another negative bay begins abruptly near Leirvogur which with the earth's rotation (note local time scales) has moved close to the satellites meridian. At 21^h39^m a second abrupt decrease in B_{XY} occurs at the satellite. In this case, however, a recovery from the decrease is not observed before the satellite moves into the equatorial low field region $\Delta B < 0$ of Figure 30. The time differences between the abrupt decreases at the earth's surface and at the satellite are 15 and 14 minutes for the two cases.

Figure 32 provides an example of the opposite behavior observed when the satellite is inside the equatorial low field intensity region, $\Delta B < 0$ of Figure 30, at the time of a sudden negative bay onset near the same meridian. In this case the satellite is inbound at a slightly lower latitude and ΔB is roughly zero between 14 and 12 R_e such that it is not clear that one can say which of the two regions, $\Delta B > 0$ and $\Delta B < 0$, applies. However, between 12 and 11 R_e it definitely enters the $\Delta B < 0$ region. There are not clearly defined negative bays near the satellite meridian until a negative bay begins abruptly in the general area of Cape Chelyuskin where it appears at 14^h09^m UT. At $14^h10.8^m$ there is a sharp increase in the B_{XY} field intensity at the satellite. Between 15^h47^m and 15^h56^m UT there is a disappearance of the magnetograph trace at Kiruna and an abrupt change at Dixon

Island marking the onset of another bay. In this case, however, a sharp change does not appear at the satellite although the field is obviously distorted abnormally as indicated by the deviation of B_Z.

Figure 33, November 15, 1964, is to be discussed relative to other phenomena in Section 13 but is included here as providing another example of bay onset correlation. In this case before $23^h04.5^m$ UT the satellite is not clearly in either the $\Delta B > 0$ or $\Delta B < 0$ regions of Figure 30 as $\Delta B \simeq 0$ and the local time, near 19^h, is such that the satellite is not necessarily in a region of tail field behavior. Although there was some negative bay, $-\Delta H$, activity prior to 22^h57^m UT it was not near the satellite meridian. At 22^h57^m UT, however, a negative bay appeared suddenly at the Julianehaab observatory which is also the auroral belt observatory closest to the satellites meridian. At $23^h04.5^m$ UT the field at the satellite abruptly increased.

To explain why increases and decreases in the field at the satellite correlate, respectively, with the satellite being in the $\Delta B < 0$ and $\Delta B > 0$ regions of Figure 30, it was initially attractive to assume that this was explained by rapid merging of field lines in the geomagnetic tail. Dungey [1966] and Axford [1966] in particular have extended their earlier work on the reconnection of field lines along a neutral sheet in the geomagnetic tail to explain the sudden onset of negative bays. Although differing in detail both theories [Dungey, 1966; Axford, 1966] assume that the sudden onset is a consequence of accelerated reconnection and merging which in turn is

produced by a sudden change in the solar wind and/or the magnetic field in the solar wind. When this occurs plasma in the neutral sheet region and newly reconnected field lines move toward the earth from the distant tail regions. Thus there is a relaxation of tail stress and the field intensity at locations remote from the neutral sheet should decrease. Similarly as more lines of force move closer to the earth an increase in field intensity is to be expected in the equatorial region of closed field lines emanating from slightly lower latitudes at the earth's surface than those extending deep into the tail.

In terms of the observations, rapid merging as a cause of the sudden bay onsets became doubtful as more examples consistently showed the onset at the earth's surface occurring prior to the change at the satellite. Furthermore these time differences couldn't be explained away in terms of propagation path in the face of two other considerations: (a) only occasionally is a surface observatory going to be ideally located where the ionospheric onset originates; thus the true onset time in the ionosphere will usually be prior to the time it appears at the nearest observatory, and (b) the fact that a correlated change at the satellite is seen only when near the meridian of the bay onset does not permit one to assume a wide variety of propagation paths whereby a change has to traverse a longer and slower path to the satellite than to the earth's surface.

Other observations which make it difficult to believe that the sudden bay onset is caused by rapid merging in the tail in response

to a sudden change in the solar wind include the following. (a) The middle latitude "quiet" tail region, Figure 30, as discussed in the next section and illustrated by Figure 34 does not vary greatly at the time of bay activity in the auroral zone. It does, however, respond sensitively to major solar wind changes as indicated, in particular, by sudden commencements [e.g., Figure 34]. One would thus expect to see a change in the middle latitude tail region at the time bay activity is triggered if the triggering comes from a change external to the cavity. This does not appear when examined on the basis of bay activity. (b) Examination of OGO-A interplanetary field data at the time of selected bay onsets has not revealed slightly earlier or coincident changes in the interplanetary field. For example, during the storm of April 17-18, 1965 (Figure 11) a negative bay appeared at College, Alaska at 06^h24^m in which ΔH decreased by about 2000^γ within the next 4 minutes. Although there are earlier changes, beginning near 06^h03^m, at Sitka at a lower latitude that cast doubt on the appropriate onset time, there are not significant changes in the interplanetary field data which was being recorded after 06^h09^m (Figure 11). Also, Vela-2 [Gosling, et al., 1967b] measurements of the solar wind did not reveal large changes during this time interval. It should be noted, however, that a statistical approach in examining bay onsets relative to solar wind and interplanetary field changes has not been made. It would not be surprising to find some correlated events as an impulse may contribute to accelerating other processes responsible for the bay onset.

Less specific, but probably even stronger, reasons for rejecting field line reconnection and merging following a solar wind change as a cause of sudden negative bay onsets come from morphological considerations. Stated briefly, these reasons relate to the following. (a) The fact that the negative bay onset is an event which occurs when a disturbed condition and aurora already exists. Thus, it does not initiate the disturbance but is instead an enhancement of the disturbance in a select region [See, e.g., Heppner, 1966]. (b) Negative bay onsets originate in a select zone of magnetic local time, centered slightly before magnetic midnight, and with a crude periodicity of several hours under average conditions in the auroral zone. Thus, an onset is roughly predictable in both time and location when the auroral distrubance pattern is known. In terms of a solar wind triggering action one thus needs to explain how the solar wind could know in advance that conditions in the auroral zone are favorable for creating a sudden onset. In brief there does not appear to be any logic in assuming that a change external to the earth's cavity is essential to produce an event whose occurrence an observer on earth can usually predict in advance through watching the development of an auroral disturbance. More specific morphological questions can also be raised. For example it is not obvious why an onset appears first at the low latitude limit of aurora (innermost field lines) and then proceeds to higher latitudes.

In rejecting accelerated field line reconnection and merging as the direct cause of auroral break-up and the negative bay onset

we are not rejecting the hypothesis that these are important processes that may take place in the geomagnetic tail. We are merely stating that a different explanation is required for the sudden onset problem.

Explanation in terms of the triggering effect occurring either within closed lines of the outer magnetosphere or within the auroral ionosphere appears to be required. The satellite data at this stage do not provide a distinction as to which (i.e., a magnetospheric or ionospheric triggering mechanism) is most likely and one must thus use surface data as a guide. As this deviates from the subject of OGO-A data, discussion here will be confined to several comments and statement as to where we think the solution may lie. Recent papers by Swift [1965, 1966] represent the only approach to this problem that we are aware of in the literature. Swift proposes that auroral break-up is caused by interchange instability in a ring current. Some of the possible pitfalls of this interpretation are also noted, Swift [1966]. It should further be noted, among other factors, that Swift assumes that electrojet currents flow only east to west and thus he does not recognize the condition that an electric field reversal occurs in the auroral break-up region. We bring up this point, independent of the possibility of interchange instability, in that it is fundamental to the approach we propose below, which is being studied further for more complete presentation in the future.

We attach primary importance to two factors: (1) the electric field geometry between latitudinally adjacent flux tubes near the break-up meridian, and (2) the local ionospheric conductivity. The

simplest model has the following features. Immediately before auroral break-up the electric field across the lowest latitude arcs is taken to be primarily south to north to drive a west to east Hall current; at a slightly higher latitude where aurora is in diffuse and rayed forms the electric field is taken to be primarily north to south to drive an east to west current. The triggering of a sudden negative bay onset occurs in this model when the ionosphere becomes a short-circuit in the meridian plane between the oppositely directed electric fields. As soon as appreciable south to north current flows in this circuit the electrostatic potentials on adjacent magnetic shells must rapidly adjust to new values. The adjustment of potentials in the meridian plane must necessarily be accompanied by both changes in the east-west potential distribution, and differences in potential along magnetic lines between ionospheric and magnetospheric regions. Thus, electrostatic particle acceleration along magnetic field lines must occur during the period of adjustment. For this brief portrayal it is essential to note the following. (a) The basic electric field configuration is assumed to come from the convective pattern in the outer magnetosphere and it is assumed that magnetic lines of force are essentially equipotentials except for the short circuiting effects in the ionosphere. (b) The general magnetopsheric configuration exists at all times with the electric field intensity varying in response to internal plasma motions. It is locally perturbed by the adjustments in potential resulting from ionospheric short circuiting and the apparent effects of these perturbations diminish with distance from the active region. (c) Minor variations in the detailed geometry of

the magnetospheric electric field, as well as the instantaneous ionospheric conductivity, influence the suddenness of the short circuit effect. (d) To some extent the potential field is short-circuited at all times by ionospheric currents. The transition from evening $+\Delta H$ variations to $-\Delta H$ (i.e., negative bay) variations within a few hours of magnetic midnight is frequently gradual, particularly during conditions of low activity. At these times relatively weak ionospheric currents are adequate to prevent further build up of the electric fields.

A basic difference in the role of the magnetospheric electric field envisaged here and that used by Dungey [1966] and Axford [1966] for the onset problem is that we attach importance to the convection that has occurred for several or more hours prior to a sudden onset. Morphologically this is dictated by the consideration of a sudden onset occurring within an existing disturbance pattern. It may also be required in the case of sudden commencement storms to explain why there is usually a lag between the time of a sudden commencement and the development of the largest bays associated with the storm.

11. The Nighttime Quiet Field at Middle Latitudes

Figure 34 illustrates the typical appearance of data along outbound passes occurring within several hours of midnight. The lack of significant field variations relative to lower latitude data leads to the designation "quiet" tail in Figure 30. As mentioned in Section 10, the field beyond roughly 10 R_e at these latitudes remains stable during bay activity in the auroral belt (e.g., note activity at Churchill between 05^h and 11^h UT, Figure 34) but responds directly to major changes in cavity compression (e.g., note activity following the SC, Figure 34). At distances < 10 R_e time variations apparently associated with auroral belt activity appear. As illustrated in Figures 34, 35, and 36 the amplitude of these short period time variations is a small fraction of the total field intensity.

In addition to its stable behavior the field in this region is characteristically more intense than anticipated from published field models. Referring specifically to the region $\Delta B > 40^\gamma$ of Figure 30, calculations furnished by G. D. Mead based on the cavity compression model of Mead [1964] and cavity compression plus tail current sheet model of Williams and Mead [1965] give a ΔB of only 10 to 20^γ. One could attempt to explain the strong field along lines of assuming that the models do not properly represent the magnetopause surface and cavity compression at high latitudes. This, however, appears to be contradicted by the rather good fit to the models at middle latitudes on the day side. For example, on the noon meridian the Mead [1964] and Williams and Mead [1965] models predict that below a certain latitude the cavity compression field will add to the dipole intensity and above this latitude it will subtract.

From 4 to 10 R_e the change in sign occurs over latitude ranges 33^o to 45^o and 30^o to 40^o, respectively, for the two models. As indicated by the dashed line on the noon meridian Figure 30, this agrees reasonably well with the OGO-A measurements beyond 7 R_e. Under non-storm conditions the change in sign of ΔB, Figure 30, is consistently found between latitudes 33^o and 45^o beyond 7 R_e. Near 7 R_e this change in sign disappears and ΔB at lower altitudes is essentially zero or slightly positive within the middle latitude range of the measurements. The deviation from the cavity models below 7 R_e on the day side can be readily explained in terms of a 10 to 20^γ contribution from an equatorial ring current centered below 4 R_e. A weak ring current below 4 R_e can also be postulated to explain why ΔB becomes essentially zero on the night side of the earth at 4 R_e on the equator, as shown in Figure 30.

There are two implications in the last paragraph relative to explaining the strong field, $\Delta B > 40^\gamma$, region on the night side: (a) the methods for computing the cavity compression field are not likely to give gross errors, and (b) the addition of an equatorial ring current below 4 R_e to the model calculations appears essential to produce better agreement with measurements in several magnetospheric regions, but it is not sufficient to account for a $\Delta B > 40^\gamma$ in the nighttime middle latitude region.

The inadequacy of existing models with the addition of a ring current to explain field intensities in the $\Delta B > 40^\gamma$ region, Figure 30, leads to the conclusion that a substantial fraction of the ΔB must be caused by a concentration of plasma at nighttime low latitudes with sufficient diamagnetism, or pressure, to bulge the field toward middle latitudes.

This is consistent with finding a persistent weak field region, $\Delta B < 0$, near the equator between 5 and 10 R_e, Figure 30. The night side low latitude diamagnetic region is thus identified as this region. Figures 35 and 36 are chosen to illustrate the arguments given above: respectively, (a) that a ring current contribution may explain a fraction of the excess intensity in the $\Delta B > 40^{\gamma}$ region, and (b) that a larger proportion of the excess intensity is probably caused by a nighttime low latitude concentration of plasma between 5 and 11 R_e that is not directly associated with ring current, D_{st}, fields.

Figure 35 shows data on the outbound pass of May 5-6, 1965 which occurred during the recovery phase of a magnetic storm when one would expect the D_{st} field to vary relatively slowly. Taking $\Delta B = 40^{\gamma}$ as a quiet day reference in this region, on grounds that it is approximately the minimum value observed on other passes, and noting that ΔB during the pass of May 5-6 is between 55 and 60^{γ}, the storm enhancement is 15 to 20^{γ}. This agrees well with the recovery phase field depression at the earth's surface which was also between 15 and 20^{γ} as shown in Figure 35 by the world-wide D_{st} and the Moca Observatory near the same local time. The geometry is such that the ring current field vectors almost totally add to either a dipole field or a tail field component directed toward the sun in the $\Delta B > 40^{\gamma}$ region whereas they totally subtract at an equatorial observatory. The exactness of agreement should probably not be taken too seriously; however the fact that agreement with storm enhancements can be found is indicative that the ring current contribution is not negligible. As noted before trouble is encountered if one tries to explain the quiet day excess of 40^{γ} by the same means.

Figure 36, an outbound pass on May 16, 1965, is an outstanding example of lack of correlation between D_{st} and a large enhancement of the field at middle latitudes. ΔB (total field) ranges from 95^{γ} at $12^{h}50^{m}$ and 5.7 R_e to 58^{γ} at $14^{h}35^{m}$ and 8.6 R_e whereas the hourly surface D_{st} varies between $+9^{\gamma}$ and -10^{γ}.

In contrast, the exceptionally strong field coincides in time with moderately intense bay activity in the auroral zone as indicated by K_p and the College, Alaska magnetogram in Figure 36. As College, Alaska is displaced roughly 2 hours in local time from the satellite meridian detailed correspondence between time variations might not be expected but it is apparent, as noted for previous examples, that there are not major rapid fluctuations in $\Delta B/B$ at the satellite. During recovery from the largest bay following $14^{h}05^{m}$ UT, ΔB at the satellite tends to decrease more rapidly. At $14^{h}37^{m}$, corresponding roughly to the end of the rapid recovery, the field at the satellite shifts rapidly in direction. Lack of data after $14^{h}40^{m}$ UT and the surface observatories near the satellite meridian do not permit more detailed study. The importance of this pass is that it provides rather clear evidence that the strong fields at middle latitudes are not to be attributed to ring current effects but are instead related primarily to plasma pressures at lower latitudes. The association with auroral zone activity further suggests that the magnetic shells passing through the low latitude, $\Delta B < 0$ region (Figure 30) are probably linked to the auroral zone.

In local time the middle latitude measurements during night hours occur mainly after 22^h30^m thus the extent of the $\Delta B > 40^\gamma$ region is not described for the evening hours. Near 04^h local time on the morning side the strong field noticeably weakens and continues to diminish proceeding toward the day side.

12. Observations Implying $B \tilde{=} 1$ in the Outer Magnetosphere at Low Latitudes near the Dawn Meridian

The OGO-A orbits during May-June 1965 were such than on inbound passes the satellite remained at very low latitudes over large distances in the local time sector 04^h30^m to 06^h30^m. This is roughly seen by visual interpolation of the geomagnetic projections shown in Figure 2. The magnetic field along these passes typically has the following characteristics: (a) between 11 R_e and the magnetopause the average gradient in total field intensity is essentially zero, (b) in a number of cases there is very little contrast between magnetospheric and transition region field behavior near the magnetopause and thus boundary identification becomes uncertain using only the field data, and (c) in a number of cases the magnetic field intensity in the transition region is greater than the field intensity in the adjacent magnetospheric region.

The distribution of these characteristics for a number of passes is shown in Figure 37. The solid lines mark the orbit segments over which the average field gradient is essentially zero or, alternatively, becomes positive as a consequence of greater field intensities in the transition region. The X marks the position of the magnetopause at the time of the boundary crossing which occurred closest to the earth on that particular pass. As indicated, the magnetopause was not identifiable on two of the nine passes shown. Difficulty in identifying the magnetopause is usually

the consequence of there being a lack of rapid fluctuations in the transition region and there not being any clearly defined persisting change in the average field behavior occurring within a time interval of several minutes.

Figure 38, May 31-June 1, 1965, illustrates the behavior for a pass which occurred under very quiet magnetic conditions. The satellite remained at magnetic latitudes $\leq$ 7.1 degrees from 20 R_e to 8 R_e. The lack of a negative field gradient beyond 11 R_e and a slight increase in field intensity after crossing the magnetopause are obvious. Between 11 R_e and 4 R_e it is also apparent that the field is not markedly different than the theoretical field.

The pass on May 21, 1965, Figure 39, illustrates another pass during quiet conditions. In this case there is a slightly greater range of latitudes but the behavior is similar to that in Figure 38. There is also some uncertainty in the magnetopause location.

Figure 40, May 26, 1965, shows a pass in which a much wider range of magnetic latitudes, roughly $\pm$ 15^{o}, is encountered beyond 11 R_e. It is also a time of weak but increasing magnetic activity at the earth's surface. Despite the latitude range the gradient behavior is similar to the lower latitude passes. In this case, as indicated by the roughness of the data, small irregular fluctuations are seen within the magnetosphere as well as in the transition region. There is uncertainty in knowing whether or not the satellite was briefly inside the magnetosphere during the interval marked M (?) near 18^{h} UT.

The June 3, 1965 pass, Figure 41, provides an example in which both the magnetic activity and magnetic latitude vary considerably during the

pass. The characteristics previously noted are again apparent. It is chosen for illustration here to note an additional characteristic behavior of the data in this region which is less readily defined or described than the others noted. This is the existence of relatively more stable, but weaker, fields within the transition region at locations which are usually several earth radii beyond the magnetopause. In examining Figures 38, 39, and 40 the reader may have noted this tendency for the transition region field to change character: for example, between 18 and 19 R_e in Figure 38 and between 16 and 17 R_e on Figures 39 and 40. Also as indicated in the projections of Figure 37 there is usually an identifiable time within the transition region where the average dB/dr is no longer zero or plus. We have not, however, found that there is a clear correlation between relatively abrupt decreases in field intensity within the transition region and distinct changes in the character of the rapid time fluctuations. Both occur, both independently and in coincidence, and considerably more study is required to establish these relationships. In Figure 41 two major changes are noted within the transition region: one following 16^h UT and the other at 13^h25^m UT. The change following 16^h UT is primarily a change in intensity on this time scale. However at 13^h25^m UT the abrupt change is proceded by a period of very stable fields in which one has to allow for the possibility that the satellite could have been inside the magnetosphere as indicated by M (?). Largely on grounds that it is not uncommon to find periods of stable field behavior within the transition region it is unlikely that the field prior to 13^h25^m is magnetospheric. Figure 42, to be discussed later, provides another example; the field prior to 20^h20^m UT, and particularly

prior to 19^h43^m UT when rapid fluctuations were not present, might be identified as magnetospheric on grounds of stable behavior. An interesting aspect of the dilemma involved in deciding whether or not an interval of stable field behavior at these locations is magnetospheric is that regardless of the assumption one most often finds that the adjacent time-space interval, definitely identified as transition region, has an equal or stronger field intensity. Thus, the arguments presented later regarding the pressure balance across the magnetopause are not made questionable by uncertainty in identifying these stable field intervals.

The June 8-9, 1965 pass, Figure 42, illustrates that during periods of moderate magnetic activity the field intensity on the transition region side of the magnetopause can greatly exceed the field intensity within the adjacent magnetospheric region. Figure 43 shows the total field intensity, $(B^2_{xy} + B^2_z)^{\frac{1}{2}}$, in an expanded view of the boundary region. This case is particularly interesting in other respects in that the simultaneous behavior of low energy electrons is suggestive of interchange behavior at the boundary. Although complicated by photoelectric effects in this part of the orbit the MIT plasma probe shows a sharp change coincident with the boundary identified at 23^h55^m in Figures 42 and 43. Vasyliunas (personal communication) identifies this as the magnetopause in good agreement with the identification made here. After this crossing the magnetic field data suggests that there may be two more crossings at 00^h15^m and 00^h37^m, as indicated in Figures 42 and 43. However, although the electron spectra and flux show considerable structure following 23^h55^m the biggest changes occur near 00:10, 01:20, and 01:55 and Vasyliunas (personal communication)

interprets these to be changes within the magnetosphere. Another way of viewing these differences is to say that the electron behavior between 00:15 and 00:37 does not lend support to identifying this interval as being a transition region field. Also, that between 23^h55^m and 01^h55^m the largest changes in the electron spectra do not coincide with the most significant field changes. We interpret this general behavior to be indicative of interchange phenomena at the boundary. As shown by Rosenbluth and Longmire [1957] the particle spectra should change markedly with field line interchange and thus if such interchange is taking place one would not expect to find exact correspondence with the electron spectra observed outside the interchange region. As the magnetopause in this sector is a boundary between two high β regions, as argued below, it seems highly likely that conditions for such interchange are favorable.

The existence of a stronger field on the transition region side of the magnetopause than in the adjacent magnetosphere theoretically gives a lower limit for the plasma pressure in the magnetospheric region which is most conveniently expressed in terms of $\beta_m = P_m/B^2_m/8\pi$. Writing the pressure balance across the magnetopause as

$$P_m + \frac{B_m^2}{8\pi} = P_t + \frac{B_t^2}{8\pi}$$

where subscripts m and t denote magnetospheric and transition regions, respectively, and assuming that B_m and B_t do not undergo a time change exactly coinciding with the boundary crossing, the lower limits for P_m are

only subject to assumptions regarding P_t. A minimum value for P_m, or alternatively minimum β_m, results if we assume either $P_t = 0$ or $P_{t\perp} = 0$ where $P_{t\perp}$ is the transition region pressure normal to the boundary. In this case $\beta_m \geq 1$ if $B_t \geq \sqrt{2}\, B_m$.

In terms of plasma measurements in the transition region it is of course unrealistic to set $P_t = 0$. Instead the measurements in general make $\beta_t >> 1$ but also suggest that in the region of interest here $P_{t\perp}$ may be considerably less than P_t; i.e., the plasma is not isotropic but instead has a dominant flow direction away from the sun and not normal to the boundary near the dawn meridian. Taking $P_{t\perp} \geq \frac{B_t^2}{8\pi}$ is thus a much less stringent assumption than taking $P_{t\perp} = 0$. For this assumption, $P_{t\perp} \geq \frac{B_t^2}{8\pi}$, one gets $\beta_m \geq 1$ if $B_t \geq B_m$.

In total these arguments imply that β_m must be close to, or greater than, one for $B_m \leq B_t$ or $\sqrt{2}\, B_m \leq B_t$ which, in turn, is typical for the observed ratios of B_m and B_t in this region. In cases where $B_t > \sqrt{2}\, B_m$ such as June 8-9, 1965, Figures 42 and 43, it appears probable than β_m exceeds one. It is also possible that the condition $\beta_m > 1$ could occur frequently in that the arguments above give only minimum values for $P_{m\perp}$. The arguments are, of course, subject to the assumption that B_m and B_t are not undergoing a major time change at the time of the boundary crossing. This would be an obvious criticism if the arguments were based on isolated measurement points and explains why we have emphasized the point that this is a general condition in this region rather than an isolated observation.

The argument that the $\beta \tilde{=} 1$, or $\beta > 1$, condition probably exists over the entire span of distance from the magnetopause to approximately 11 R_e is

primarily intuitive and stems from two considerations: (a) the lack of a field gradient implies approximate equilibrium whereas internal field structure would be likely to appear if P_m was only large very close to the boundary, and (b) the consistency with which a normal field gradient appears in the data as the satellite moves toward the earth from 11 R_e suggests that the plasma regime external to 11 R_e is quite different than that closer to the earth.

The range of geomagnetic latitudes for the $\beta \simeq 1$ condition between 04^h30^m and 06^h30^m UT appears to be approximately $\pm 15^o$. It cannot be substantially greater because the characteristics described are not observed on outbound passes where the magnetopause is crossed at geomagnetic latitudes of 25^o to 45^o. At the higher latitudes the magnetopause is generally very distinct and readily identified from both the fluctuations and having $B_m > B_t$. An interesting pecularity near the magnetopause on a number of outbound passes in this local time sector is the appearance of one or several brief intervals in which the field magnitude and/or direction changes greatly but the general fluctuation behavior differs from that encountered in the transition region. When these intervals appear they are usually tens of seconds to one or two minutes in duration and usually occur within ten or twenty minutes of the magnetopause crossing. Their existence suggests some degree of blobbiness near the boundary. Hopefully future correlations with other measurements will help resolve whether the blobs are temporal or spatial features and how they may be related to the lower latitude high β region.

The reasons for designating the two local time limits, 4^h30^m and 06^h30^m, are different. The 4^h30^m LT limit is not to be taken as a real limit as it comes only from the fact that data on inbound passes earlier than 4^L30^m is not continuous with distance and thus one cannot clearly demonstrate that the same characteristics are present. This is the consequence of the spacecraft entering a reduced power, and consequently reduced duty cycle, in mid-June. It seems quite probable that these characteristics do exist at slightly earlier local times than 4^h30^m.

The 6^h30^m local time limit is given on the basis that at this and slightly later local times the characteristics described may or may not be observed on a given pass (i.e., the behavior is not consistent). Particularly in the local time sector of 6^h30^m to 07^h near the magnetopause several inbound low latitude passes available during May 1965 show such complex time sequences of stable fields, highly irregular fields, and high frequency fluctuations occurring with different combinations of total field magnitude that detailed identification in terms of magnetospheric or transition region field becomes very uncertain using only field data. A more complete study with additional data from May 1966, OGO-B data, and correlation with other OGO-A and B experiments is required to determine if this chaotic behavior is a common feature of the 6^h30^m to 07^h sector and to achieve a better understanding. Tentatively we are inclined to believe that this boundary behavior is related to the change from a high β outer magnetosphere at earlier local times to a lower β outer magnetosphere at later local times and further infer that it is at this, and earlier, local times that solar wind plasma readily enters the magnetosphere at low latitudes.

Figure 44 is an attempt to illustrate several speculative consequences of these observations. First it is probable that the magnetopause surface bounding the high β region and the magnetopause surface bounding the adjacent lower β regions will not expand and contract equally in response to changes in energy density in the adjacent transition region. The consequence of this differential movement is likely to be warping, or development of localized bumps, on the surface. Such bumps would be expected to be unstable and thus they should be regarded as temporal features. However, if allowed to develop to appreciable dimensions before being destroyed by instabilities they will become an obstacle to the normal solar wind flow within the transition region which at this location will again be supersonic. Secondary shocks stemming from the bumps would then be expected. As criteria for recognizing such shocks inside the transition region have not been established, the data at present neither prove or disprove their existence. It is, however, tempting to speculate that isolated large amplitude, short duration (e.g., 5 to 10 sec) 'spikes' found in the transition region field data could be caused by secondary shocks. Alternatively, one can speculate that the discontinuities within the transition region separating time-space intervals of markedly different field behavior, such as discussed earlier in this section, could be attributed to weak shocks. As illustrated by the low Mach number shocks discussed for the April 19, 1965 storm, Section 6, and their contrast with theoretical expectation, criteria for recognizing weak shocks may be difficult to establish. Similarly, more study to achieve a better understanding of the variety of distinct types of fluctuations in the transition region is required to resolve this question.

The growth and duration of bumps on the magnetopause surface is probably limited by the development of instabilities. Existing theoretical treatments of instabilities [e.g., Northrop, 1956; Rosenbluth and Longmire, 1957, Lehnert, 1962] treat the problem in which β is high on only one side of the magnetopause and in these cases finding the condition for the onset of instability from an initial small perturbation is usually considered a solution. The problem posed here (i.e., high β on both sides of the boundary) is quite different. In fact, since the initial conditions are an unstable condition in terms of most theories there does not appear to be a theoretical need for finding a perturbation to initiate the instability. Although this is probably an over simplification of the problem it indicates that one can view the instability from two extreme views. One view is that a bump never really grows but is instead continuously prevented from growing by exchange between the transition region and the magnetosphere. The other view involves the assumption that a bump can grow until it breaks down as a consequence of a major instability exchange. The difference thus lies in the rate at which instability occurs and whether it is continuous or intermittent.

In either of the above cases the magnetopause bounding the high β region becomes open. Although the data do not reveal whether the net plasma flow is into or out of the magnetosphere one assumes "a priori" that the net flow will be into the magnetosphere where it is rapidly convected into the magnetospheric tail as a consequence of the earth's rotation. If this occurs continuously or frequently it will provide a nearly continuous supply of new plasma to the tail which possibly explains the formation of a high β neutral sheet deep in the tail.

Relating the above discussion to Figure 44 it should be noted that the bumps and the secondary shocks may not develop if the instability is more or less continuous. Similarly although it is appealing to view the instability as a form of intermittent or nearly continuous interchange the process is likely to be influenced by the geometry of the transition region field. At present there does not appear to be any answer regarding the importance in the interchange process of field line connection between magnetospheric and transition fields in this region (e.g., similar to that proposed by Dungey [1961, 1963] at the sub-solar point).

13. Observations in the Outer Magnetosphere at Low Latitudes near the Dusk Meridian

It is important to know whether or not the characteristics described in the previous section for local times 4^h30^m to 6^h30^m also appear near the evening meridian such as between 17^h30^m and 19^h30^m. Unfortunately the latitude vs. distance path of the satellite in this local time zone does not permit an equally clear picture. There are also limitations in data availability at low latitudes near the magnetopause in this local time zone imposed by a gap in data transmission. This is indicated by the scarcity of low latitude magnetopause crossings shown in Figure 9 for these local times. Frequently, however, data became available on inbound passes shortly after a magnetopause crossing should have occurred such that information on gradients is available. From this information the principal conclusion is that if a persistent low latitude $\beta \simeq 1$, or $\beta > 1$, condition exists, as indicated by the lack of a field gradient between some distance such as 11 R_e and the magnetopause, its latitudinal width is probably less than the $\pm 15^o$ width found near the dawn meridian. In general, when one

examines a series of orbits within the latitude range ± 15° and local times 17^h30^m to 19^h30^m both cases of a nearly normal dipole gradient and cases of a reduced gradient are observed. Thus, near the dusk meridian we have not found a particular distance at which the field gradient becomes zero that repeats persistently from orbit to orbit in the manner observed near 11 R_e in the dawn sector, as illustrated in the Figures of Section 12. Remarkably, however, Vasyliunas [1966] has found a sharp boundary in the low energy electron flux and spectra in the low latitude dusk sector that occurs most frequently close to 11 R_e. (Note: because of the spacecraft orientation, photoelectric effects on the plasma cup prohibit similar electron measurements from being made in the dawn sector). Thus it is possible that there may be more similarity between the dawn and dusk sectors than might appear from the field gradient argument.

In one outstanding case, shown in Figure 33, the condition $B_t > B_m$ is evident near 18^h LT. This cannot, however, be treated as a normal case inasmuch as it occurs following a storm commencement at 10^h08^m UT, November 15, 1964 and also following a period when the shock front was abnormally close to the earth for this local time. In Figure 33 the first of a sequence of three shock crossings between 14^h42^m and 15^h05^m is indicated. The abnormal location is evident in Figure 8 near $Y_{se} = 17$, $X_{se} = -1.4$. The magnetopause, also shown in Figure 8 near $Y_{se} = 13.5$, $X_{se} = -2.3$, is only slightly closer to earth than during average conditions. Using the same criteria as in the previous section, it appears probable that in this case the magnetospheric plasma pressure must have been such that either $\beta_m \simeq 1$ or $\beta_m > 1$ conditions were present.

It is probably not an accidental coincidence that the positive bay activity in the auroral zone near the same meridian was unusually strong at this time. As shown by the sequence of Dixon Island, Kiruna, Leirvogur, and Julianehaab magnetogram traces, Figure 33, the $+\Delta H$ disturbance was not only large but also persisted over a wide range in longitude for a number of hours preceding and coincident with the time of the magnetopause crossing. Assuming that this is not an accidental coincidence one would like to know whether the high β condition results from the auroral activity or instead arises directly from flow of plasma through the magnetopause. The data does not discriminate between these alternatives. They are noted here to bring out one point. That is, if plasma enters the magnetosphere near dawn and dusk near the equator the subsequent influence of this plasma on geomagnetic activity is likely to be quite different for the two regions of entry. As noted in the previous section near the dawn meridian the plasma would usually be expected to convect to large distances in the geomagnetic tail as a consequence of the earth's rotation [see e.g., Axford and Hines, 1961]. There is thus likely to be a time delay in the subsequent effects of this plasma. In contrast, plasma entering near 18^h is expected to convect more directly to the near earth tail region which we believe is more directly related to auroral activity than the distant tail. In this case the time delay between an unusual level of plasma entry and the surface activity is likely to be small by comparison: i.e., nearly simultaneous or within a few hours. The November 15th, Figure 22, example could be indicative of this behavior.

14. Summary

The following statements briefly summarize the principal observations reported in this paper.

(1) The variability in the location of the magnetopause and bow shock discontinuities cannot be simply related to solar wind velocity or any other single parameter. In particular, variations in plasma pressures within the magnetosphere probably play an important role in determining the boundary locations. In contrast to some previous reports the correlation of boundary locations with Kp indices is found to be poor.

(2) During the main phase of the magnetic storm of April 17-18, 1965 the bow shock is encountered at an abnormally large distance from the earth. The principal cause of this abnormal location is the existence of an exceptionally strong, 20 to 27$^{\gamma}$, interplanetary magnetic field which drops the Alfvén Mach number to values < 2 and thus increases the bow shock stand-off distance.

(3) The detailed field structure of the low Mach number, $M_A < 2$, bow shocks encountered on April 18, 1965 differs significantly from frequently quoted theoretical expectations and from the typical shock structures described in this paper for higher Mach numbers. These shocks are characterized by the presence of an exceptionally stable magnetic field on the transition region side of the shock and the absence of field oscillations associated with the shock.

(4) Gross movements of the bow shock associated with occurrences of sudden impulses at the earth's surface caused by changes in the solar wind compression of the magnetosphere are found to occur at times later than

the sudden impulse. The time differences are consistent with the shock response occurring after the solar wind change has encountered the magnetospheric obstruction and with propagation of the effect from the magnetopause to the bow shock at the Alfvén velocity. There is also some evidence that the shock location may respond to a lesser extent at the time the solar wind change first encounters the bow shock.

(5) The change in the magnetic field in crossing the magnetopause in the sunward hemisphere is frequently seen as a smooth transition over a time interval which is typically of the order of one minute. When related to arguments regarding the relative velocity of the satellite and the magnetopause the crossing times are consistent with the magnetopause thickness being of the same order of magnitude as the ion Larmor radius.

(6) A large fraction of bow shock crossings exhibit a similar average (i.e., rapid oscillations removed) magnetic field structure. This permits construction of a model profile for the shock structure based on: (a) the sharpness of the change in field gradient at the interface with the interplanetary field, (b) the rise time over which most of the change in field magnitude occurs, and (c) the total time interval between the interface time and the time at which the field reaches its average level in the transition region behind a "bump" in field intensity often found on the transition region side of the interface. When related to the average relative velocity of the satellite and the shock based on the existence of multiple crossings resulting from small amplitude changes in the shock location, these characteristic times can be converted to typical lengths or "thicknesses". Three "thicknesses" are thus obtained corresponding

to the uncertainty in (a) above and the dimensions of (b) and (c) above. Roughly, the dimension (c) resembles the ion Larmor radius, the dimension (b) resembles the characteristic ion Larmor radius, and the uncertainty in (a) corresponds to an interface dimension less than 20 km which could possibly be only hundreds of meters and thus is suggestive of an electrostatic influence at the interface.

(7) Two classes of rapid fluctuations are frequently, but not always, encountered at the bow shock. One of these is a coherent, circularly polarized wave whose frequency in the satellite frame of reference often lies between 0.5 and 1.5 cps. The other appears as high frequency noise relative to the magnetometer sampling rate and thus has an equivalent frequency > 3 cps and probably > 7 cps. These two classes of oscillation appear independently or in combinations at the bow shock, superimposed on the average structure, Item 6 above, and reach maximum amplitude immediately adjacent to the shock interface. The oscillations on some occasions extend into the interplanetary medium where their amplitude diminishes with distance away from the shock. The waves are thus believed to be generated at the shock. An additional property of the coherent oscillations is that they are usually confined to discrete wave packets of 4 to 6 cycles. The identity of the high frequency, > 3 cps., fluctuations is unknown. The coherent, roughly 1 cps, waves are identified as propagating in the whistler mode. It is suggested that their frequencies in a frame of reference stationary in the plasma are also close to 1 cps. This preference in frequency is shown by calculating the phase velocity for the condition that the group velocity of the waves be nearly equal to the solar wind velocity.

(8) Detailed correlation between the onset of negative bays in the auroral belt at the earth's surface and sudden changes in the magnetospheric field in the tail region is apparent only when the satellite is near the meridian of a surface observatory showing a sharp onset. In these cases the field intensity at the satellite is found to: (a) decrease when the satellite is located away from the equator where normally ΔB, relative to a dipole field, is positive; and (b) increase when the satellite is in the equatorial region between 5 and 11 R_e where normally ΔB, relative to a dipole field, is negative. The onset at the earth's surface is found to occur prior to the sudden change at the satellite. These characteristics support arguments, based more generally on morphological consideration, that reconnection and merging of field lines in the geomagnetic tail caused by changes external to the geomagnetic cavity does not explain the sudden onset of negative bays and auroral break-up. Explanation of the onset in terms of effects occurring within the closed magnetosphere or auroral ionosphere appears to be required. It is proposed that accelerated short-circuiting of the convective electric field pattern within the auroral ionosphere creates the local sudden reversal of the electric field which marks the occurrence of auroral break-up.

(9) At middle latitudes at distances > 5 R_e in the mid-night sector the field is found to be considerably stronger than predicted by existing models of the magnetosphere and geomagnetic tail. Near 5 R_e ΔB, relative to a dipole field, has been found to be as large as 95^{γ} in this region

under disturbed conditions. Although rapid time variations at times of high latitude disturbances are seen between 5 and 10 R_e at these latitudes their amplitude is relatively small and diminishes with distance. At greater distances in the middle latitude tail the field is found to be exceptionally stable. The strong fields between 5 and roughly 10 R_e are believed to be the consequence of high plasma pressures near the equator in the same local time sector over similar distances.

(10) The behavior of ΔB on the dayside of the earth as well as near 4 R_e near the equator on the night side of the earth suggests that a weak equatorial ring current located at distances less than 4 R_e persists during quiet periods.

(11) Near the magnetopause within the local time sector 4^h30^m to 6^h30^m and geomagnetic latitudes of $\pm$ 15° the intensity of magnetospheric fields, B_m is generally found to be $\leq B_t$, the intensity of fields in the adjacent transition region. This condition and the lack of a field gradient between 11 R_e and the magnetopause leads to the conclusion that β in this magnetospheric region must be close to, or greater than, one.

(12) The contrast between the field behavior in the high β region, Item 11 above, and adjacent higher latitude regions and the later local time sector between 6^h30^m and 7^h00 suggests that there will be local differential expansion and contraction of the magnetopause surface near the dawn meridian in response to relative changes in the solar wind and internal plasma pressures. One consequence is that bumps may develop on the magnetopause surface which could cause secondary shock fronts

within the transition region. A more significant consequence is that the magnetopause in this sector is likely to be highly unstable. It is proposed that solar plasma may continuously or intermittently enter the magnetosphere through this unstable boundary.

(13) Although the distribution of data in the dusk sector (e.g., 17^h30^m to 19^h30^m) does not permit an ideal comparison with the behavior in the dawn sector it appears that a comparable high β region may be limited to a narrower range of low latitudes if it exists as a persistent feature. One case, during a disturbed period, definitely indicates the existence of a $\beta \geq 1$ condition within the magnetosphere near 18^h local time.

Acknowledgment

Exchange of information and discussions with Dr. V. Vasyliunas of the Massachusetts Institute of Technology regarding the OGO-A plasma measurements have frequently been helpful in the analysis and we are grateful for this communication.

Reference

Auer, P. L., H. Hurwitz, Jr., and R. W. Kilb, Phys. Fluids, 5, 298-316, 1962.

Axford, W. I., Proc. of ESRO Colloquium, Stockholm, Nov. 1965; Sp. Sci. Reviews, to be published, 1966.

Axford, W. I. and C. O. Hines, Can. J. Phys., 39, 1433-1463, 1961.

Behannon, K. W. and N. F. Ness, J. Geophys. Res., 71, 2327-2351, 1966.

Bonetti, A., H. S. Bridge, A. J. Lazarus, B. Rossi, and F. Scherb, J. Geophys. Res., 68, 4017-4063, 1963.

Bridge, H. S., A. Egidi, A. Lazarus, E. Lyon, and L. Jacobson, Space Research V, North-Holland Publ. Co., Amsterdam, 969, 1965.

Cahill, L. J., J. Geophys. Res., 71, 4505-4519, 1966.

Cahill, L. J. and Amazeen, P. G., J. Geophys. Res., 68, 1835-1844, 1963.

Camac, M., A. B. Kantrowitz, M. M. Litvak, R. M. Patrick, and H. E. Petschek, Nuclear Fusion, Suppl., Pt. 2, 423-445, 1962.

Davis, T. N., J. Geophys. Res., 67, 59-110, 1962.

Dessler, A. J., W. E. Francis, and E. N. Parker, J. Geophys. Res., 65, 2715-2719, 1960.

Dungey, J. W., Phys. Rev. Letters, 6, 47, 1961.

Dungey, J. W., Planet, Space Sci., 10, 233-237, 1963.

Dungey, J. W., Proc. of ESRO Colloquium, Stockholm, Nov. 1965; to be published Sp. Sci., Reviews, 1966.

Fairfield, D. H. and N. F. Ness, GSFC Preprint X-612-66-530, Nov. 1966.

Ferraro, V. C. A., J. Geophys. Res., 57, 15-49, 1952.

Fishman, F. J., A. R. Kantrowitz, and H. E. Pelschek, Rev. Mod. Phys. 32, 959-966, 1960.

Frank, L. A. and J. A. Van Allen, J. Geophys. Res., 69, 4923-4932, 1964.

Freeman, J. W., J. A. Van Allen, and L. J. Cahill, J. Geophys. Res., 68, 2121-2130, 1963.

Freeman, J. W., J. Geophys. Res., 69, 1691-1723, 1964.

Gosling, J. T., J. R. Asbridge, S. J. Bame, A. J. Hundhausen, and I. B. Strong, Measurements of the Interplanetary Solar Wind during the Large Geomagnetic Storm of April 17-18, 1965, (Preprint) 1967(b).

Gosling, J. T., J. R. Asbridge, S. J. Bame, and I. B. Strong, J. Geophys. Res., 72, 101-112, 1967(a).

Heppner, J. P., Defence Res. Board, Canada, Report DR-135, 1958; Thesis, Calif. Inst. of Tech. (1954).

Heppner, J. P., Proc., ESRO Colloquium, Stockholm, Nov. 1965; (to be published, Space Sci. Rev., 1966); GSFC preprint X-612-65-490, 1965.

Heppner, J. P., Proc of Advanced Study Institute, Keele, England, Aug. 1966; to be published, Reinhold Publ. Co., New York, 1967; GSFC preprint X-612-66-455, Aug. 1966.

Heppner, J. P., N. F. Ness, C. S. Scearce, and T. L. Skillman, J. Geophys. Res., 68, 1-46, 1963.

Holzer, R. E., M. G. McLeod, and E. J. Smith, J. Geophys. Res., 71, 1481-1486, 1966.

Jensen, D. C. and J. C. Cain, J. Geophys. Res., 67, 3568-3569, 1962.

Kennel, C. F., and R. Z. Sagdeev, Collisionless shock waves in high β plasmas, Intern. Center for Theor. Phys., IC-66-68, Trieste, 1966.

Lehnert, B., Phys. Fluids, 5, 432-438, 1962.

Ludwig, G. H., Space Sci. Rev., 2, 175-218, 1963.

Mead, G. D., J. Geophys. Res., 69, 1181-1195, 1964.

Mead, G. D. and D. B. Beard, J. Geophys. Res., 69, 1169-1180, 1964.

Morozov, A. I., and L. S. Solov'ev, Soviet Phys. JETP, 13, 927-932, 1961.

Ness, N. F., C. S. Scearce, and J. B. Seek, J. Geophys. Res., 69, 3531-3569, 1964.

Nishida, A., Report of Ionosphere and Space Research (Japan), 20, 42-44, 1966.

Nishida, A. and L. J. Cahill, J. Geophys. Res., 69, 2243-2255, 1964.

Northrop, T. G., Phys. Rev., 103, 1150-1154, 1956.

Patel, V. L. and A. J. Dessler, J. Geophys. Res., 71, 1940-1942, 1966.

Rosenbluth, M. N. and Longmire, C. L., Annals of Phys., 1, 120-140, 1957.

Shabanskiy, V. P., Soviet Phys. JETP, 13, 746-750, 1961.

Sigov, Yu. S., and B. A. Tverskoy, Geomagn. Aeron., 3, 32-36, 1963.

Snyder, C. W., M. Neugebauer, and U. R. Rao, J. Geophys. Res., 68, 6361-6370, 1963.

Spreiter, J. R. and W. P. Jones, J. Geophys. Res., 68, 3555-3564, 1963.

Stix, T. H., The Theory of Plasma Waves, McGraw-Hill Book Co., Inc., New York, 1962.

Sugiura, M., Radio Sci., J. of Res. NBS/USNC-URSI, 69D, 1133-1147, 1965.

Sugiura, M. and J. P. Heppner, Chapter 1, Introduction to Space Science, ed. by W. N. Hess, Gordon and Breach, New York, 1965.

Swift, D. W., Geophys. Inst., Univ. of Alaska, Report UAGIR-165, July 1965.

Swift, D. W., Paper submitted to Planet, and Sp. Sci., December 1966.

Tidman, D. A., Turbulent shock waves in plasmas (submitted to Phys. Fluids) August, 1966a.

Tidman, D. A., The earth's bow shock wave (submitted to J. Geophys. Res.) September, 1966b.

Vasyliunas, V. M., Observations of Low Energy Electrons with the OGO-A satellite, Ph.d. thesis, Mass. Inst. of Tech., August 1966.

Walters, G. K., J. Geophys. Res., 69, 1769-1783, 1964.

Wiggins, E. T., TRW Systems Report No. 2336-6011-RU000 under Contract NAS 5-9100 (1965).

Wilcox, J. M., K. H. Schatten, and N. F. Ness, J. Geophys. Res., 72, 19-26, 1967.

Williams, D. J. and G. D. Mead, J. Geophys. Res., 70, 3017-3029, 1965.

Wolfe, J. H., R. W. Silva, and M. A. Myers, Space Res., 6, 1965.

Wolfe, J. H., R. W. Silva, and M. A. Myers, J. Geophys. Res., 71, 1319-1340, 1966.

Table 1: Data Characteristics

	Sensitive Scale	Insensitive Scale
Field Range (Nominal):	$\pm$ 30$^{\gamma}$	$\pm$ 500$^{\gamma}$
Digital Resolution (Nominal):	0.24$^{\gamma}$	3.5$^{\gamma}$
Readings per 12 sec. spin period per axis for data modes (a), (b), (c) below:		
(a) 1 kilobit	20.5	10.3
(b) 8 kilobit	165.	83.
(c) 64 kilobit	1322.	661.

Table 2. Statistical results on movements of the shock: $\bar{n}'$, $\bar{V}_s'$, and $\bar{A}'$ signify the average values of N', V_s, and A', and P. E. is the probable error.

		Velocity				Amplitude			
n'	$\bar{n}'$	$\bar{V}_s$	P.E.	maximum	minimum	$\bar{A}'$	P. E.	maximum	minimum
		km/sec	km/sec	km/sec	km/sec	km	km	km	km
≥ 3	4.20	9.3	4.2	28.2	3.6	3159	1288	8536	536
< 3	1.65	3.4	0.8	5.2	1.8	1590	693	3866	451
all cases	3.02	6.5	3.7	28.2	1.8	2430	1167	8536	451

FIGURE CAPTIONS

Figure 1: Illustration of magnetometer sensor locations with 22 ft. boom in the undeployed configuration. X,Y, and Z designate the body coordinates of the spacecraft. The spacecraft's spin is right handed, as indicated, with a period of approximately 12 seconds.

Figure 2: Sequence of three OGO-A orbits in geomagnetic projection following launch (top) and one year later (bottom).

Figure 3: Projections of the OGO-A spin axis and orbit onto the equatorial plane of the earth.

Figure 4: Typical calibration curves for the two ranges. Curves shown are for the Y axis of the flight instrument.

Figure 5: Fluxgate magnetometer response curves.

Figure 6: Method of obtaining B_{XY} and B_Z

Figure 7: Spacecraft magnetic field intensities along the X and Y fluxgate axes. Each point represents an average of values sampled over periods of several hours to a day. See text for value of the Z axis spacecraft field.

Figure 8: OGO-A magnetopause and bow shock encounters. Number of crossings is indicated (see text).

Figure 9: Geomagnetic latitudes, or ranges of latitude, are given for the boundary crossings of Figure 8.

Figure 10: Kp indices, or ranges of the Kp index, are given for the boundary crossings of Figure 8.

Figure 11: Measurements during the April 17-18, 1965 magnetic storm

Figure 12: Crossings of the magnetosphere boundary and the bow shock as seen in the sensitive Y component plotted on a condensed time scale. The vertical width is twice the magnitude of the magnetic field in the plane normal to the spin axis.

Figure 13: Comparison of the horizontal component, H, observed at Tucson and Honolulu with movements of the bow shock as deduced from shock crossings by the satellite.

Figure 14: Crossings of the magnetosphere boundary and the bow shock observed in the sensitive Y component and in the insensitive Z component. For the latter, 1-minute averages $\bar{Z}$ and the standard deviations $\delta(Z)$ for the same intervals are shown. Satellite coordinates are indicated by radial distance in earth-radii (R_e), geomagnetic and geocentric latitudes, and solar ecliptic longitude ϕ, measured eastward from the longitude of the subsolar point.

Figure 15: Variations in the magnetic field during an outward traversal of the magnetosphere boundary. The satellite position at $10^h\ 58^m\ 0^s$ is: radial distance 94,802 km ($14.86R_e$), geographic latitude 26.8^o, geomagnetic latitude 21.3^o, and local time 14.8^h. The reference field, Bo, is from Jensen and Cain (1962) coefficients.

Figure 16: Variations in the magnetic field during a period in which the magnetosphere boundary moved outward overtaking the satellite, 9 minutes after the end of Fig. 15. The satellite position at $11^h\ 9^m\ 0^s$ is: radial distance 95,905 km ($15.04\ R_e$), geographic latitude 28.5^o, geomagnetic latitude 21.6^o, and local time 14.8^h.

Figure 17: Variations in the magnetic field while the satellite crossed the magnetosphere boundary outward, about 17 minutes after the end of Fig. 16. The satellite position at $11^h\ 29^m\ 0^s$ is: radial distance 97,869 km (15.34 R_e), geographic latitude 28.3^o, geomagnetic latitude 22.1^o, and local time 14.8^h.

Figure 18: Magnetic field variations during a traversal of the bow shock on November 25, 1964. From top to bottom: 1-second averages of the sensitive Y component; the standard deviation σ (Z) and the mean value of Z taken over the spin period; the amplitude of the sensitive Y component determined by taking one-half of the separation between the upper and lower envelopes of the top curve; and the magnitude of the total scalar field B. The position of the satellite at $0^h\ 2^m\ 0^s$ is: radial distance 144,420 km (22.64R_e), geographic latitude 23.4^o, local time 15.7^h.

Figure 19: Magnetic field variations during a traversal of the bow shock on December 18, 1964. From top to bottom: the field component in the plane normal to the spin axis, as determined from the sensitive Y component; the field along the spin axis; and the magnitude of the total scalar field. The position of the satellite at $13^h\ 54^m\ 0^s$ is: radial distance 110,827 km (17.38 R_e), geographic latitude 27.3^o, geomagnetic latitude 32.0^o, local time 13.5^h.

Figure 20: An illustrative model of the bow shock to deomonstrate different characteristic scale lengths: t_o uncertainly $\simeq \pm 2$ sec., $|t_o - t_1| \simeq$ 8 sec. $\pm$ 6 sec., $|t_o - t_2| \simeq 35$ sec. $\pm$ 20 sec.

Figure 21: A sawtooth model for the fluctuations of the shock position. The satellite motion is represented by the near-straight line. A is the amplitude of the shock oscillation: A' is the apparent amplitude.

Figure 22: The bow shock with coherent waves of frequencies near 1 cps, observed on November 25, 1964. Scales both uncorrected (the farthest left) and corrected for the spacecraft field are given. The 12 second periodicity is the satellite spin.

Figure 23: Rapid magnetic field fluctuations with frequencies above 7 cps at the bow shock for a case in which the front of the bow shock "touched" but did not completely cross the satellite location, March 24, 1965. Scales both uncorrected (the farthest left) and corrected for the spacecraft field are given.

Figure 24: Classification of different appearances of the bow shock: (a) without regular waves of frequency near 1 cps; (b) with regular waves of frequency near 1 cps associated with the sharp rise of the field; (b') with such waves spreading out on both sides of the shock; (c) with high frequency fluctuations at the sharp rise of the field; (c') with high frequency fluctuations spreading out on both sides of the shock.

Figure 25: Example showing rapid, unresolved, fluctuations at the shock and on the interplanetary side of the shock, with coherent waves near 1 cps at the shock and on the transition region side of the shock. The Y-axis sensitive scale is shown uncorrected for the 9^{γ} spacecraft field

Figure 26: Estimates of the power spectrum densities for the sensitive Y component for the two 144-second intervals on both sides of the shock: (A) on the solar-wind side of the shock, and (B) behind the shock. In each power spectrum the peak at about 0.08 cps is due to the spin modulation, and estimates of the first four positive side lobes are indicated by 1, 2, 3, and 4. The record is for the same shock crossing as shown in Figure 22, i.e., about $0^h\ 2^m\ 10^s$ UT on November 25, 1964.

Figure 27: Power spectra for the sensitive Y component for a series of 144-second intervals in close succession. The beginning of each time interval is indicated.

Figure 28: An example of a quasi-sinusoidal wave with a period of 1.5 seconds associated with a sudden change in a quiet interplanetary magnetic field, suggesting a steepening of a finite amplitude hydromagnetic wave.

Figure 29: An example of a large amplitude wave observed in the transition region.

Figure 30: Classification of regions by gross characteristics to facilitate discussion of field behavior in the midday and midnight time sectors relative to dipole coordinates.

Figure 31: Correlation with bay onsets on September 28, 1964.

Figure 32: Correlation with bay onset on October 1, 1964.

Figure 33: November 15-16, 1964 (See text Sections 10 and 13).

Figure 34: Middle latitude "quiet" tail field, June 15, 1965.

Figure 35: Middle latitude, night time pass on May 5, 1965.

Figure 36: Middle latitude, night time pass on May 16, 1965

Figure 37: Orbital segments along inbound passes near the dawn meridian projected onto the solar-ecliptic equatorial plane. See text for a description of the features noted.

Figure 38: Inbound pass of May 31-June 1, 1965.

Figure 39: Inbound pass on May 21, 1965.

Figure 40: Inbound pass on May 26, 1965. Symbols T and M stand for transition and magnetospheric regions, respectively.

Figure 41: Inbound pass on June 3, 1965.

Figure 42: Inbound pass of June 8-9, 1965.

Figure 43: Total field intensity during the period of magnetopause crossing on June 8-9, 1965.

Figure 44: To illustrate the speculative consequences of differential expansion and contraction of the magnetopause bounding the low latitude high β region.

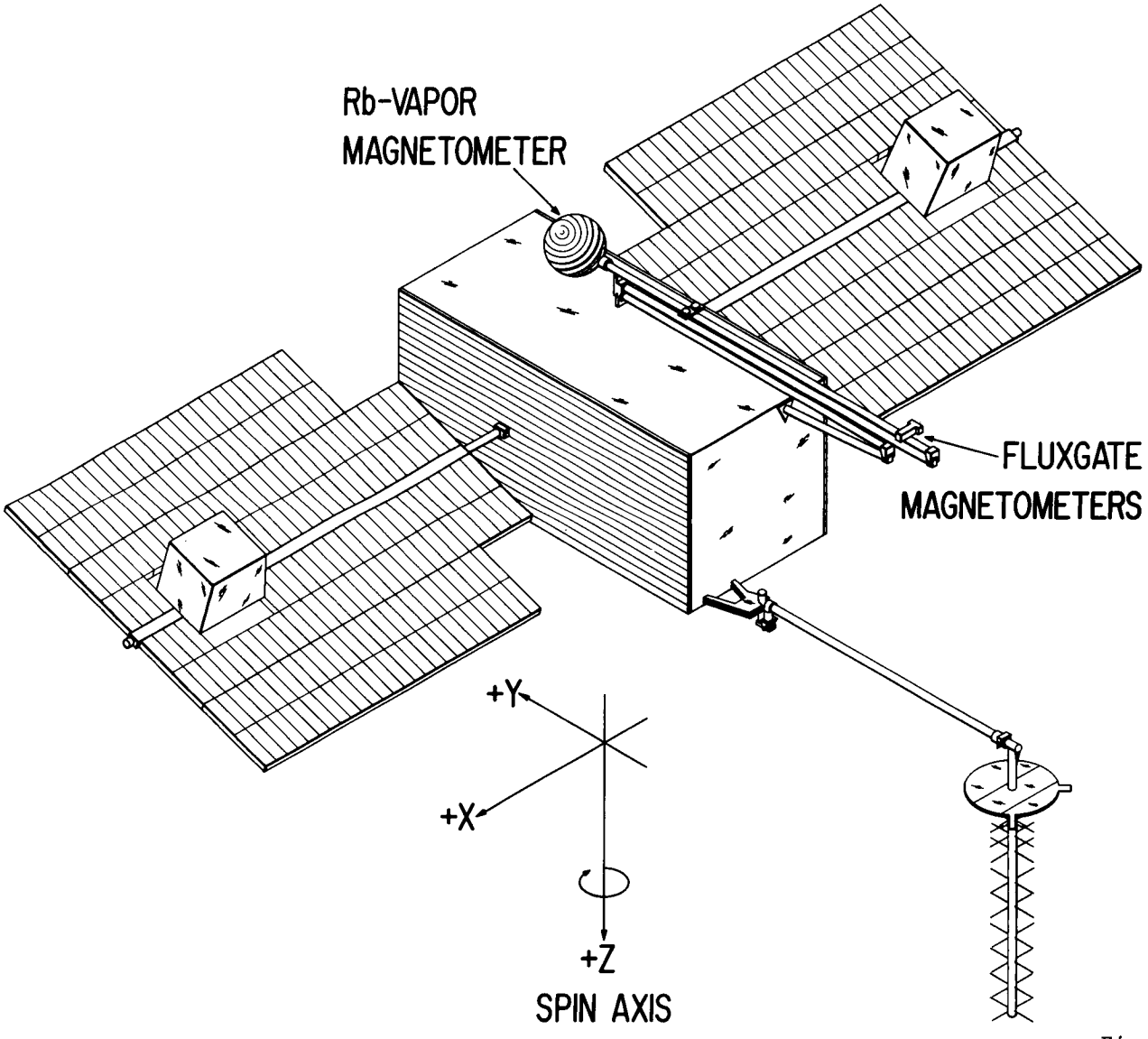
Rb-VAPOR
MAGNETOMETER
FLUXGATE
MAGNETOMETERS
+Y
+X
+Z
SPIN AXIS

Figure 1

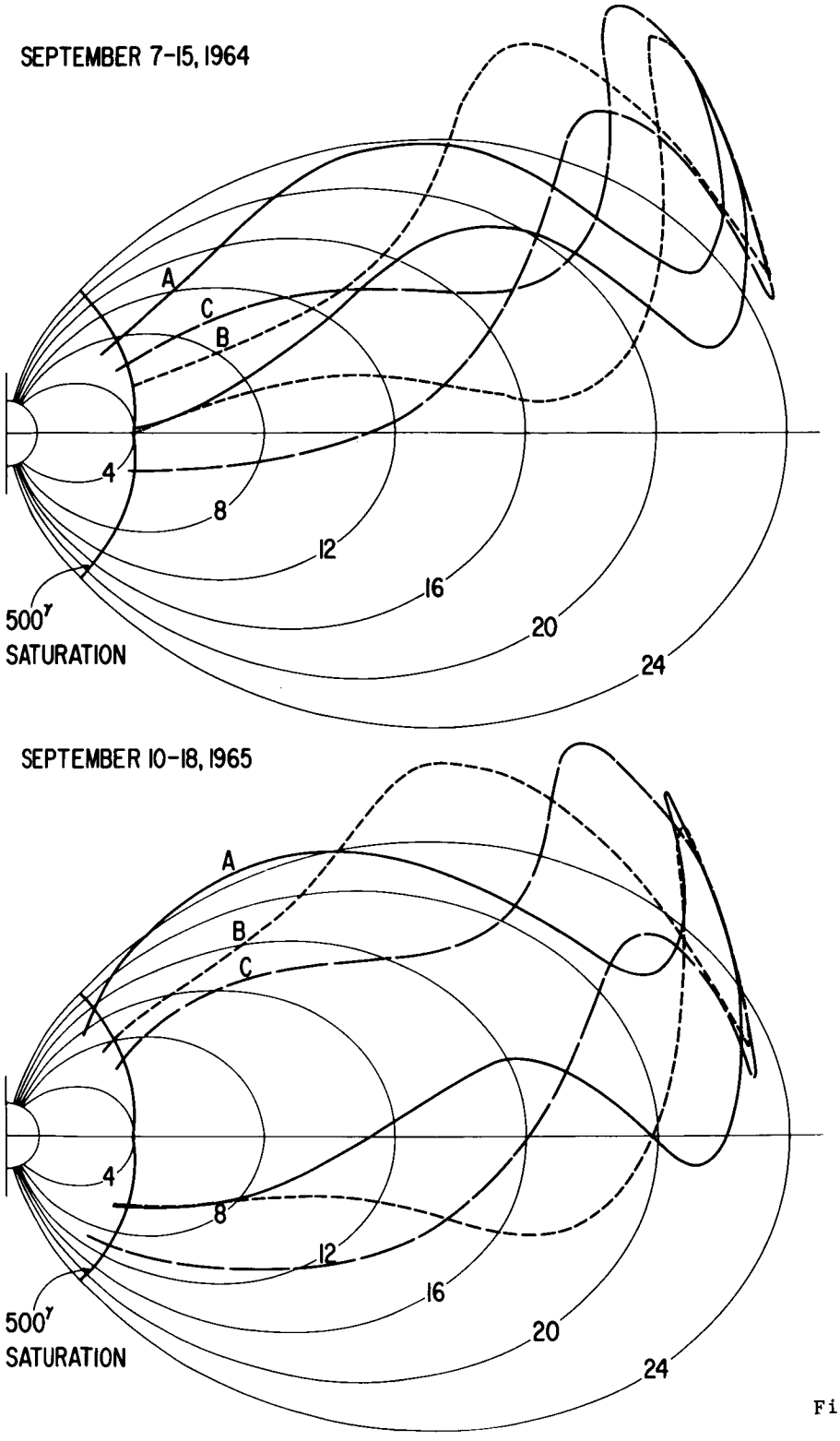
SEPTEMBER 7-15, 1964
A
C
B
4
8
12
16
20
24
500γ
SATURATION
SEPTEMBER 10-18, 1965
A
B
C
4
8
12
16
20
24
500γ
SATURATION

Figure 2

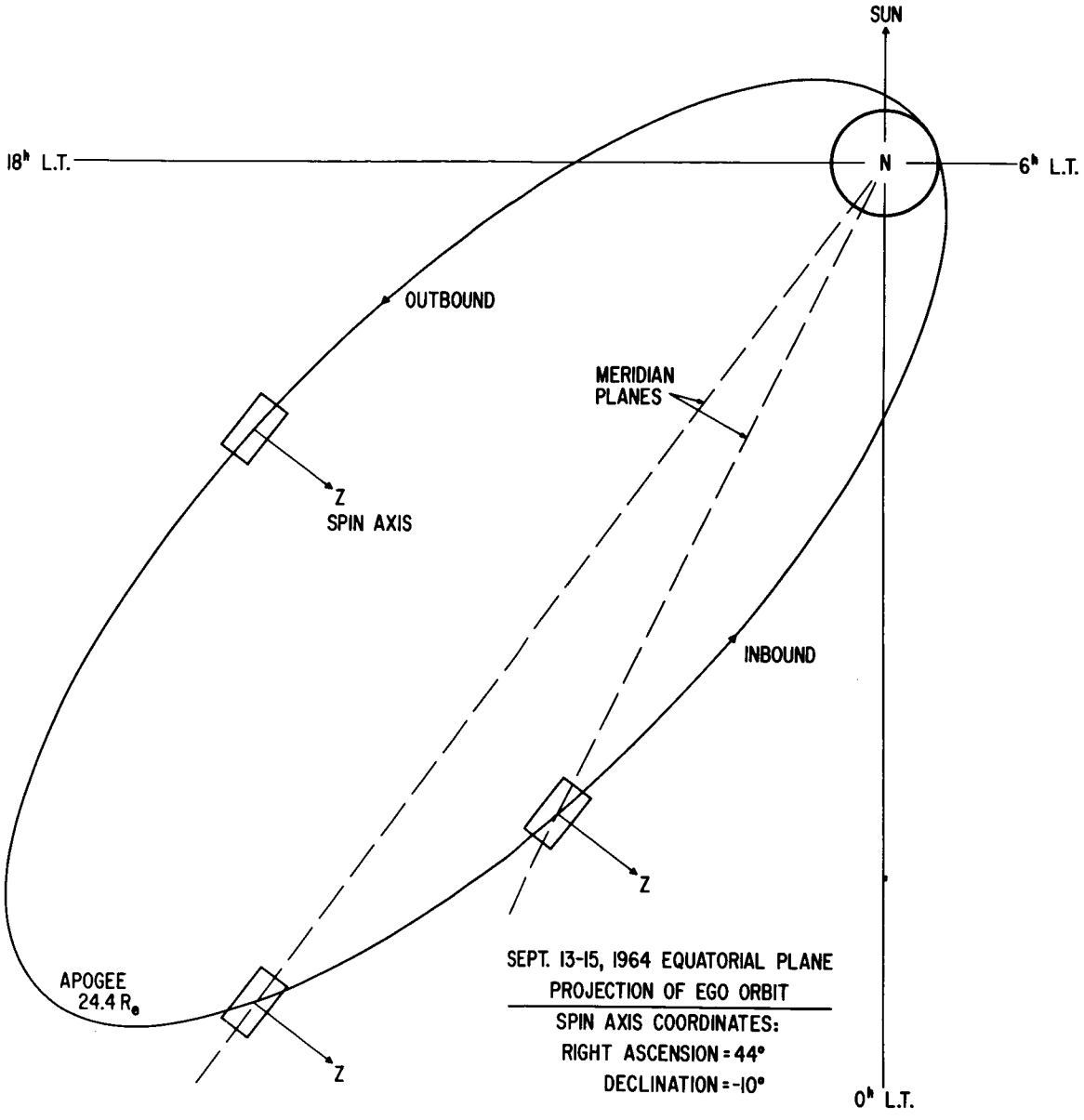
SUN
18h L.T.
N
6h L.T.
OUTBOUND
MERIDIAN
PLANES
Z
SPIN AXIS
INBOUND
Z
APOGEE
24.4 Re
Z
SEPT. 13-15, 1964 EQUATORIAL PLANE
PROJECTION OF EGO ORBIT
SPIN AXIS COORDINATES:
RIGHT ASCENSION = 44°
DECLINATION = -10°
0h L.T.

Figure 3

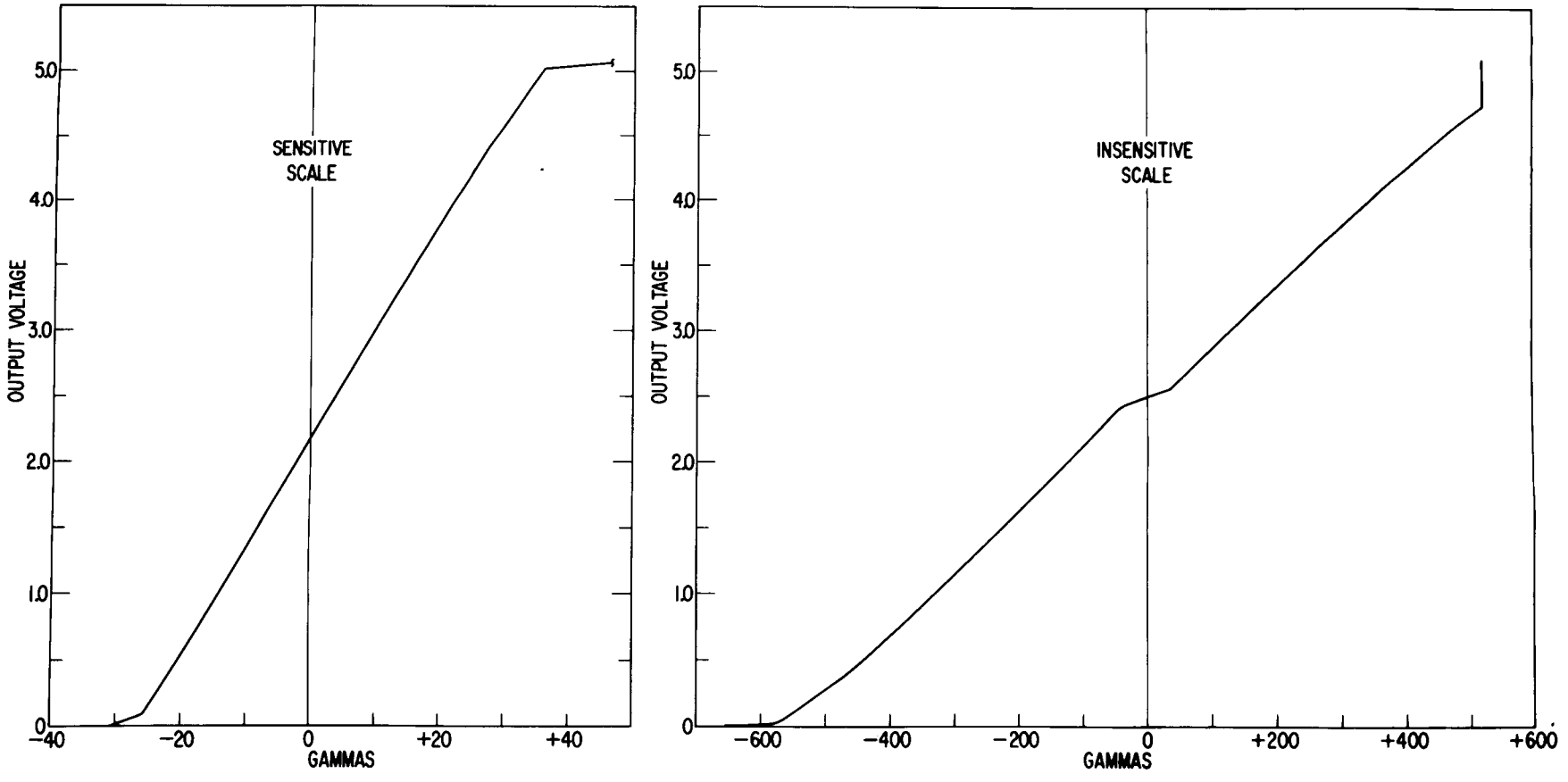
SENSITIVE
SCALE
OUTPUT VOLTAGE
5.0
4.0
3.0
2.0
1.0
0
−40
−20
0
+20
+40
GAMMAS
INSENSITIVE
SCALE
OUTPUT VOLTAGE
5.0
4.0
3.0
2.0
1.0
0
−600
−400
−200
0
+200
+400
+600
GAMMAS

Figure 4

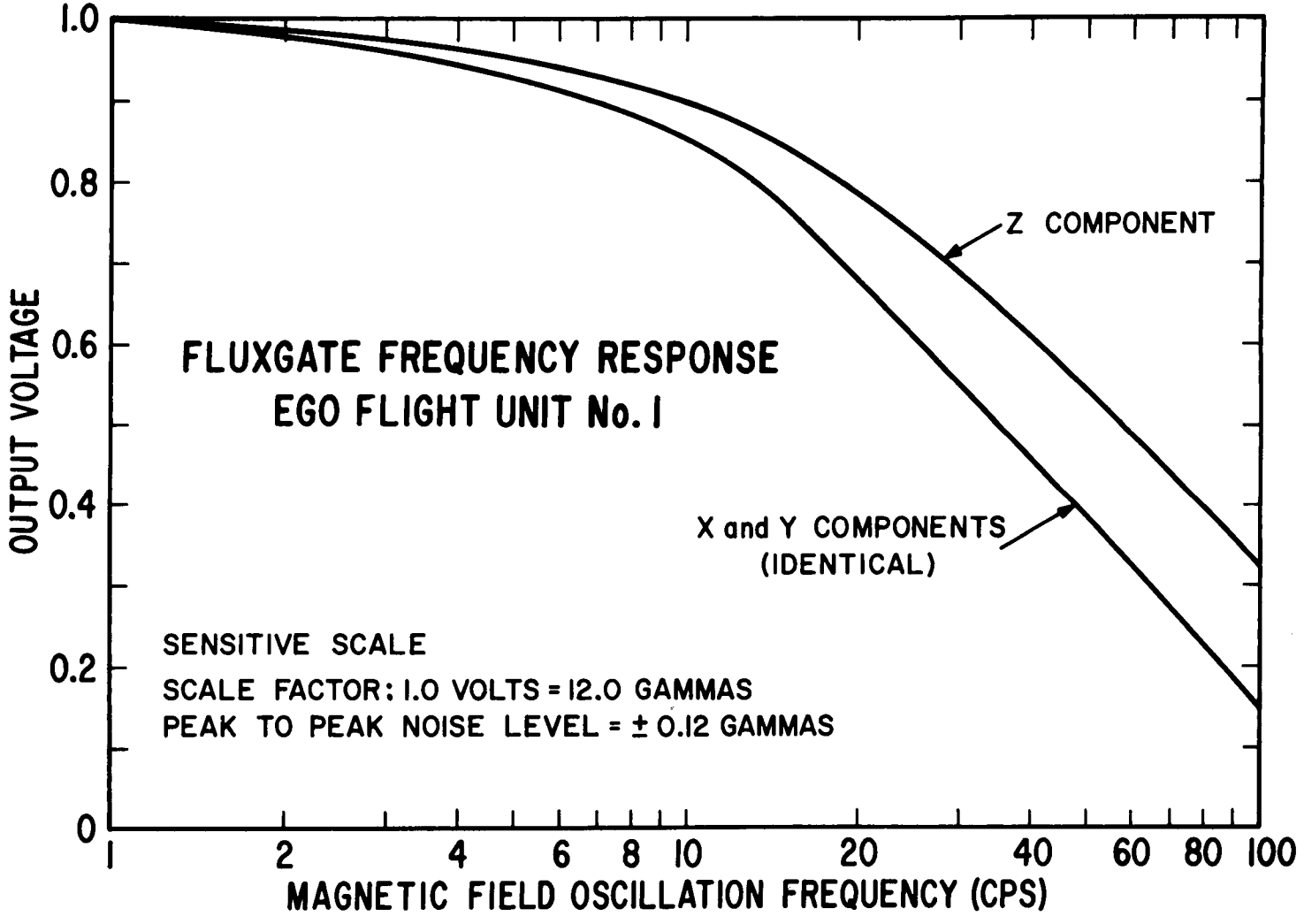
1.0
0.8
0.6
0.4
0.2
0
OUTPUT VOLTAGE
FLUXGATE FREQUENCY RESPONSE
EGO FLIGHT UNIT No. 1
Z COMPONENT
X and Y COMPONENTS
(IDENTICAL)
SENSITIVE SCALE
SCALE FACTOR: 1.0 VOLTS = 12.0 GAMMAS
PEAK TO PEAK NOISE LEVEL = ± 0.12 GAMMAS
1
2
4
6
8
10
20
40
60
80
100
MAGNETIC FIELD OSCILLATION FREQUENCY (CPS)

Figure 5

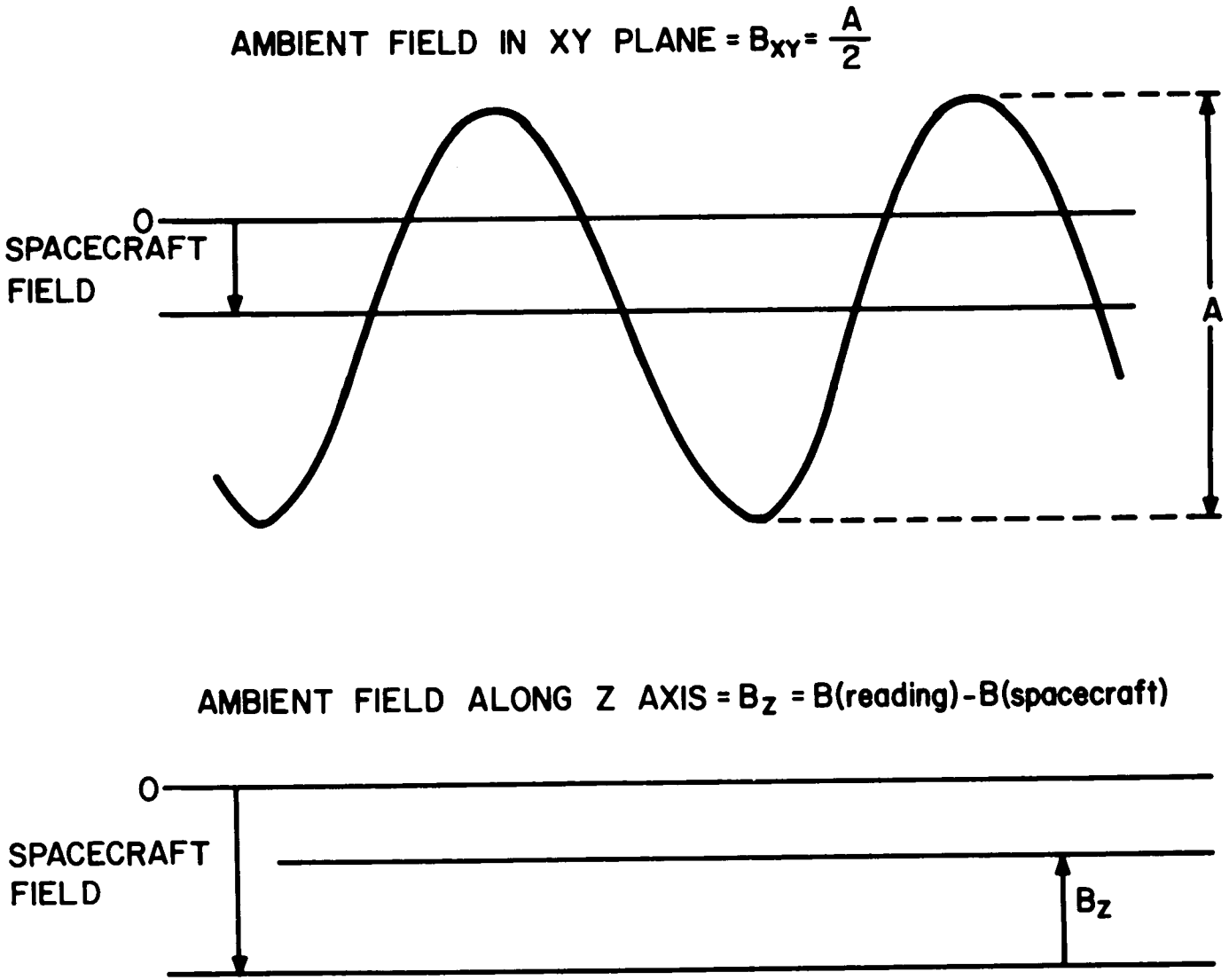
AMBIENT FIELD IN XY PLANE = $B_{XY} = \frac{A}{2}$
0
SPACECRAFT FIELD
A
AMBIENT FIELD ALONG Z AXIS = B_Z = B(reading) - B(spacecraft)
0
SPACECRAFT FIELD
B_Z

Figure 6

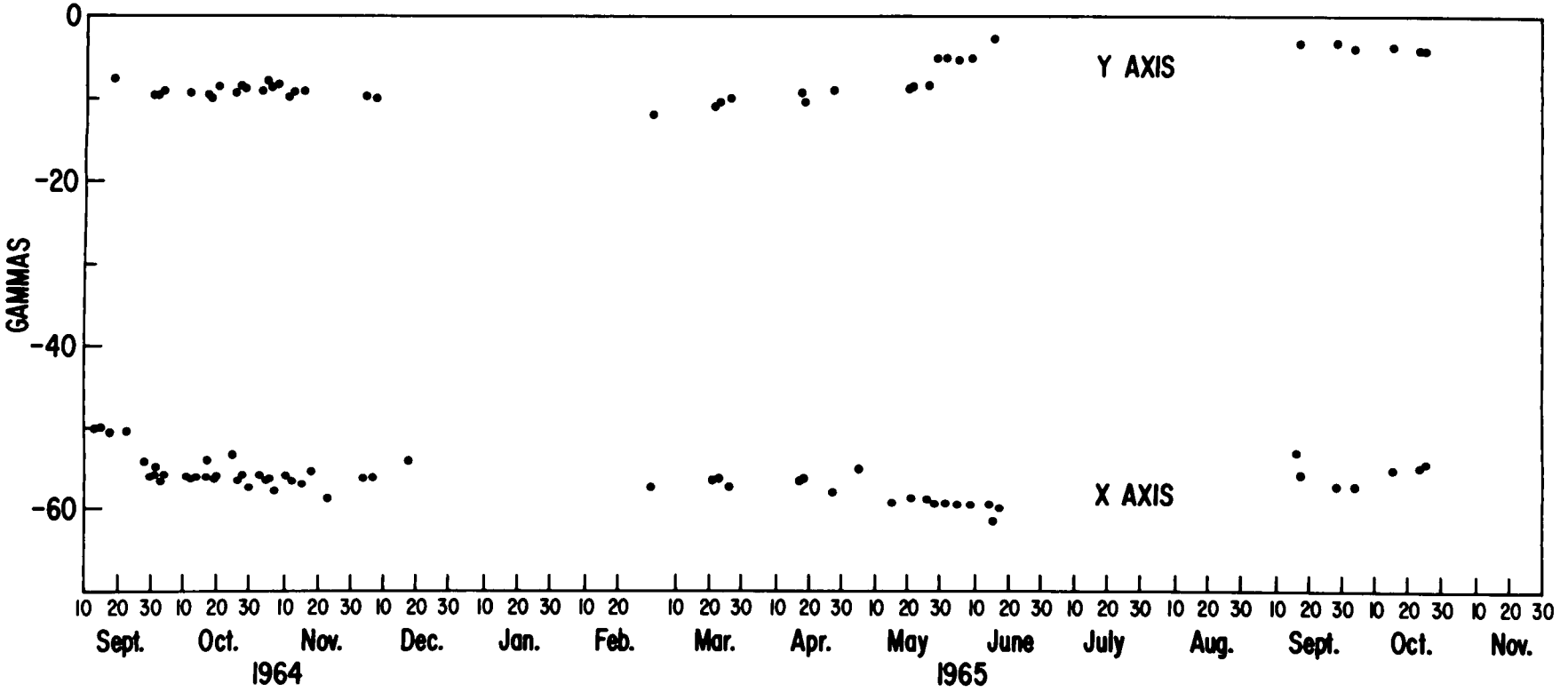
0
-20
-40
-60
GAMMAS
Y AXIS
X AXIS
10 20 30 10 20 30 10 20 30 10 20 30 10 20 30 10 20 10 20 30 10 20 30 10 20 30 10 20 30 10 20 30 10 20 30 10 20 30 10 20 30 10 20 30 10 20 30
Sept. Oct. Nov. Dec. Jan. Feb. Mar. Apr. May June July Aug. Sept. Oct. Nov.
1964
1965

Figure 7

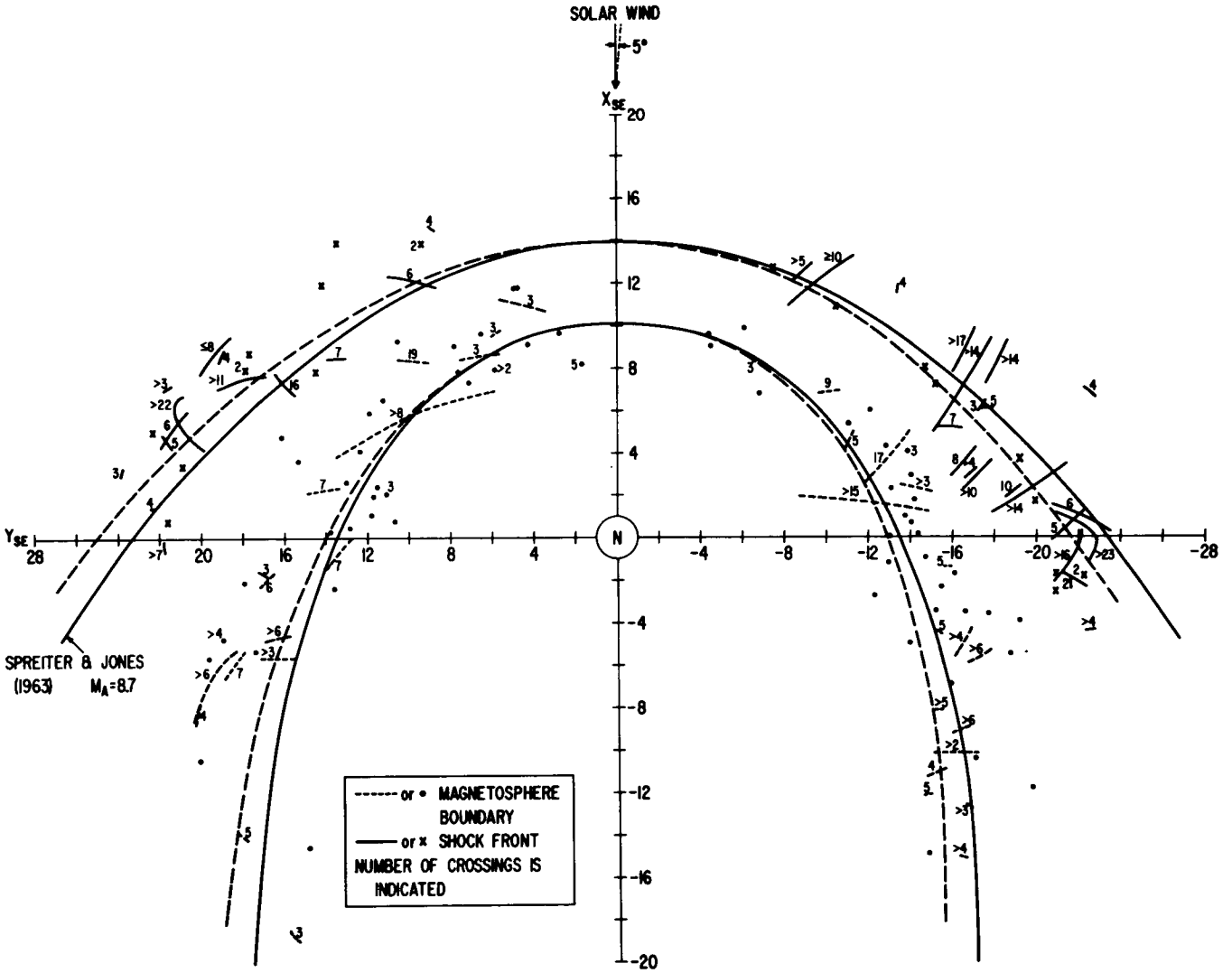
SOLAR WIND
5°
X_{SE}
Y_{SE}
N
SPREITER & JONES
(1963) M_A=8.7
------ or • MAGNETOSPHERE BOUNDARY
—— or x SHOCK FRONT
NUMBER OF CROSSINGS IS INDICATED

Figure 8

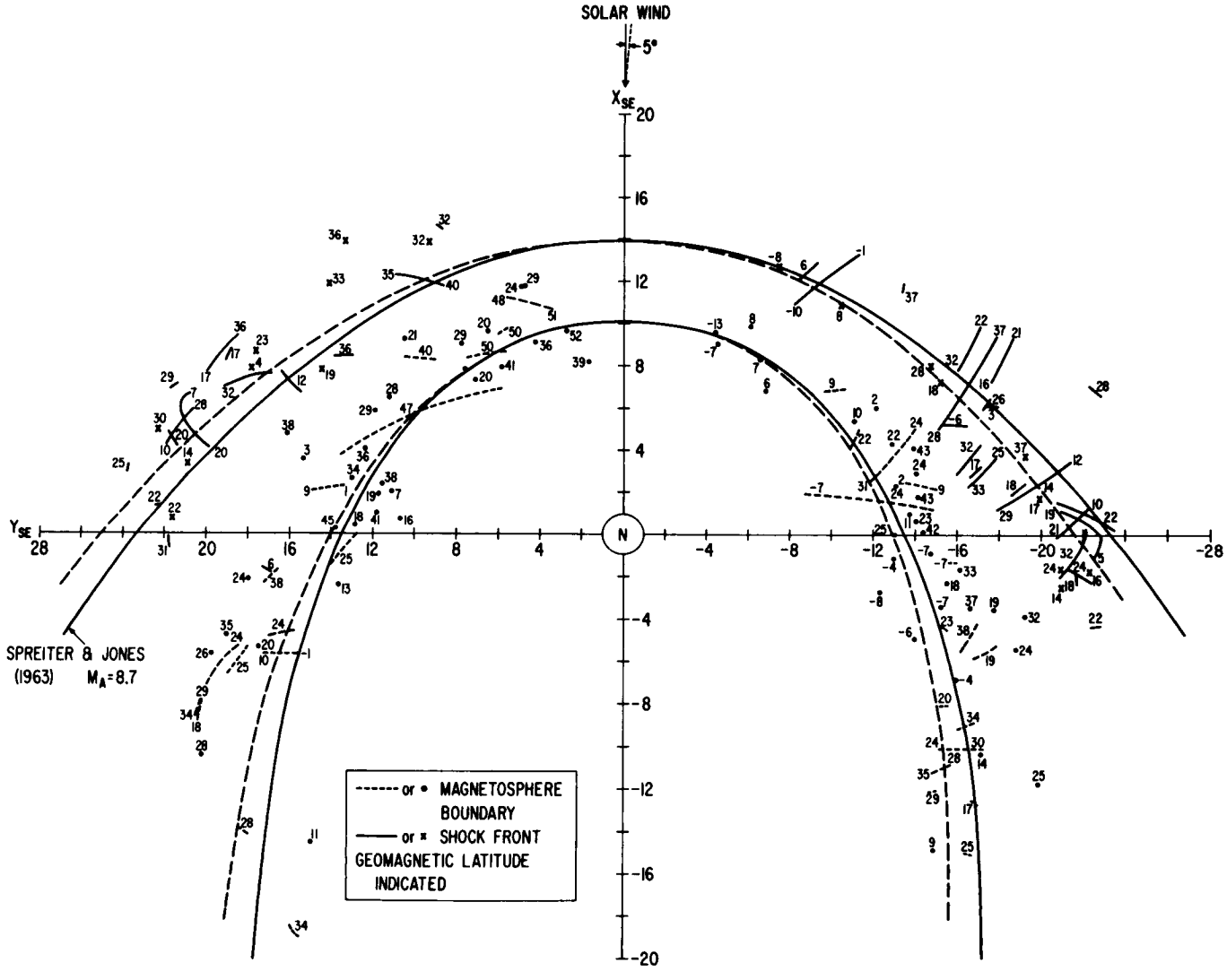
SOLAR WIND
5°
X_{SE}
Y_{SE}
N
SPREITER & JONES
(1963) M_A=8.7
------ or • MAGNETOSPHERE BOUNDARY
—— or x SHOCK FRONT
GEOMAGNETIC LATITUDE INDICATED

Figure 9

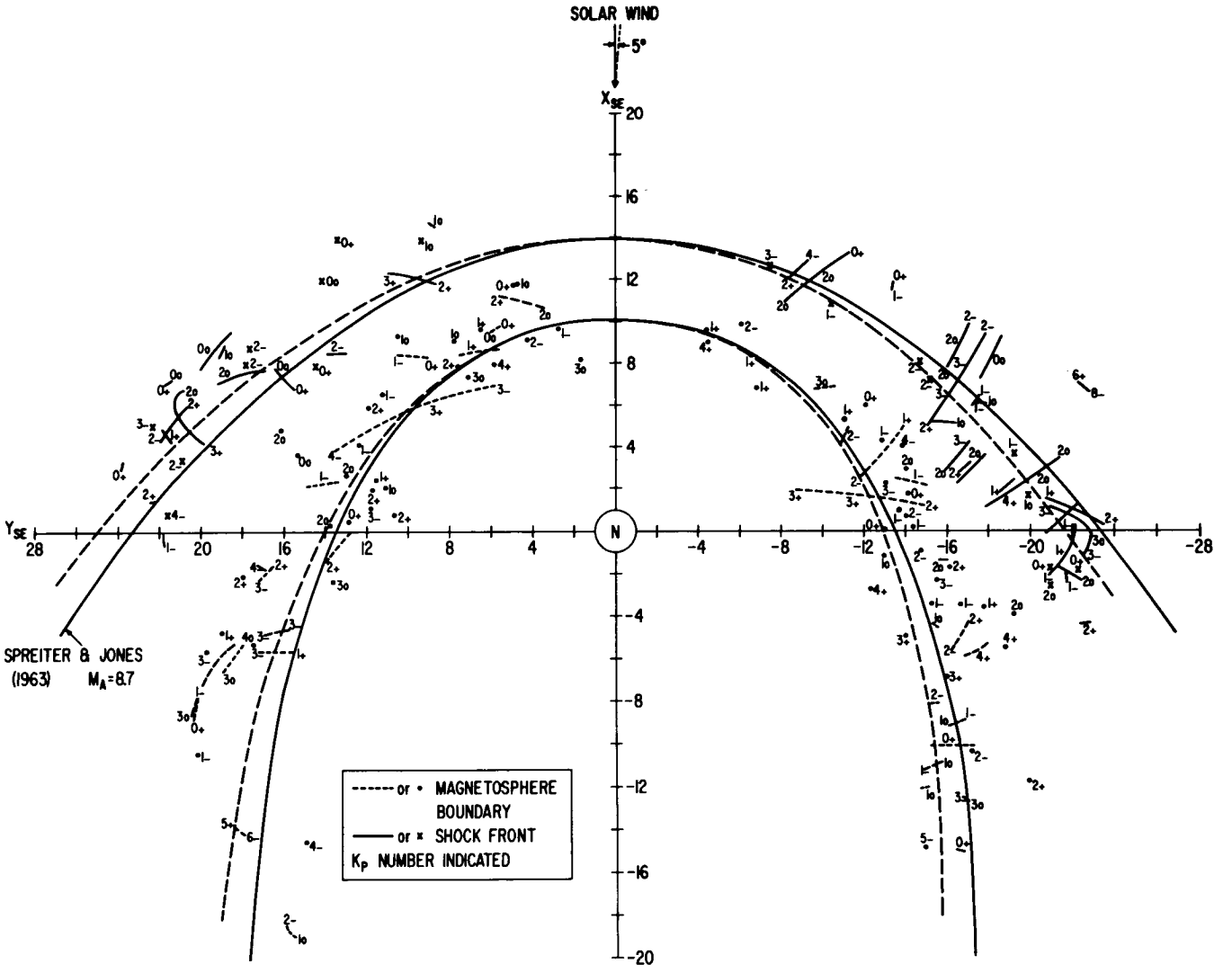
SOLAR WIND
5°
X_{SE}
Y_{SE}
N
SPREITER & JONES
(1963) M_A=8.7
or • MAGNETOSPHERE BOUNDARY
or × SHOCK FRONT
K_P NUMBER INDICATED

Figure 10

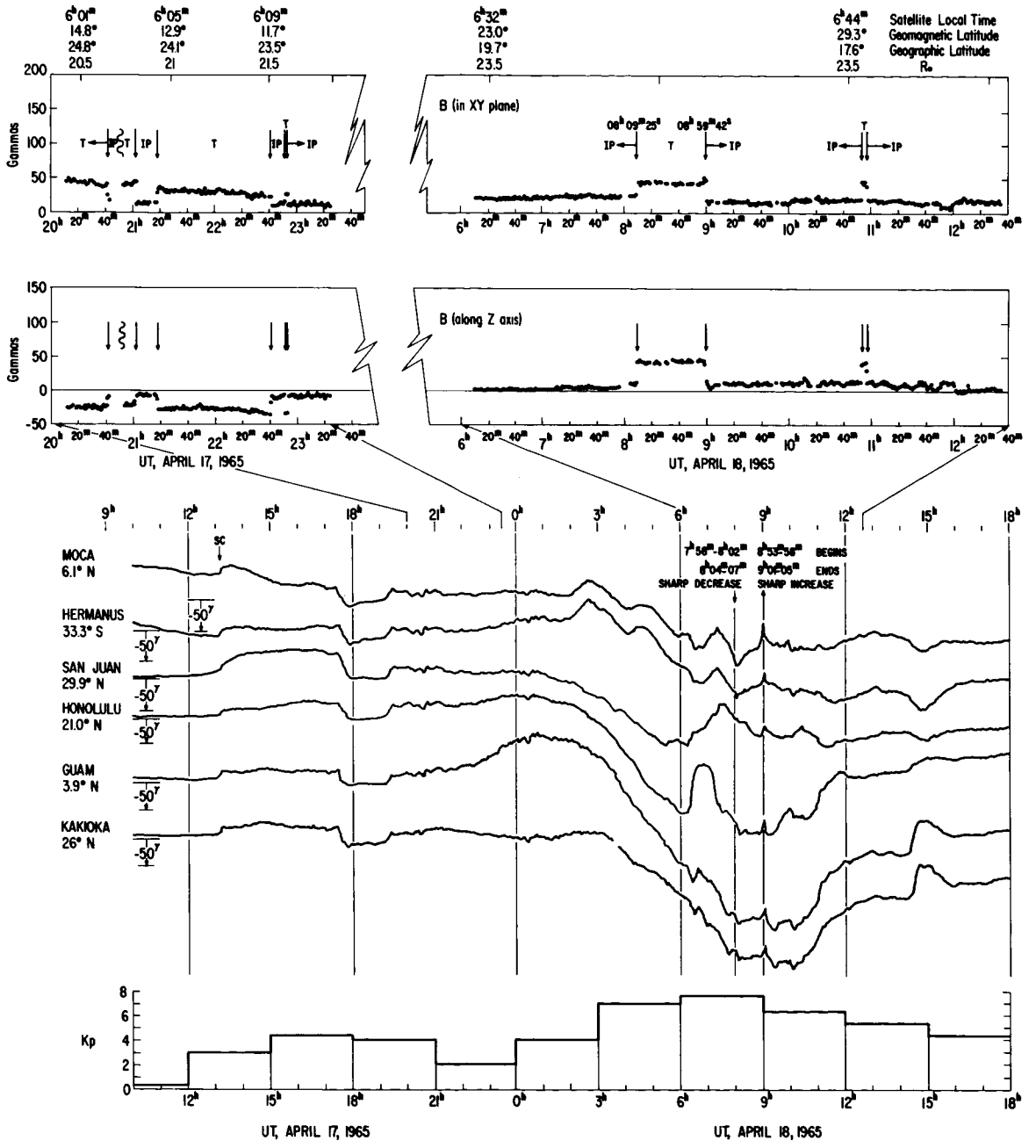
Satellite Local Time
Geomagnetic Latitude
Geographic Latitude
R
B (in XY plane)
B (along Z axis)
Gammas
UT, APRIL 17, 1965
UT, APRIL 18, 1965
SC
SHARP DECREASE
SHARP INCREASE
BEGINS
ENDS
MOCA
6.1° N
HERMANUS
33.3° S
SAN JUAN
29.9° N
HONOLULU
21.0° N
GUAM
3.9° N
KAKIOKA
26° N
Kp

Figure 11

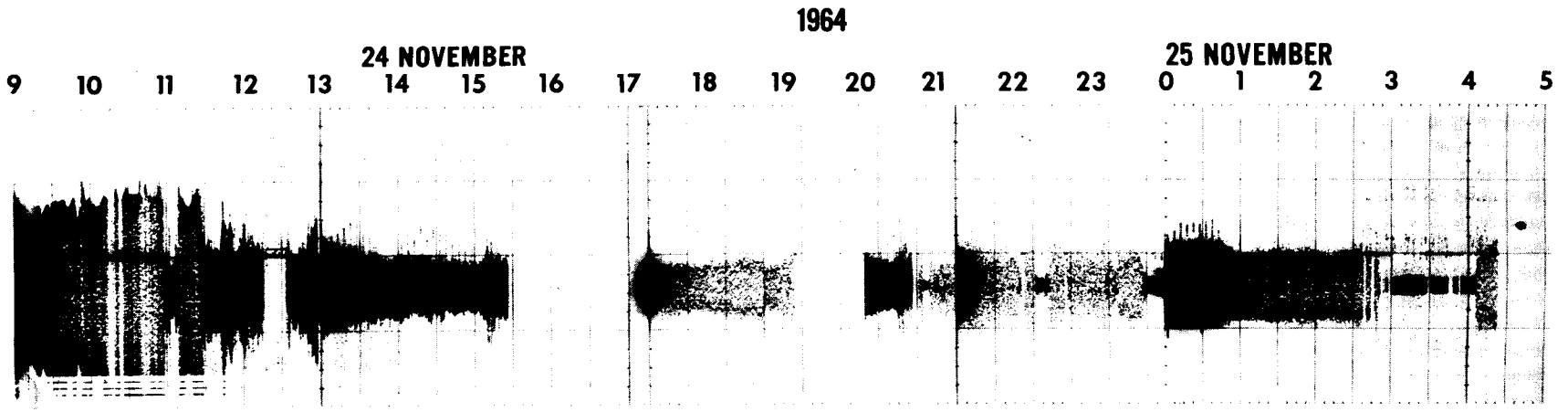
1964
24 NOVEMBER
25 NOVEMBER
9 10 11 12 13 14 15 16 17 18 19 20 21 22 23 0 1 2 3 4 5
M : MAGNETOSPHERE
T : TRANSITION REGION
I : INTERPLANETARY SPACE

Figure 12

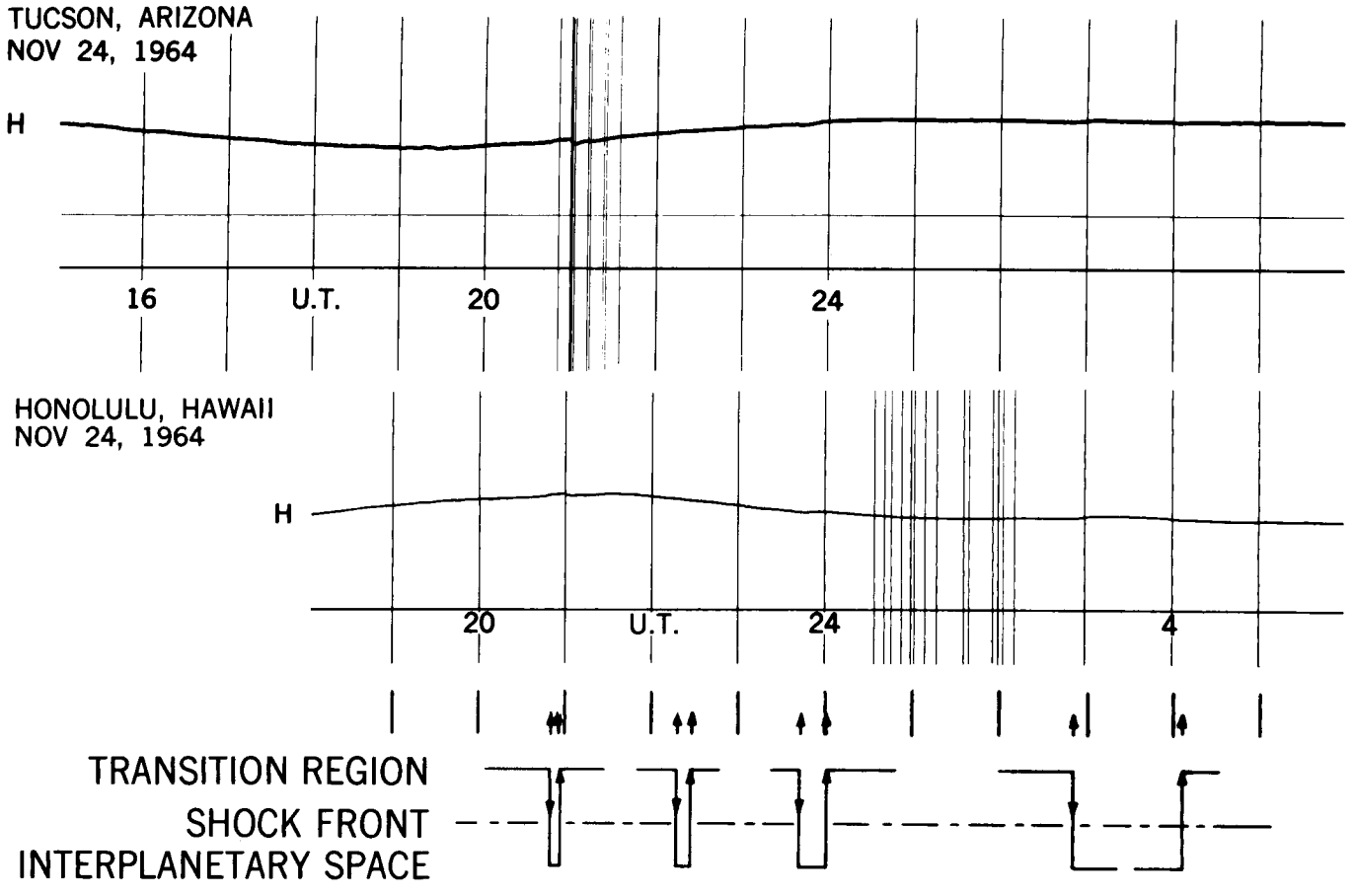
TUCSON, ARIZONA
NOV 24, 1964
H
16
U.T.
20
24
HONOLULU, HAWAII
NOV 24, 1964
H
20
U.T.
24
4
TRANSITION REGION
SHOCK FRONT
INTERPLANETARY SPACE

Figure 13

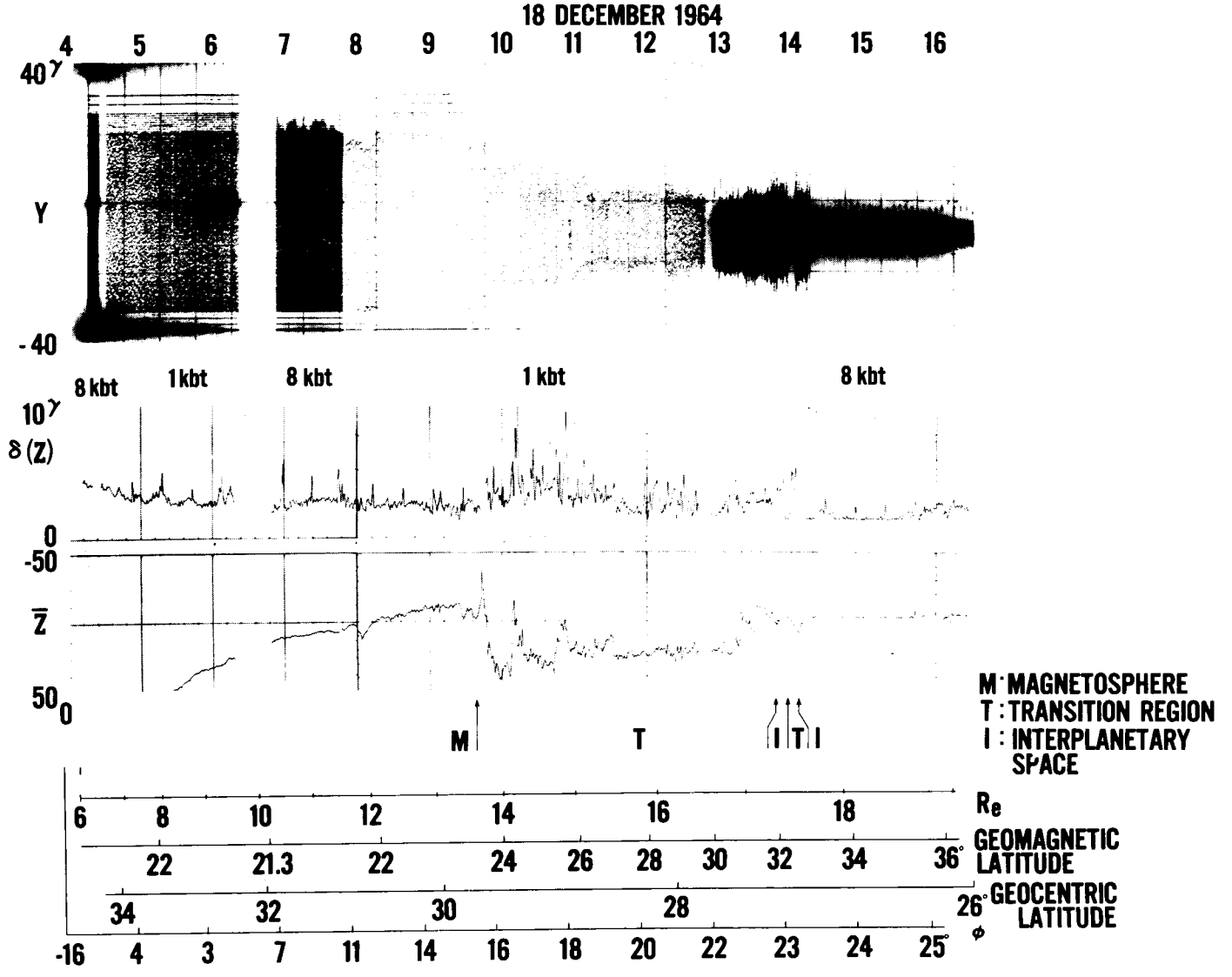
18 DECEMBER 1964
4 5 6 7 8 9 10 11 12 13 14 15 16
40γ
Y
-40
8 kbt 1 kbt 8 kbt 1 kbt 8 kbt
10γ
δ(Z)
0
-50
Z
50 0
M
T
I T I
M: MAGNETOSPHERE
T: TRANSITION REGION
I: INTERPLANETARY SPACE
6 8 10 12 14 16 18 Re
22 21.3 22 24 26 28 30 32 34 36° GEOMAGNETIC LATITUDE
34 32 30 28 26° GEOCENTRIC LATITUDE
-16 4 3 7 11 14 16 18 20 22 23 24 25
φ

Figure 14

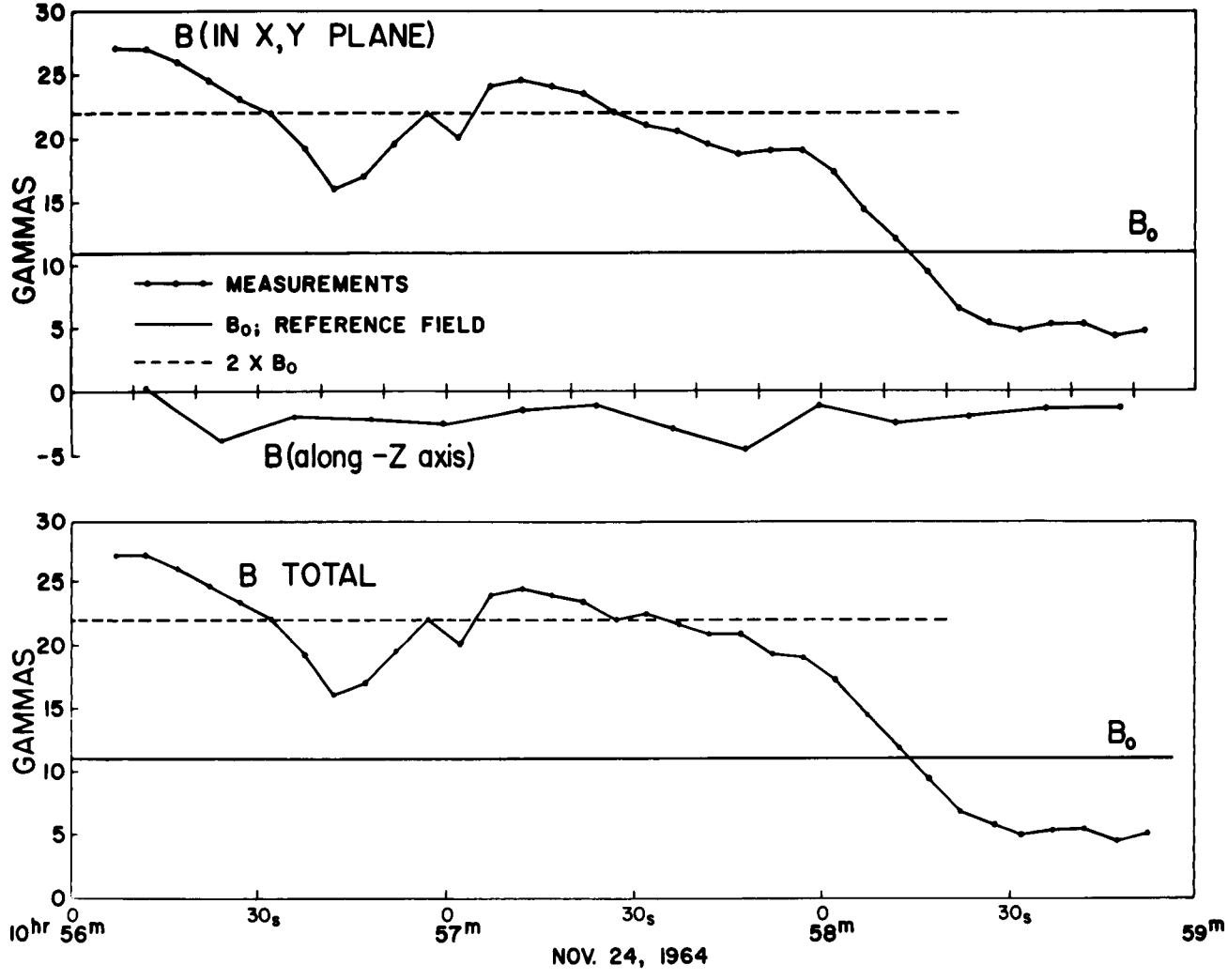
B(IN X,Y PLANE)
GAMMAS
30
25
20
15
10
5
0
-5
B_o
MEASUREMENTS
B_o; REFERENCE FIELD
2 X B_o
B(along -Z axis)
B TOTAL
GAMMAS
30
25
20
15
10
5
0
B_o
10^{hr} 0 56^m
30_s
0 57^m
30_s
0 58^m
30_s
59^m
NOV. 24, 1964

Figure 15

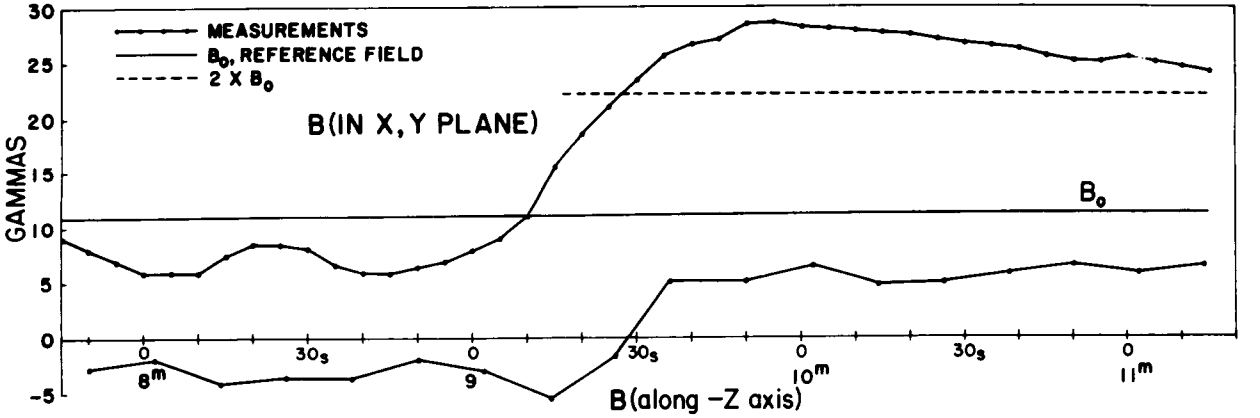
MEASUREMENTS
B_o, REFERENCE FIELD
2 X B_o
B(IN X, Y PLANE)
GAMMAS
30
25
20
15
10
5
0
-5
B_o
0
30s
0
30s
0
30s
0
8m
9
10m
11m
B(along −Z axis)

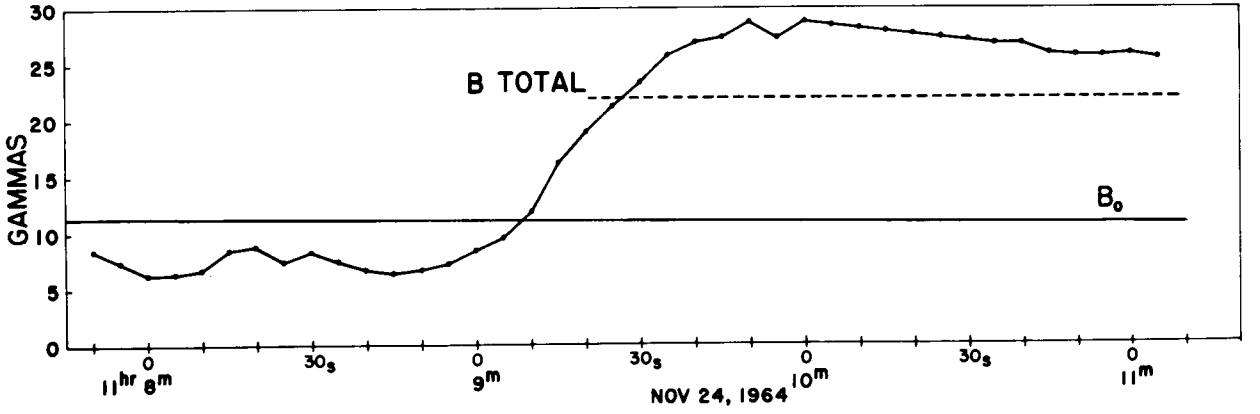
B TOTAL
GAMMAS
30
25
20
15
10
5
0
B_o
0
30s
0
30s
0
30s
0
11hr 8m
9m
10m
11m
NOV 24, 1964

Figure 16

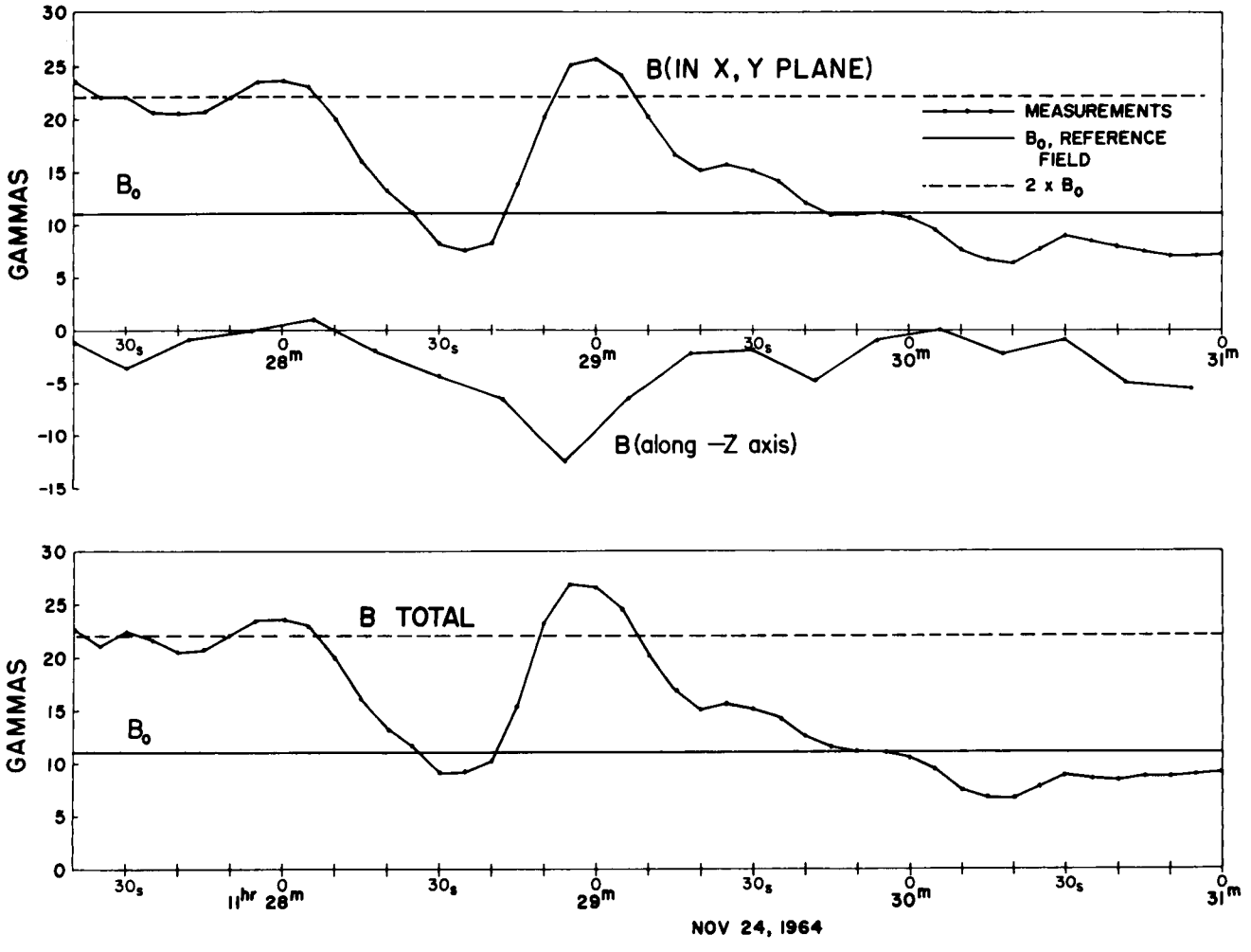
B(IN X, Y PLANE)
MEASUREMENTS
B_0, REFERENCE FIELD
2 x B_0
GAMMAS
B_0
B(along −Z axis)
B TOTAL
B_0
GAMMAS
30
25
20
15
10
5
0
-5
-10
-15
30s
0
28m
30s
0
29m
30s
0
30m
0
31m
11hr 28m
NOV 24, 1964

Figure 17

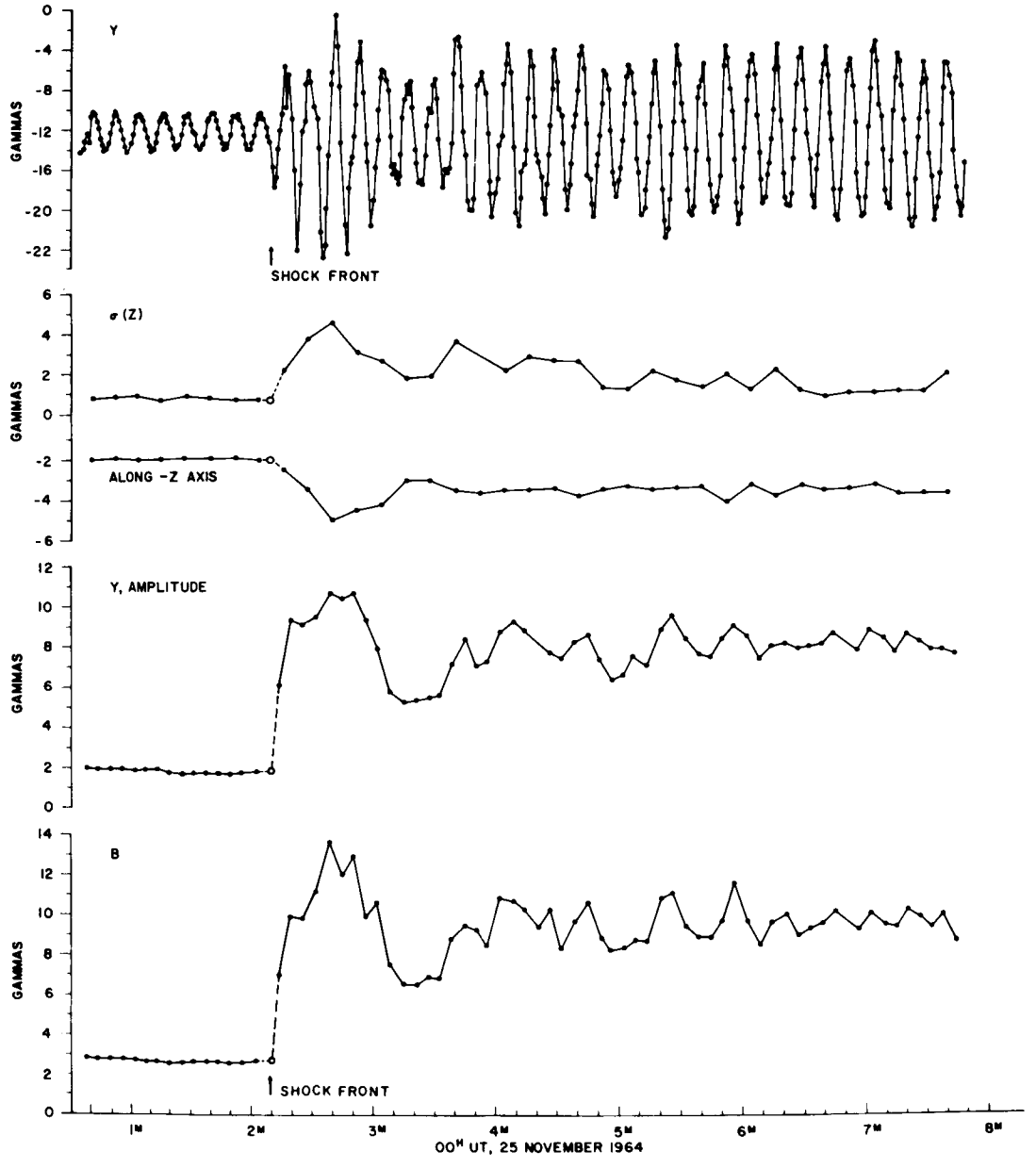
Y
GAMMAS
SHOCK FRONT
σ (Z)
ALONG -Z AXIS
Y, AMPLITUDE
B
SHOCK FRONT
00M UT, 25 NOVEMBER 1964

Figure 18

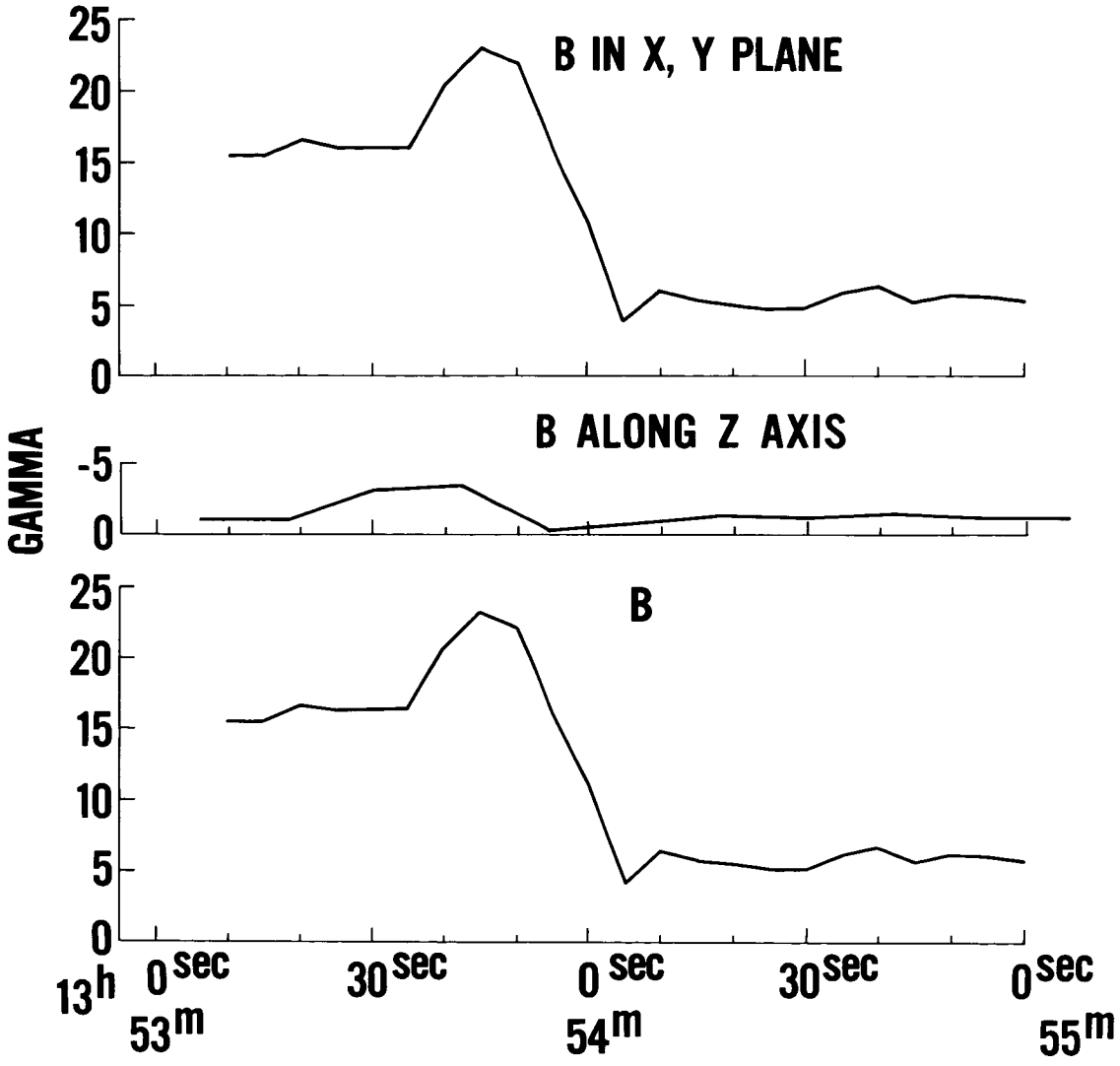
B IN X, Y PLANE
B ALONG Z AXIS
B
GAMMA
25
20
15
10
5
0
-5
0
13h 0sec 30sec 0sec 30sec 0sec
53m 54m 55m

Figure 19

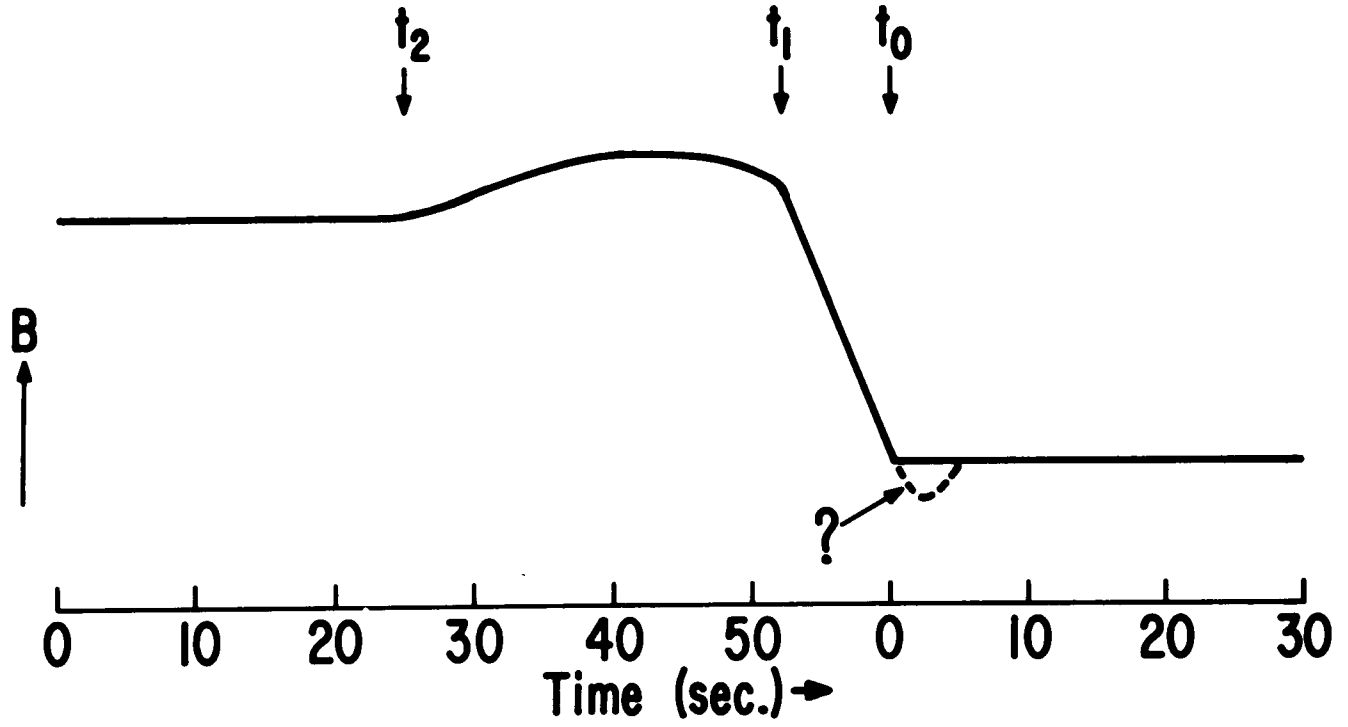

Figure 20

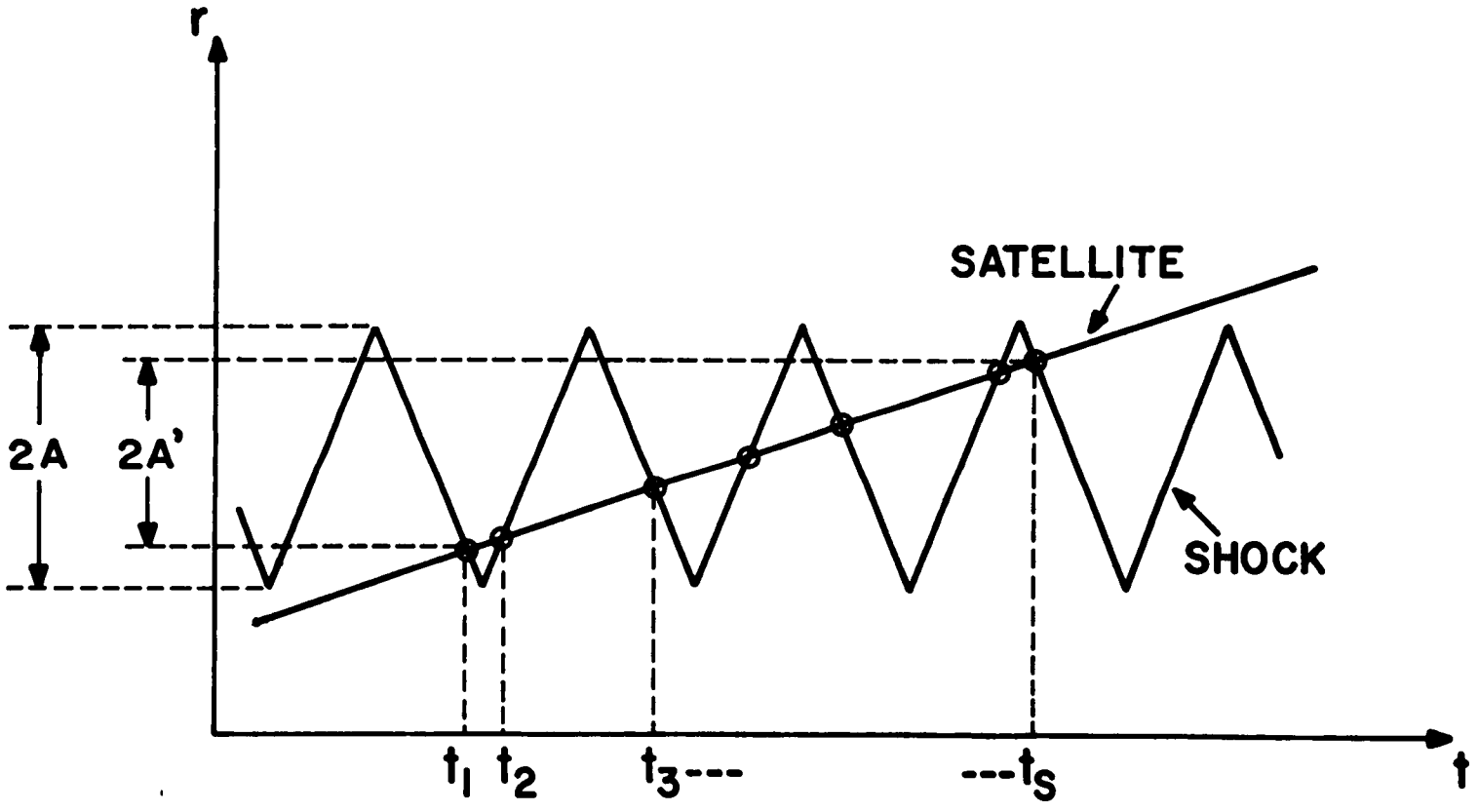

Figure 21

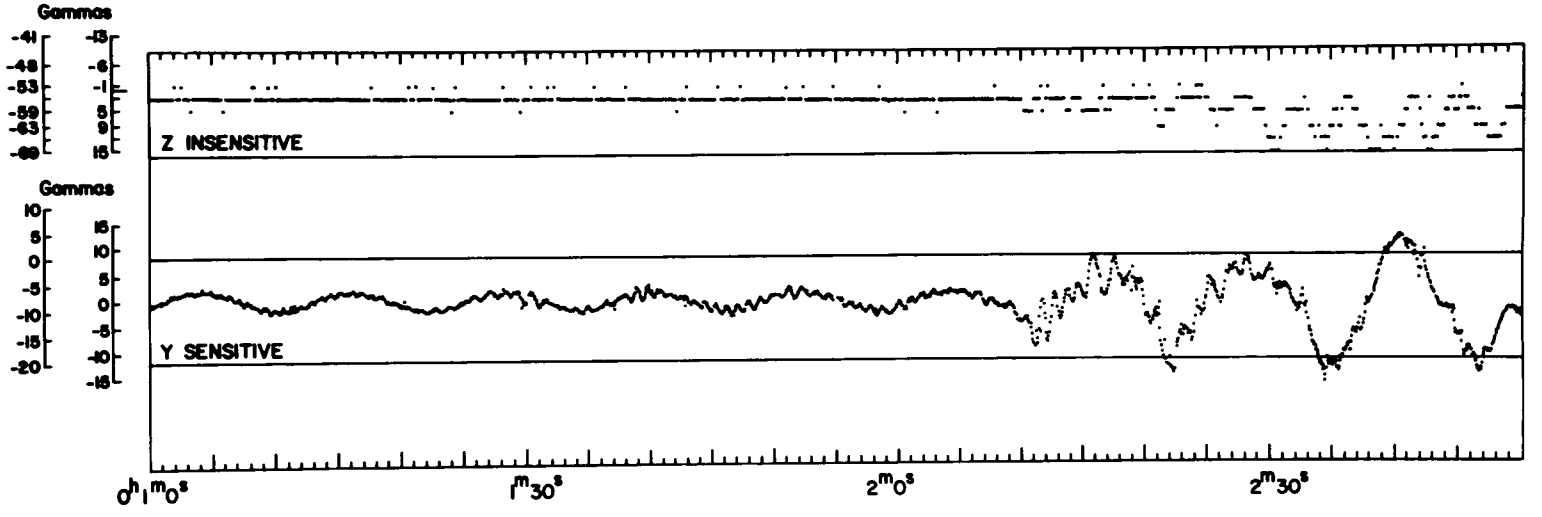
Gammas
-41
-48
-53
-59
-63
-69
-13
-6
-1
5
9
15
Z INSENSITIVE
Gammas
10
5
0
-5
-10
-15
-20
15
10
5
0
-5
-10
-15
Y SENSITIVE
0h1m0s
1m30s
2m0s
2m30s

Figure 22

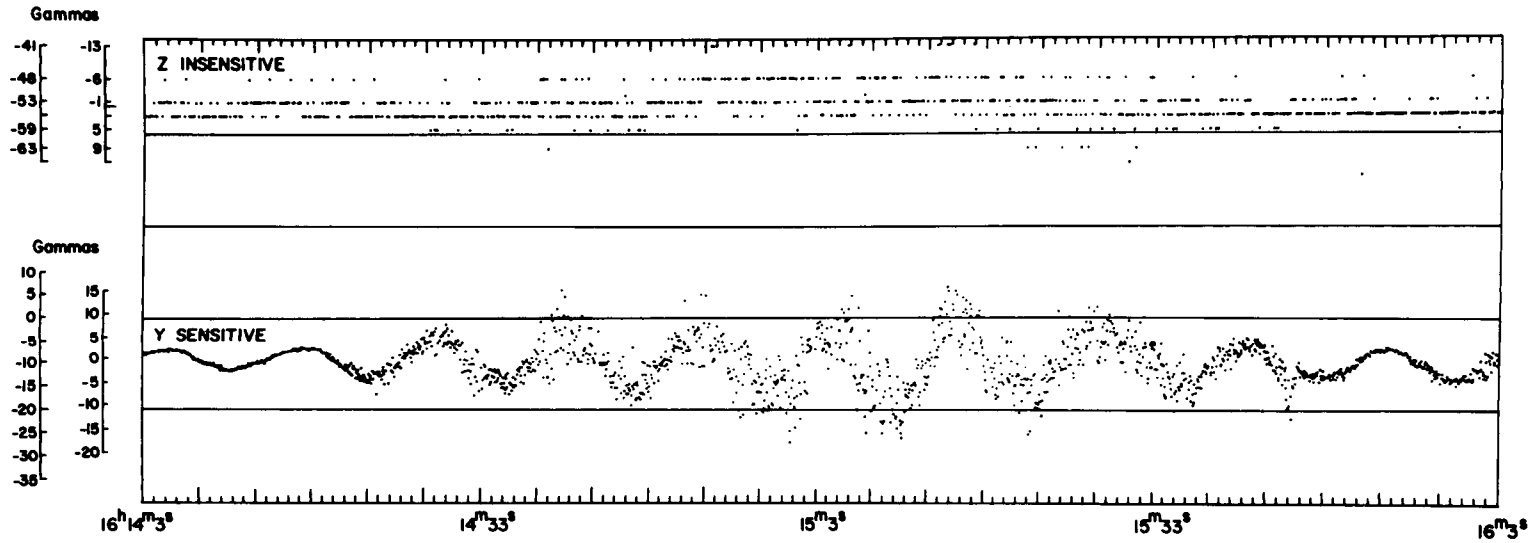
Gammas
-41
-48
-53
-59
-63
-13
-6
-1
5
9
Z INSENSITIVE
Gammas
10
5
0
-5
-10
-15
-20
-25
-30
-35
15
10
5
0
-5
-10
-15
-20
Y SENSITIVE
16h14m3s
14m33s
15m3s
15m33s
16m3s

Figure 23

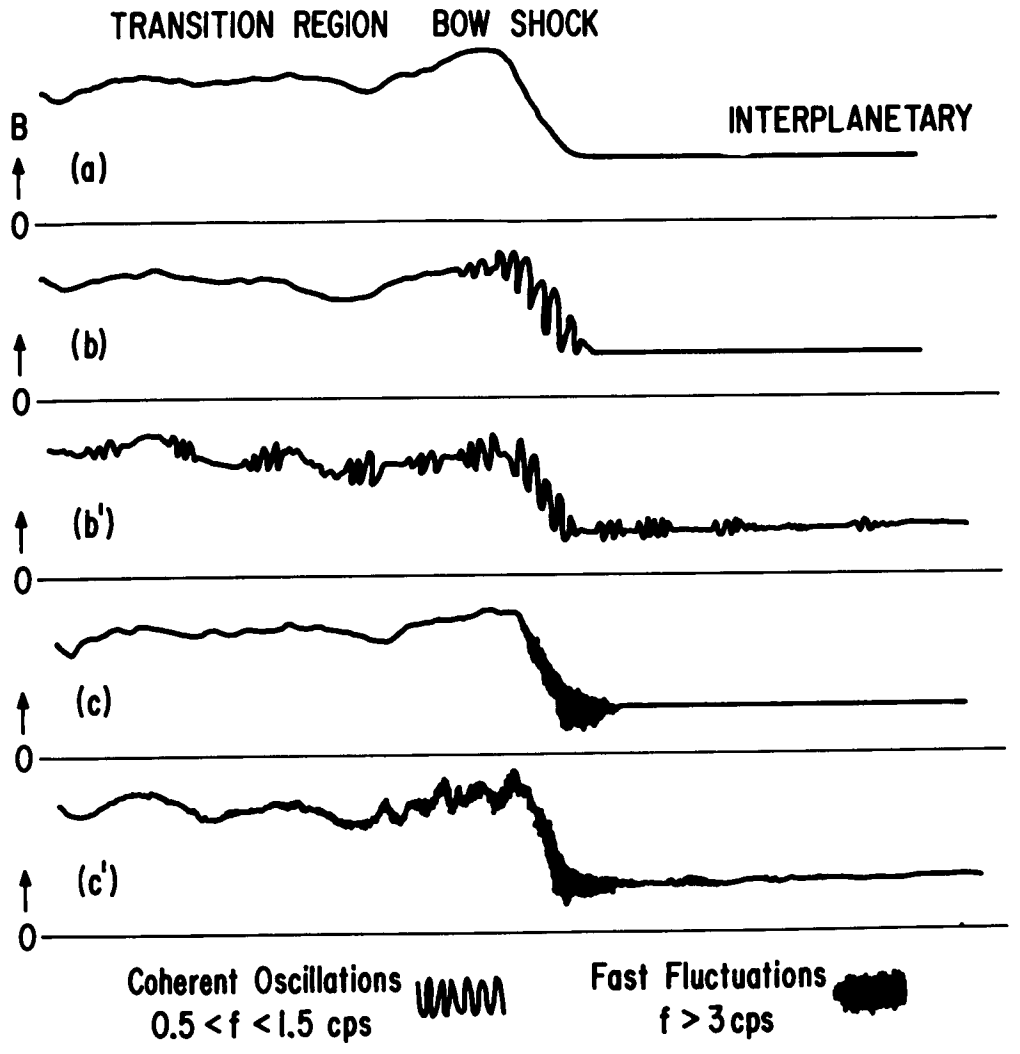
TRANSITION REGION
BOW SHOCK
INTERPLANETARY
B
(a)
0
(b)
0
(b')
0
(c)
0
(c')
0
Coherent Oscillations
0.5 < f < 1.5 cps
Fast Fluctuations
f > 3 cps

Figure 24

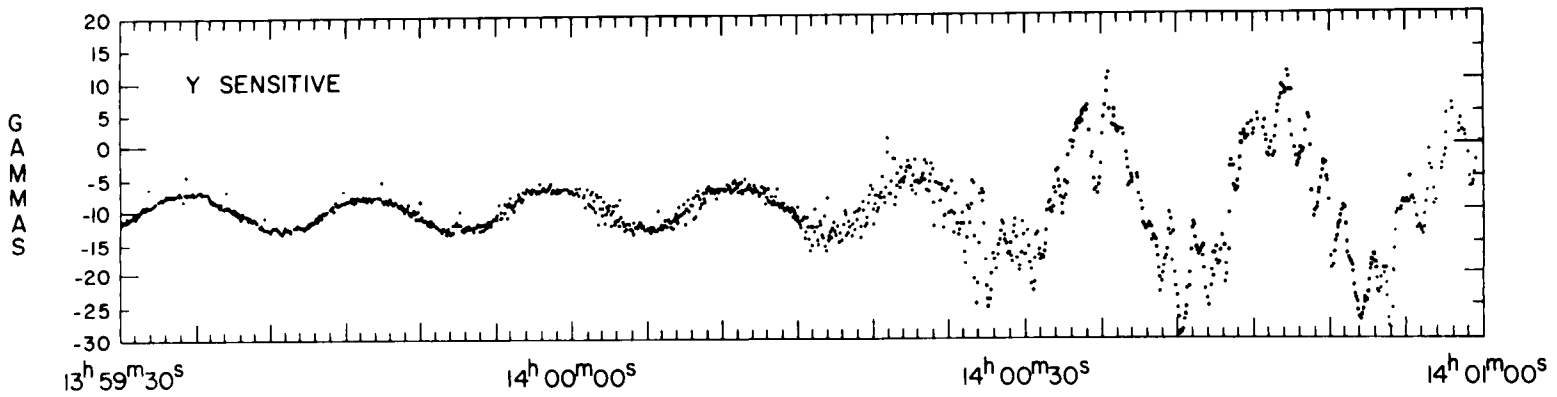
Y SENSITIVE
GAMMAS
20
15
10
5
0
-5
-10
-15
-20
-25
-30
13h 59m 30s
14h 00m 00s
14h 00m 30s
14h 01m 00s

Figure 25

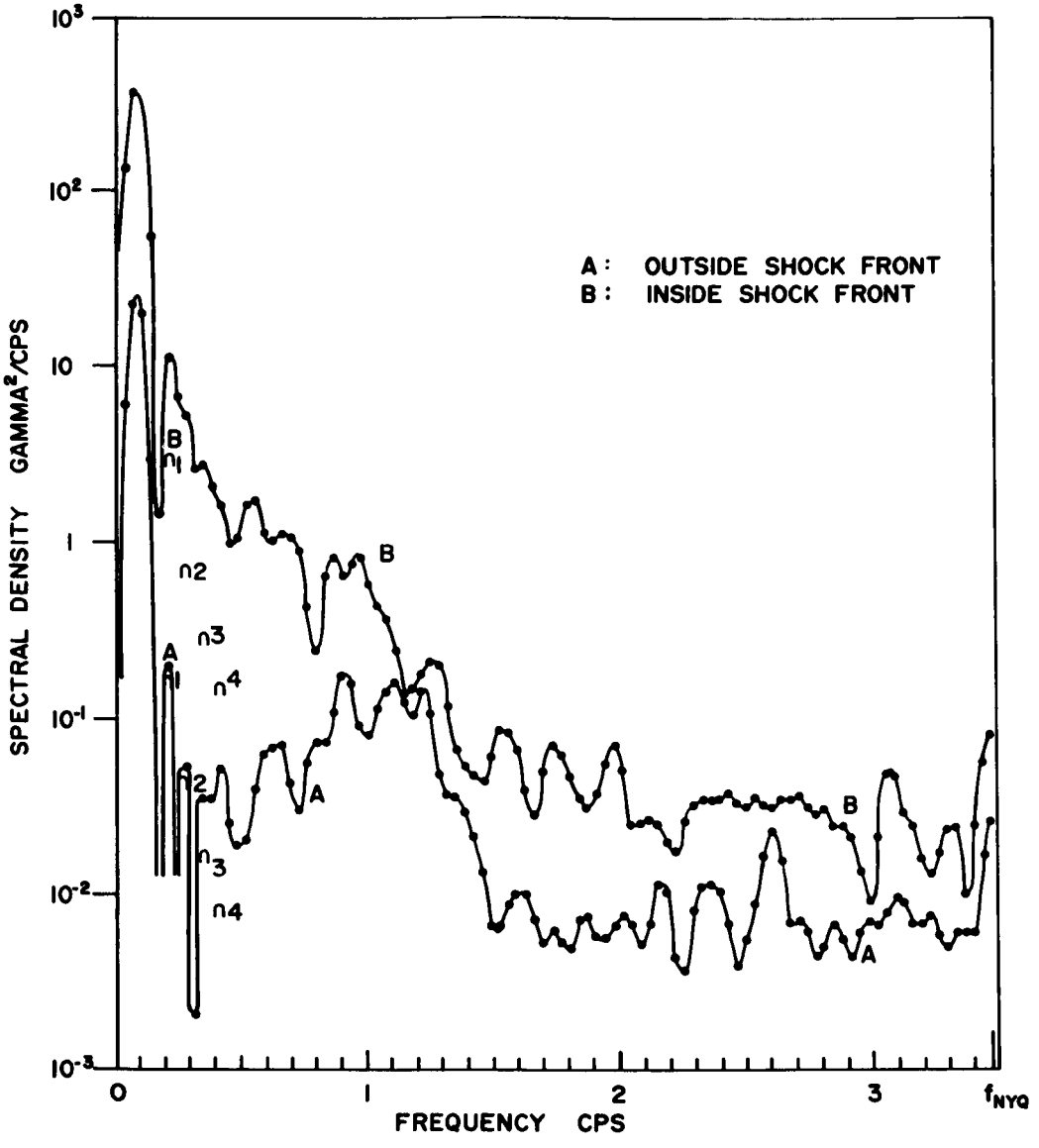
A : OUTSIDE SHOCK FRONT
B : INSIDE SHOCK FRONT
SPECTRAL DENSITY GAMMA²/CPS
FREQUENCY CPS
10^3
10^2
10
1
10^{-1}
10^{-2}
10^{-3}
0
1
2
3
f_{NYQ}
B
n1
n2
n3
n4
A
n1
n2
n3
n4
B
A

Figure 26

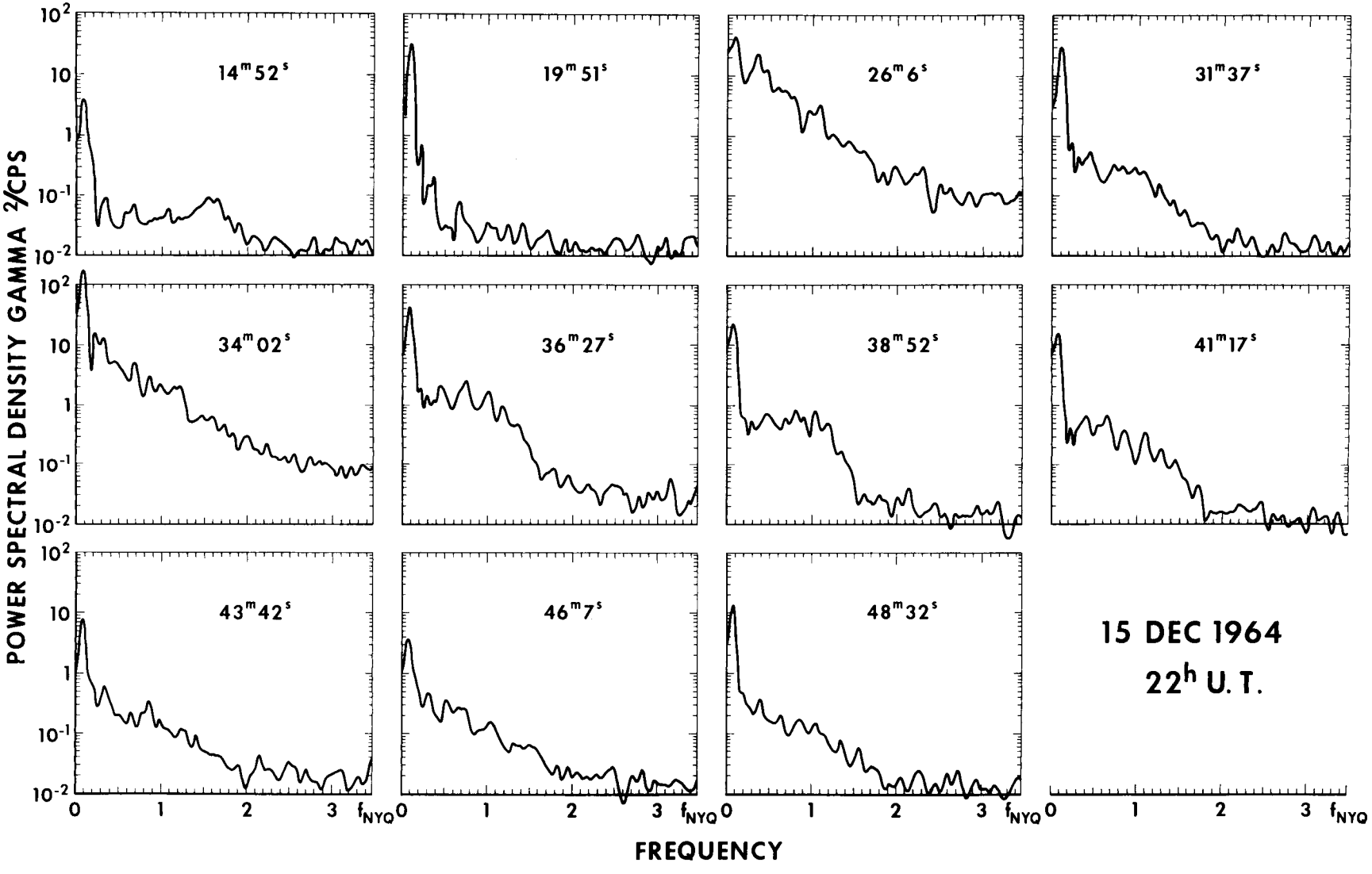
POWER SPECTRAL DENSITY GAMMA 2/CPS
10^2
10
1
10^{-1}
10^{-2}
14^m52^s
19^m51^s
26^m6^s
31^m37^s
34^m02^s
36^m27^s
38^m52^s
41^m17^s
43^m42^s
46^m7^s
48^m32^s
15 DEC 1964
22^h U.T.
0
1
2
3
f_{NYQ}
FREQUENCY

Figure 27

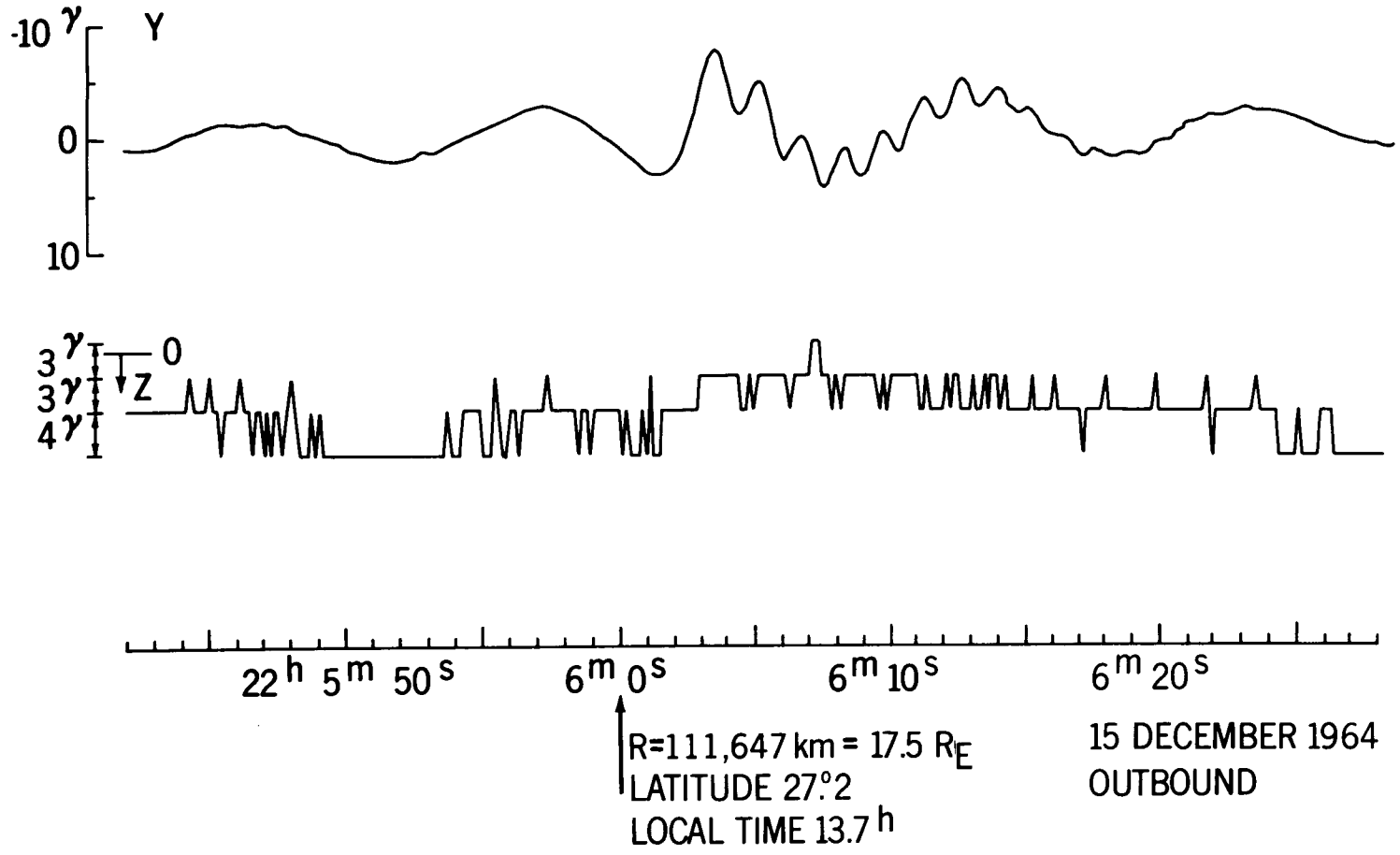
-10 γ
Y
0
10
3 γ
3 γ
4 γ
0
Z
22h 5m 50s
6m 0s
6m 10s
6m 20s
R=111,647 km = 17.5 RE
LATITUDE 27°.2
LOCAL TIME 13.7 h
15 DECEMBER 1964
OUTBOUND

Figure 28

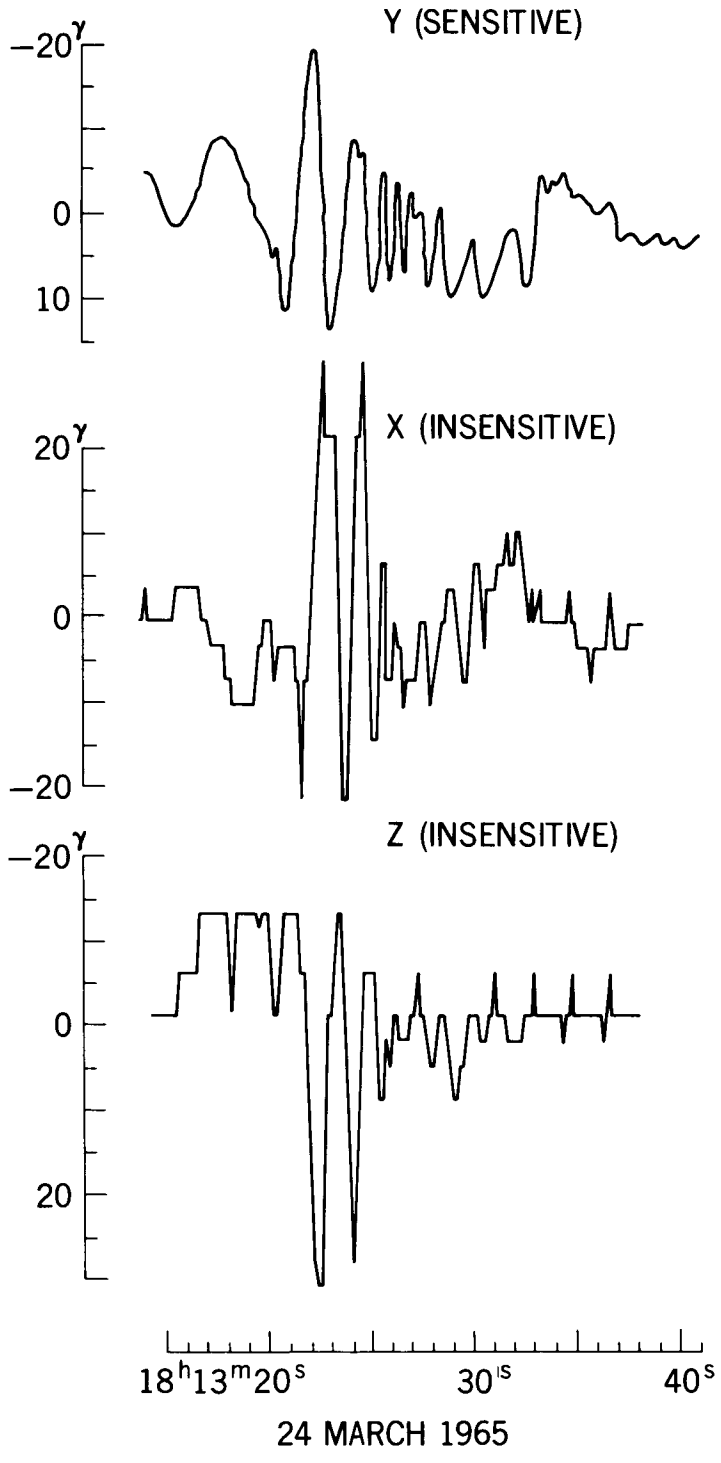
Y (SENSITIVE)
−20γ
0
10
X (INSENSITIVE)
20γ
0
−20
Z (INSENSITIVE)
−20γ
0
20
18h13m20s
30s
40s
24 MARCH 1965

Figure 29

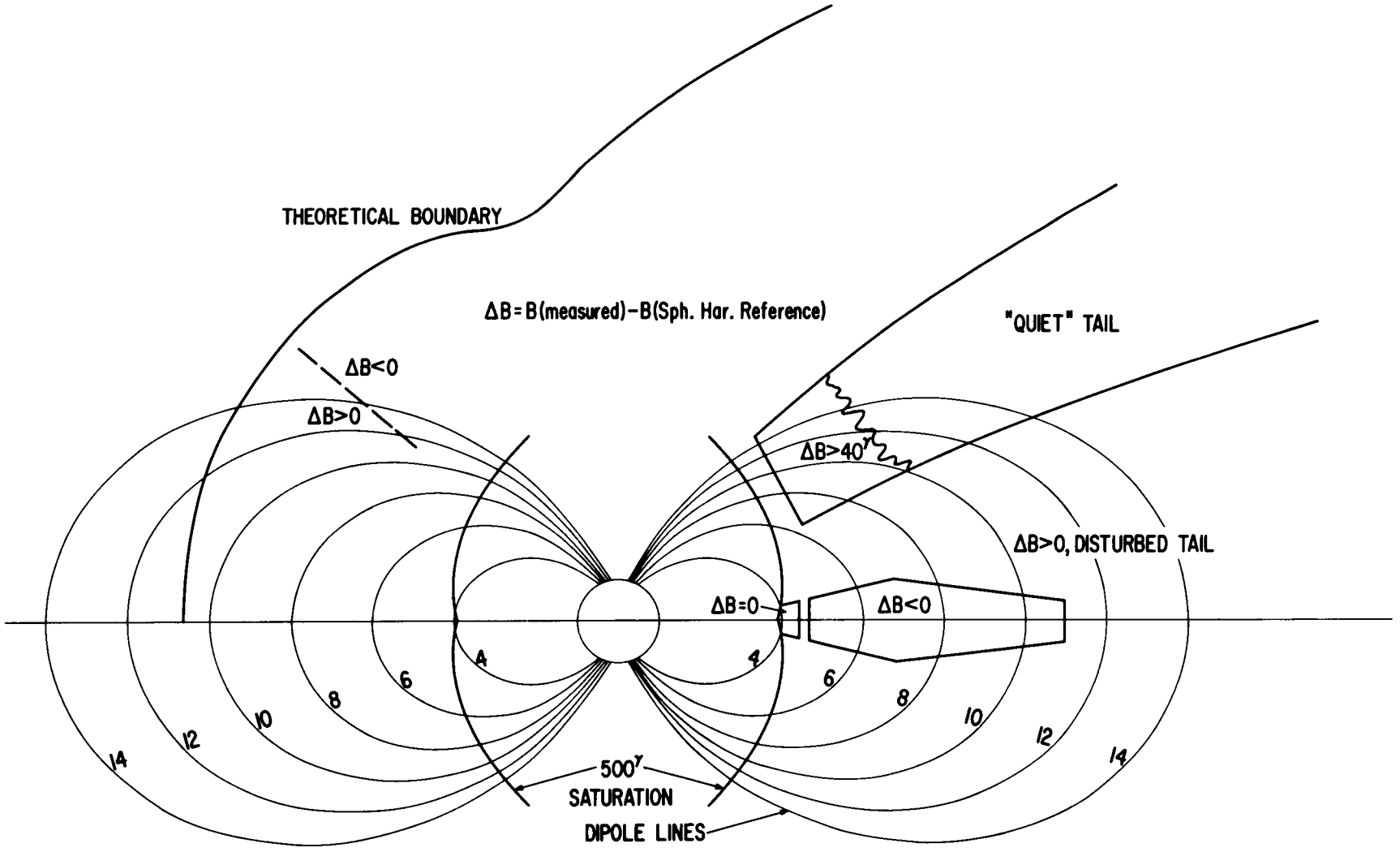
THEORETICAL BOUNDARY
ΔB = B(measured) − B(Sph. Har. Reference)
"QUIET" TAIL
ΔB<0
ΔB>0
ΔB>40γ
ΔB>0, DISTURBED TAIL
ΔB=0
ΔB<0
4
6
8
10
12
14
500γ
SATURATION
DIPOLE LINES

Figure 30

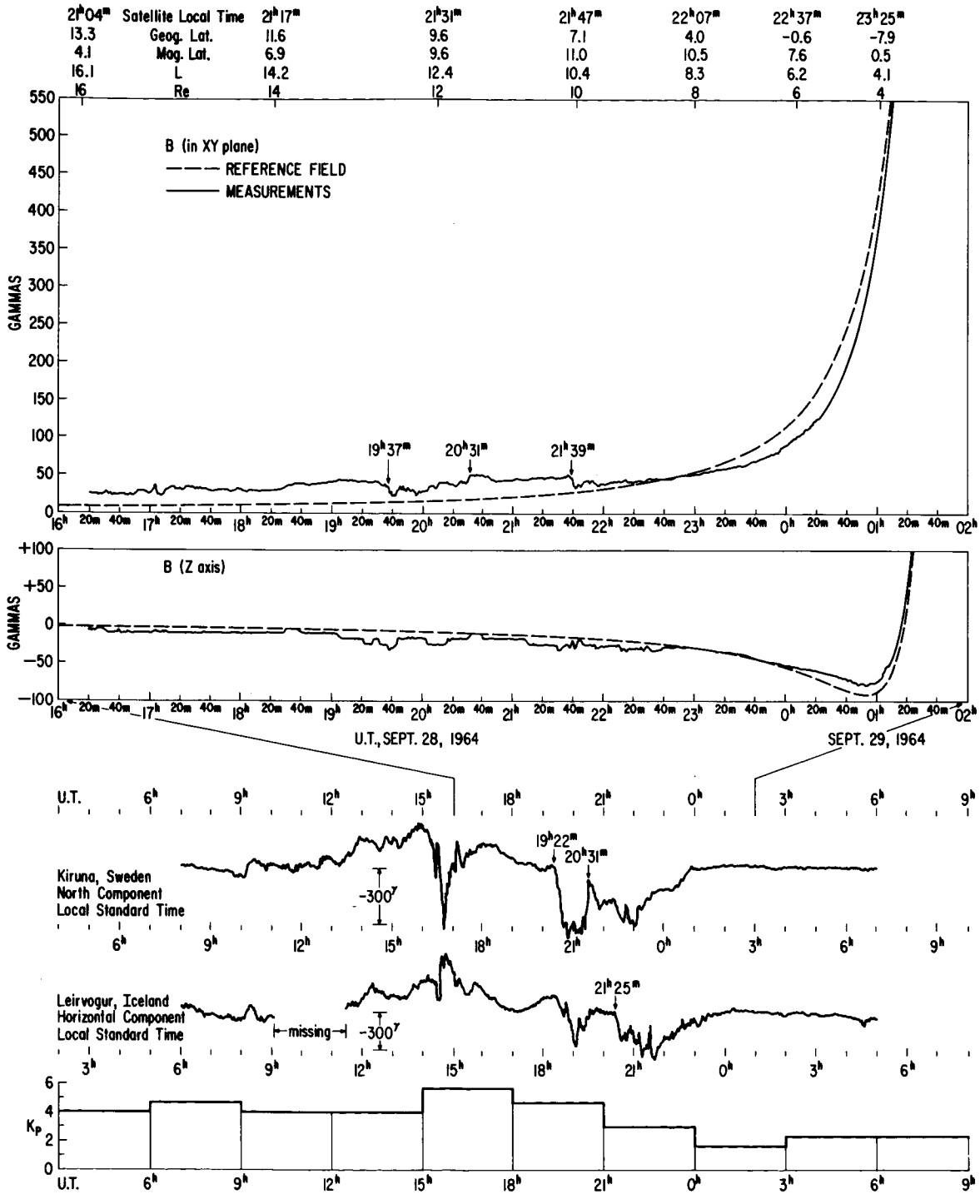
21h04m Satellite Local Time 21h17m 21h31m 21h47m 22h07m 22h37m 23h25m
13.3 Geog. Lat. 11.6 9.6 7.1 4.0 -0.6 -7.9
4.1 Mag. Lat. 6.9 9.6 11.0 10.5 7.6 0.5
16.1 L 14.2 12.4 10.4 8.3 6.2 4.1
16 Re 14 12 10 8 6 4
B (in XY plane)
REFERENCE FIELD
MEASUREMENTS
GAMMAS
19h37m
20h31m
21h39m
B (Z axis)
U.T., SEPT. 28, 1964
SEPT. 29, 1964
U.T.
Kiruna, Sweden
North Component
Local Standard Time
-300γ
19h22m
20h31m
Leirvogur, Iceland
Horizontal Component
Local Standard Time
missing
-300γ
21h25m
Kp
U.T.

Figure 31

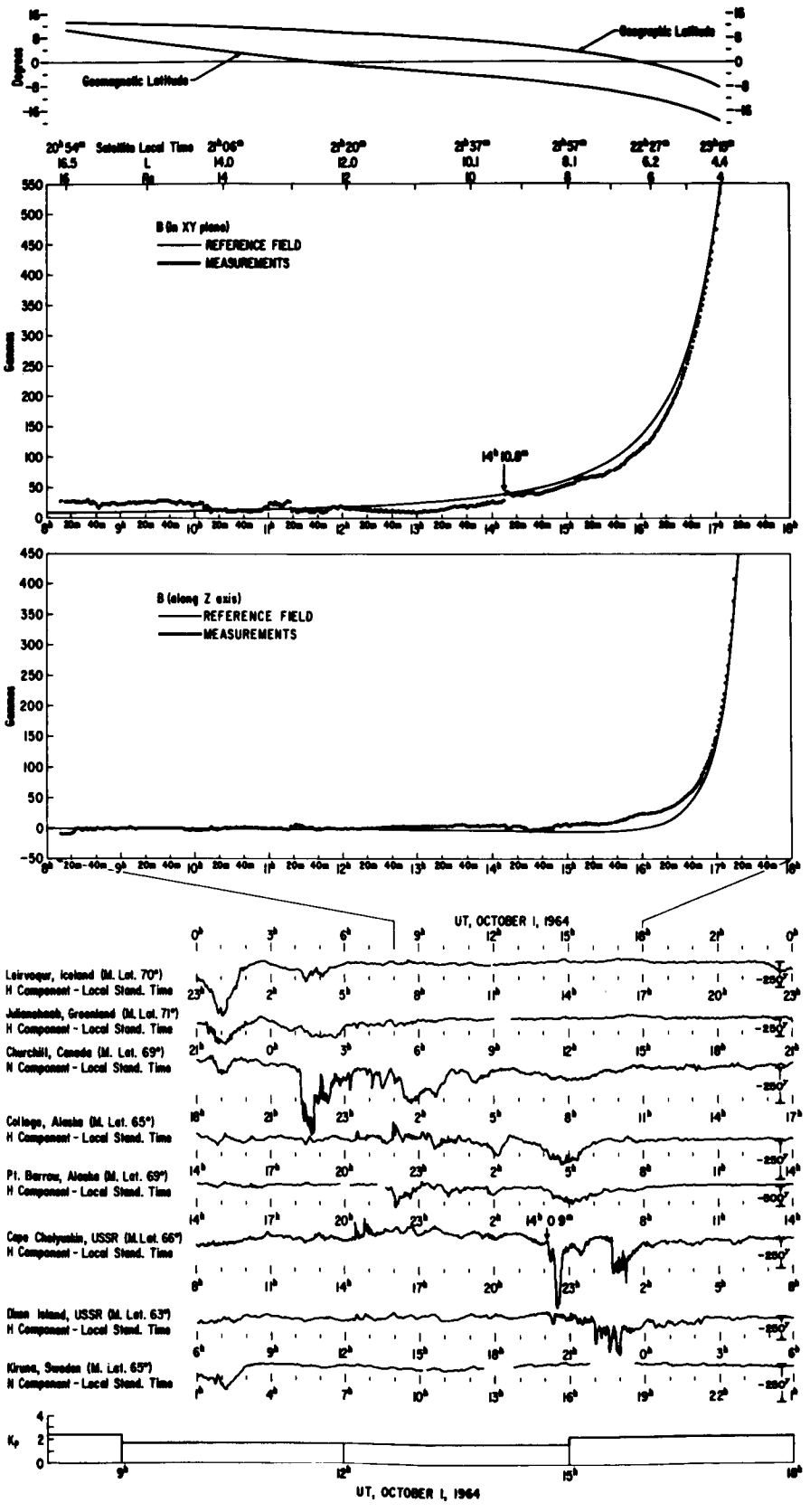
Geographic Latitude
Geomagnetic Latitude
Degrees
Satellite Local Time
B (in XY plane)
REFERENCE FIELD
MEASUREMENTS
Gammas
B (along Z axis)
REFERENCE FIELD
MEASUREMENTS
Gammas
UT, OCTOBER 1, 1964
Leirvogur, Iceland (M. Lat. 70°)
H Component - Local Stand. Time
Julianehaab, Greenland (M. Lat. 71°)
H Component - Local Stand. Time
Churchill, Canada (M. Lat. 69°)
N Component - Local Stand. Time
College, Alaska (M. Lat. 65°)
H Component - Local Stand. Time
Pt. Barrow, Alaska (M. Lat. 69°)
H Component - Local Stand. Time
Cape Chelyuskin, USSR (M. Lat. 66°)
H Component - Local Stand. Time
Dixon Island, USSR (M. Lat. 63°)
H Component - Local Stand. Time
Kiruna, Sweden (M. Lat. 65°)
N Component - Local Stand. Time
Kp
UT, OCTOBER 1, 1964

Figure 32

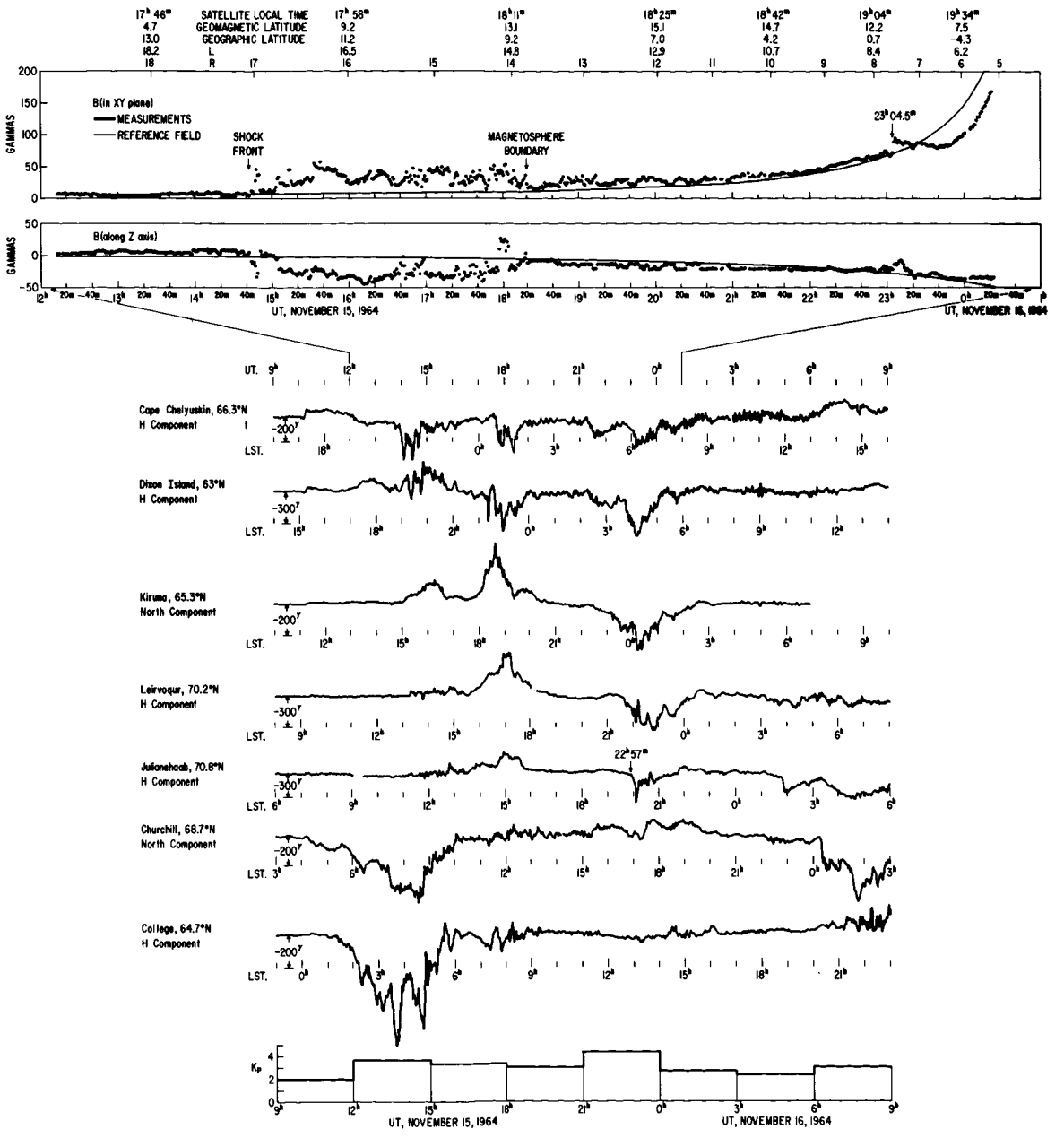
SATELLITE LOCAL TIME
GEOMAGNETIC LATITUDE
GEOGRAPHIC LATITUDE
L
B(in XY plane)
MEASUREMENTS
REFERENCE FIELD
SHOCK FRONT
MAGNETOSPHERE BOUNDARY
GAMMAS
B(along Z axis)
UT, NOVEMBER 15, 1964
UT, NOVEMBER 16, 1964
Cape Chelyuskin, 66.3°N
H Component
Dixon Island, 63°N
H Component
Kiruna, 65.3°N
North Component
Leirvogur, 70.2°N
H Component
Julianehaab, 70.8°N
H Component
Churchill, 68.7°N
North Component
College, 64.7°N
H Component
LST.
UT.
Kp

Figure 33

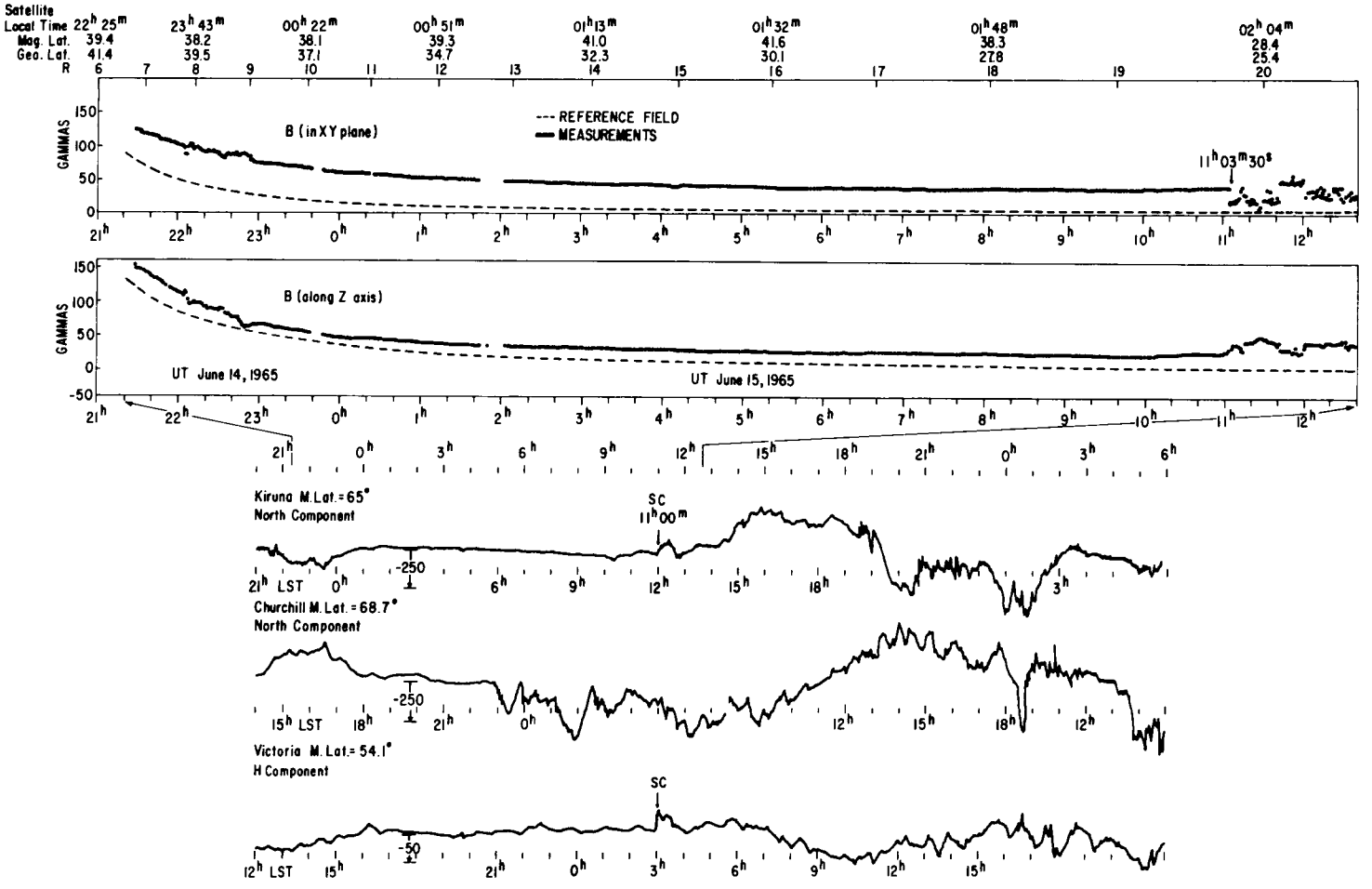
Satellite
Local Time 22h 25m 23h 43m 00h 22m 00h 51m 01h 13m 01h 32m 01h 48m 02h 04m
Mag. Lat. 39.4 38.2 38.1 39.3 41.0 41.6 38.3 28.4
Geo. Lat. 41.4 39.5 37.1 34.7 32.3 30.1 27.8 25.4
R 6 7 8 9 10 11 12 13 14 15 16 17 18 19 20
B (in XY plane)
--- REFERENCE FIELD
— MEASUREMENTS
11h03m30s
GAMMAS
B (along Z axis)
UT June 14, 1965
UT June 15, 1965
Kiruna M.Lat.=65°
North Component
SC
11h00m
-250
21h LST
Churchill M.Lat.=68.7°
North Component
15h LST
Victoria M.Lat.=54.1°
H Component
-50
12h LST

Figure 34

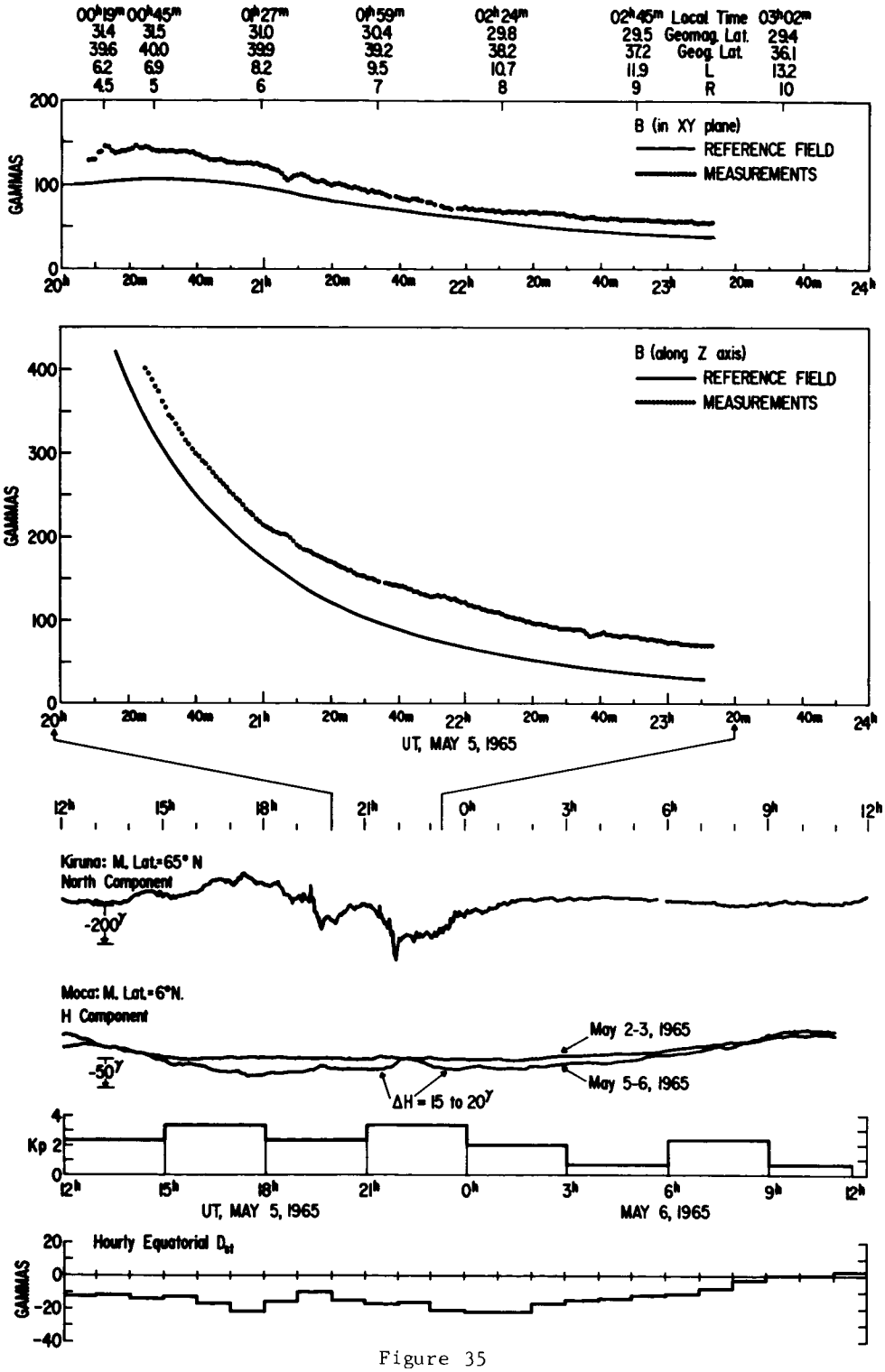
00h19m 00h45m 01h27m 01h59m 02h24m 02h45m Local Time 03h02m
31.4 31.5 31.0 30.4 29.8 29.5 Geomag. Lat. 29.4
39.6 40.0 39.9 39.2 38.2 37.2 Geog. Lat. 36.1
6.2 6.9 8.2 9.5 10.7 11.9 L 13.2
4.5 5 6 7 8 9 R 10
GAMMAS
B (in XY plane)
REFERENCE FIELD
MEASUREMENTS
B (along Z axis)
REFERENCE FIELD
MEASUREMENTS
UT, MAY 5, 1965
Kiruna: M. Lat.=65° N
North Component
-200γ
Moca: M. Lat.=6°N.
H Component
-50γ
May 2-3, 1965
May 5-6, 1965
ΔH = 15 to 20γ
Kp
UT, MAY 5, 1965
MAY 6, 1965
Hourly Equatorial Dst
GAMMAS

Figure 35

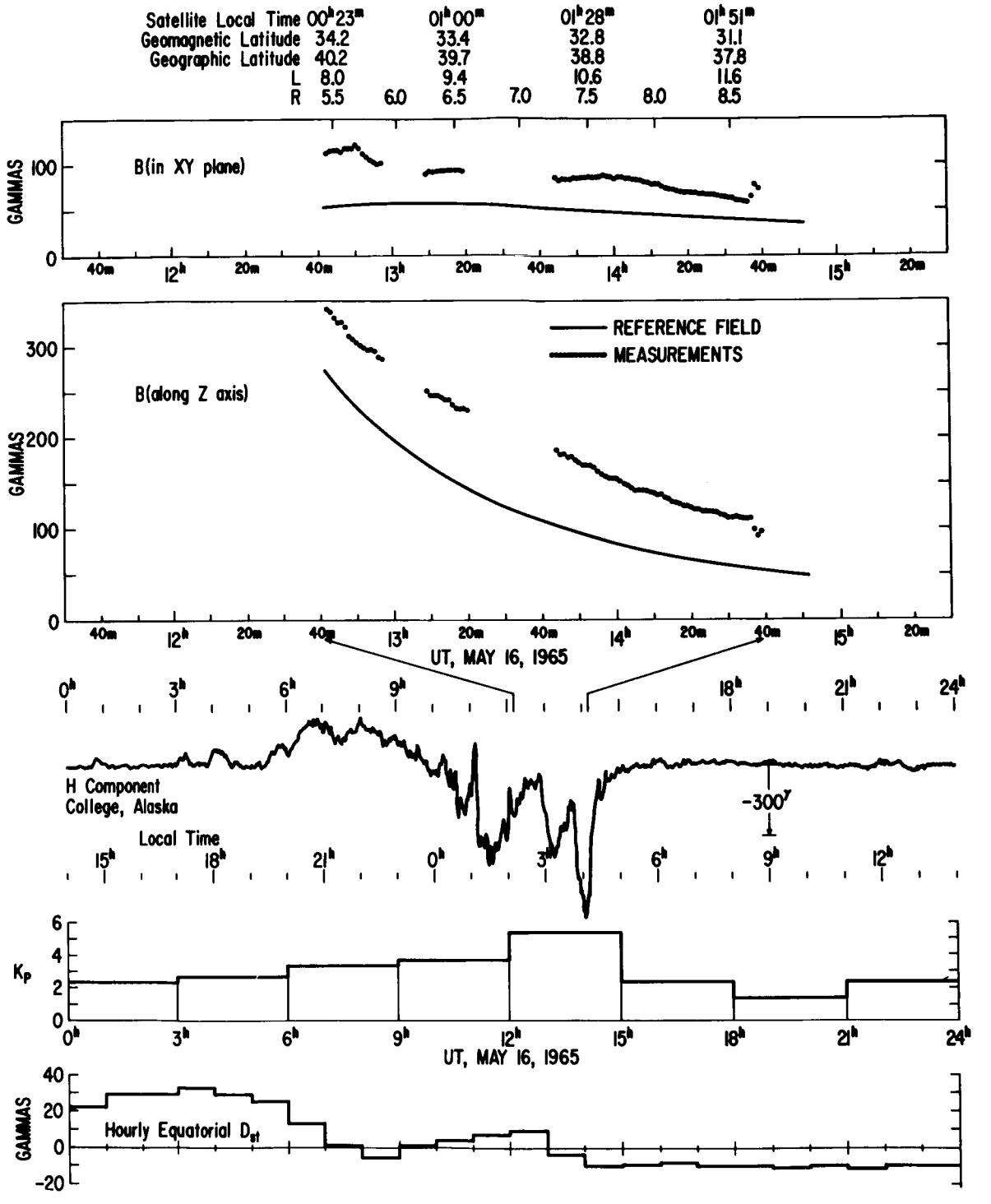
Satellite Local Time 00h23m 01h00m 01h28m 01h51m
Geomagnetic Latitude 34.2 33.4 32.8 31.1
Geographic Latitude 40.2 39.7 38.8 37.8
L 8.0 9.4 10.6 11.6
R 5.5 6.0 6.5 7.0 7.5 8.0 8.5
B(in XY plane)
GAMMAS
B(along Z axis)
REFERENCE FIELD
MEASUREMENTS
UT, MAY 16, 1965
H Component
College, Alaska
Local Time
-300γ
Kp
UT, MAY 16, 1965
Hourly Equatorial Dst
GAMMAS

Figure 36

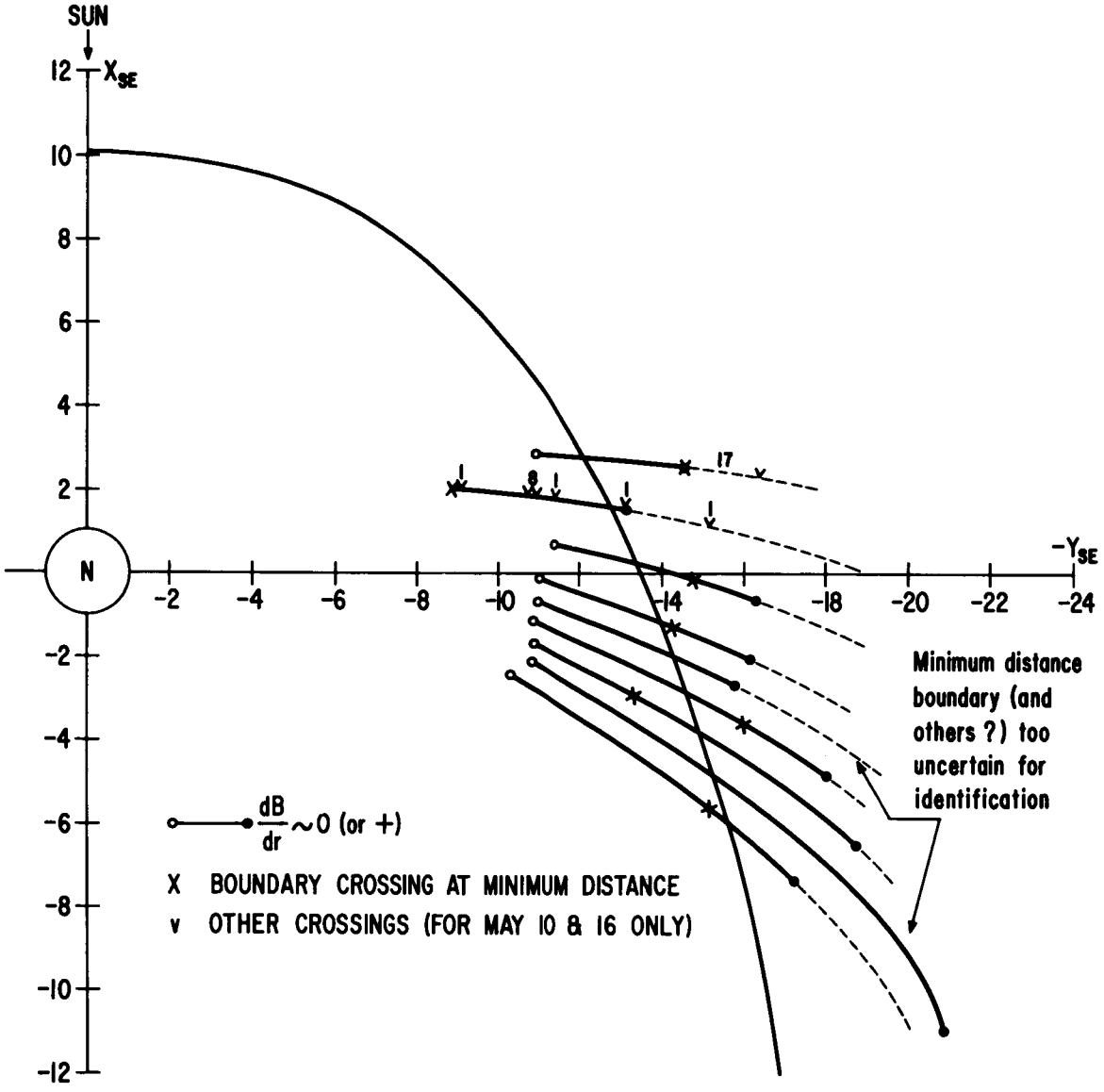
SUN
12
X_{SE}
10
8
6
4
2
N
-2
-4
-6
-8
-10
-12
-14
-18
-20
-22
-24
$-Y_{SE}$
17
8
$\frac{dB}{dr} \sim 0$ (or +)
X BOUNDARY CROSSING AT MINIMUM DISTANCE
v OTHER CROSSINGS (FOR MAY 10 & 16 ONLY)
Minimum distance boundary (and others ?) too uncertain for identification

Figure 37

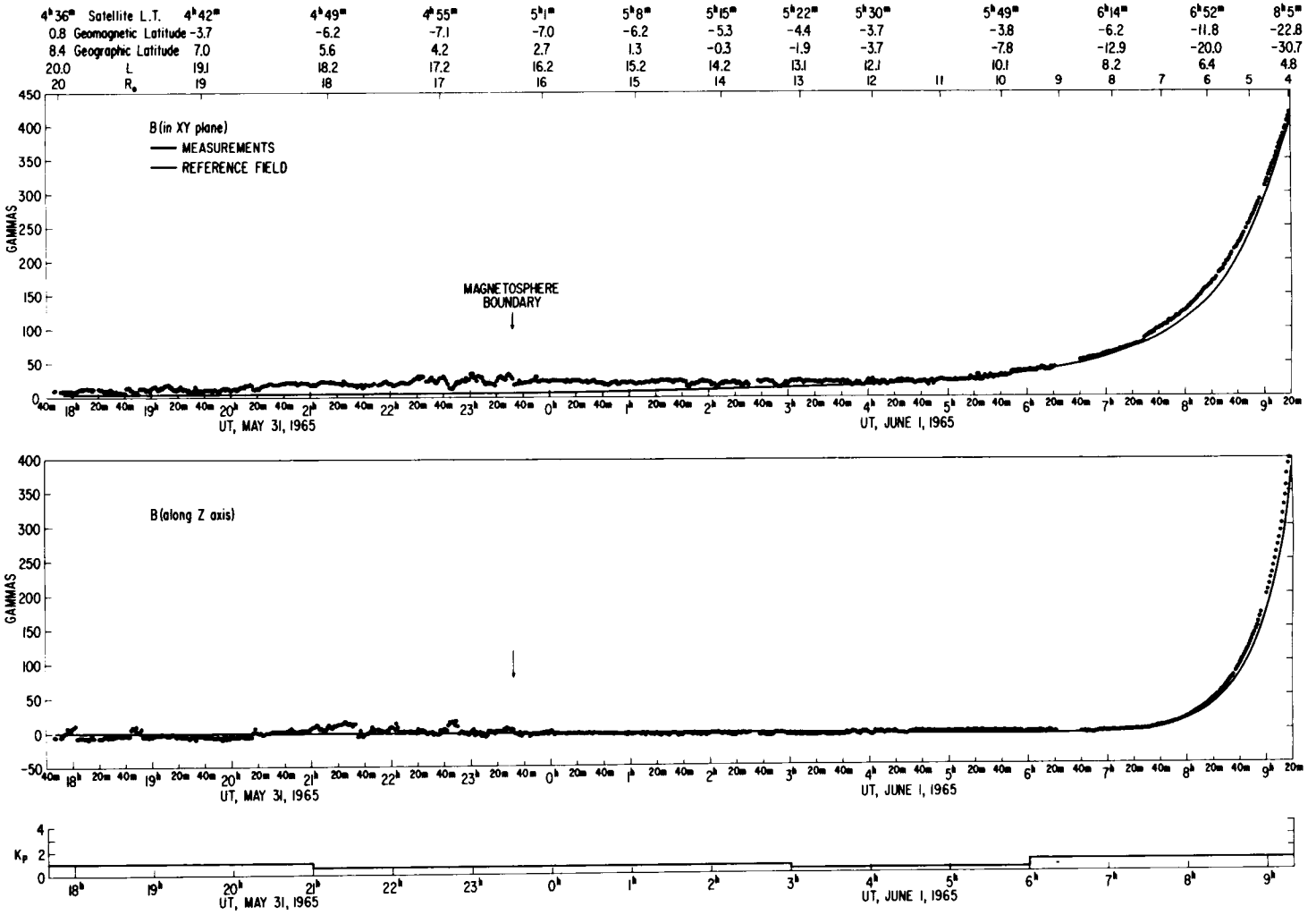
4h36m Satellite L.T. 4h42m 4h49m 4h55m 5h1m 5h8m 5h15m 5h22m 5h30m 5h49m 6h14m 6h52m 8h5m
0.8 Geomagnetic Latitude -3.7 -6.2 -7.1 -7.0 -6.2 -5.3 -4.4 -3.7 -3.8 -6.2 -11.8 -22.8
8.4 Geographic Latitude 7.0 5.6 4.2 2.7 1.3 -0.3 -1.9 -3.7 -7.8 -12.9 -20.0 -30.7
20.0 L 19.1 18.2 17.2 16.2 15.2 14.2 13.1 12.1 10.1 8.2 6.4 4.8
20 Re 19 18 17 16 15 14 13 12 11 10 9 8 7 6 5 4
B (in XY plane)
MEASUREMENTS
REFERENCE FIELD
GAMMAS
MAGNETOSPHERE BOUNDARY
UT, MAY 31, 1965
UT, JUNE 1, 1965
B (along Z axis)
GAMMAS
UT, MAY 31, 1965
UT, JUNE 1, 1965
Kp
UT, MAY 31, 1965
UT, JUNE 1, 1965

Figure 38

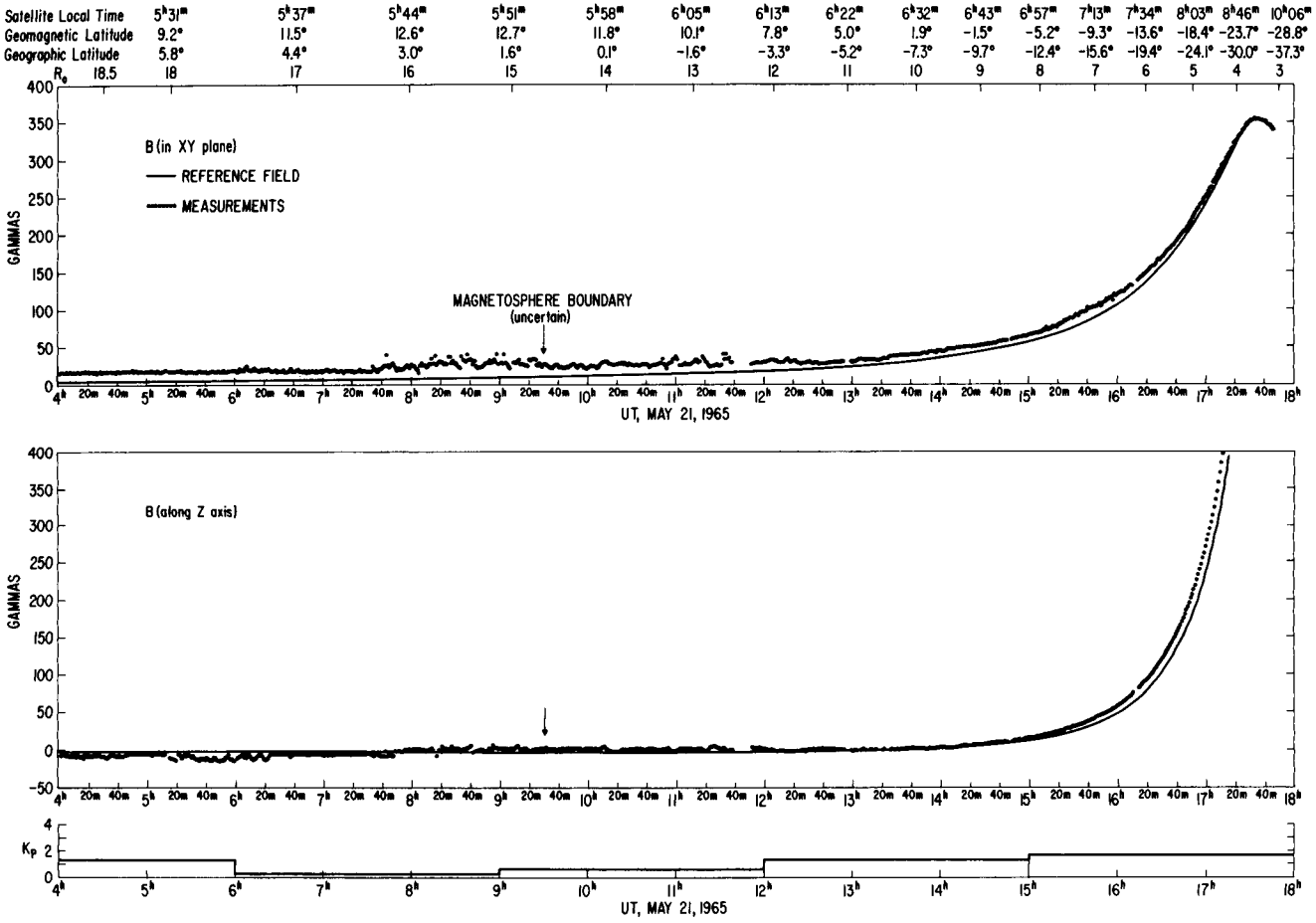
Satellite Local Time 5h31m 5h37m 5h44m 5h51m 5h58m 6h05m 6h13m 6h22m 6h32m 6h43m 6h57m 7h13m 7h34m 8h03m 8h46m 10h06m
Geomagnetic Latitude 9.2° 11.5° 12.6° 12.7° 11.8° 10.1° 7.8° 5.0° 1.9° -1.5° -5.2° -9.3° -13.6° -18.4° -23.7° -28.8°
Geographic Latitude 5.8° 4.4° 3.0° 1.6° 0.1° -1.6° -3.3° -5.2° -7.3° -9.7° -12.4° -15.6° -19.4° -24.1° -30.0° -37.3°
R_e 18.5 18 17 16 15 14 13 12 11 10 9 8 7 6 5 4 3
B (in XY plane)
REFERENCE FIELD
MEASUREMENTS
MAGNETOSPHERE BOUNDARY
(uncertain)
GAMMAS
UT, MAY 21, 1965
B (along Z axis)
GAMMAS
K_p
UT, MAY 21, 1965

Figure 39

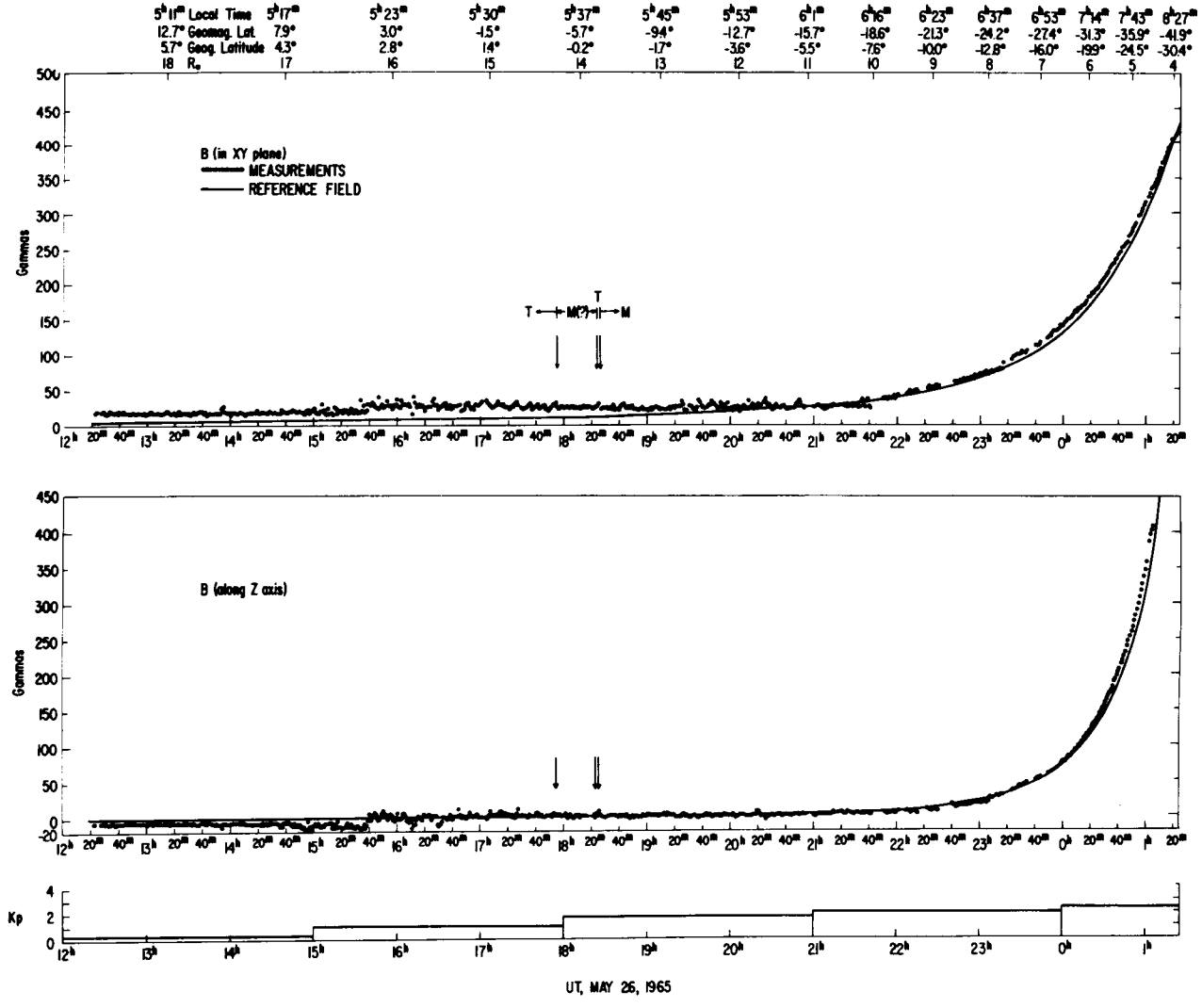
B (in XY plane)
MEASUREMENTS
REFERENCE FIELD
Gammas
B (along Z axis)
Kp
UT, MAY 26, 1965

Figure 40

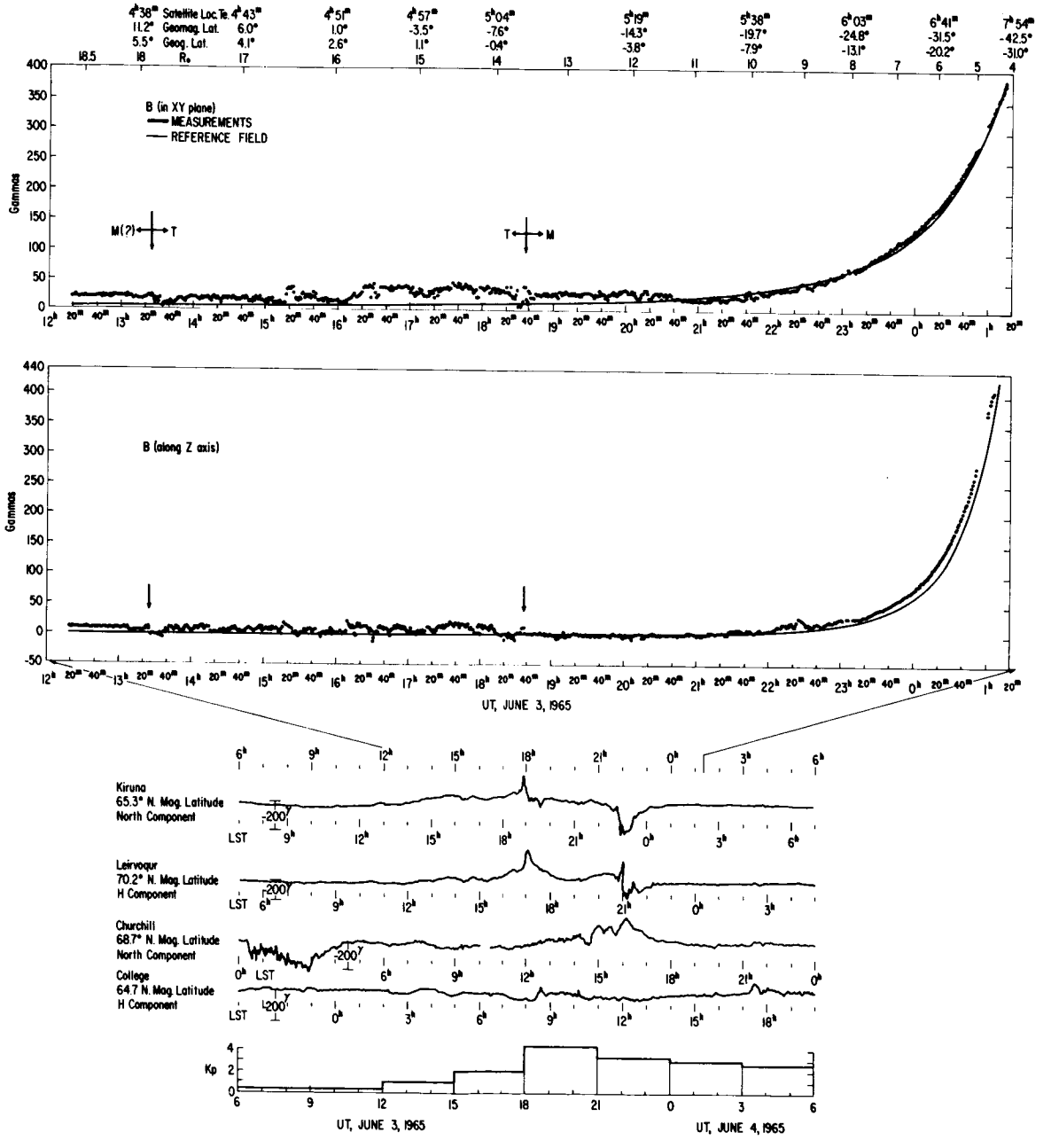
B (in XY plane)
MEASUREMENTS
REFERENCE FIELD
Gammas
B (along Z axis)
UT, JUNE 3, 1965
Kiruna
65.3° N. Mag. Latitude
North Component
Leirvogur
70.2° N. Mag. Latitude
H Component
Churchill
68.7° N. Mag. Latitude
North Component
College
64.7 N. Mag. Latitude
H Component
LST
Kp
UT, JUNE 3, 1965
UT, JUNE 4, 1965

Figure 41

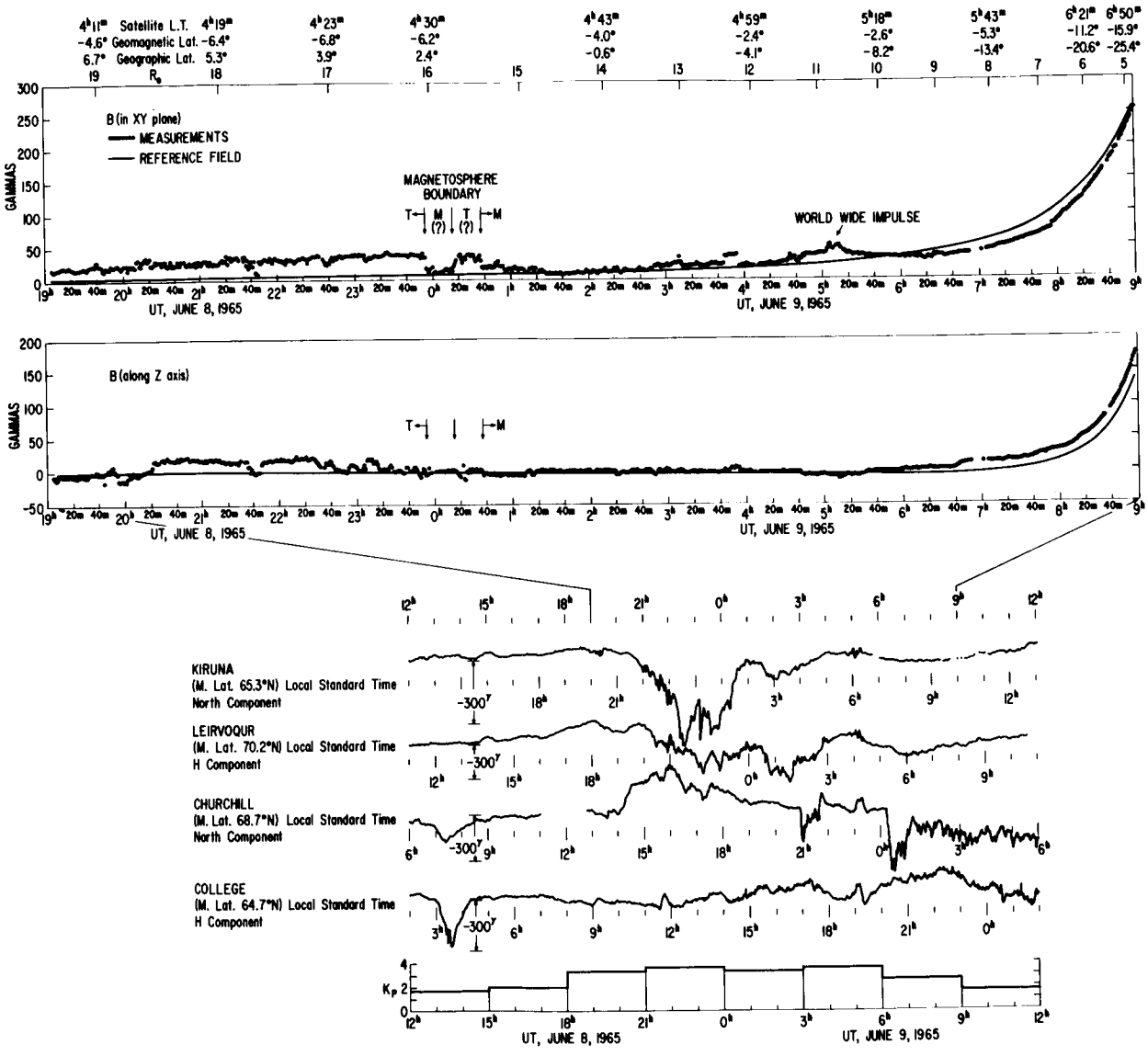
4h11m Satellite L.T. 4h19m 4h23m 4h30m 4h43m 4h59m 5h18m 5h43m 6h21m 6h50m
-4.6° Geomagnetic Lat. -6.4° -6.8° -6.2° -4.0° -2.4° -2.6° -5.3° -11.2° -15.9°
6.7° Geographic Lat. 5.3° 3.9° 2.4° -0.6° -4.1° -8.2° -13.4° -20.6° -25.4°
19 R0 18 17 16 15 14 13 12 11 10 9 8 7 6 5
B (in XY plane)
MEASUREMENTS
REFERENCE FIELD
GAMMAS
MAGNETOSPHERE BOUNDARY
T M (?) T (?) M
WORLD WIDE IMPULSE
UT, JUNE 8, 1965
UT, JUNE 9, 1965
B (along Z axis)
KIRUNA
(M. Lat. 65.3°N) Local Standard Time
North Component
-300γ
LEIRVOGUR
(M. Lat. 70.2°N) Local Standard Time
H Component
CHURCHILL
(M. Lat. 68.7°N) Local Standard Time
North Component
COLLEGE
(M. Lat. 64.7°N) Local Standard Time
H Component
Kp
UT, JUNE 8, 1965
UT, JUNE 9, 1965

Figure 42

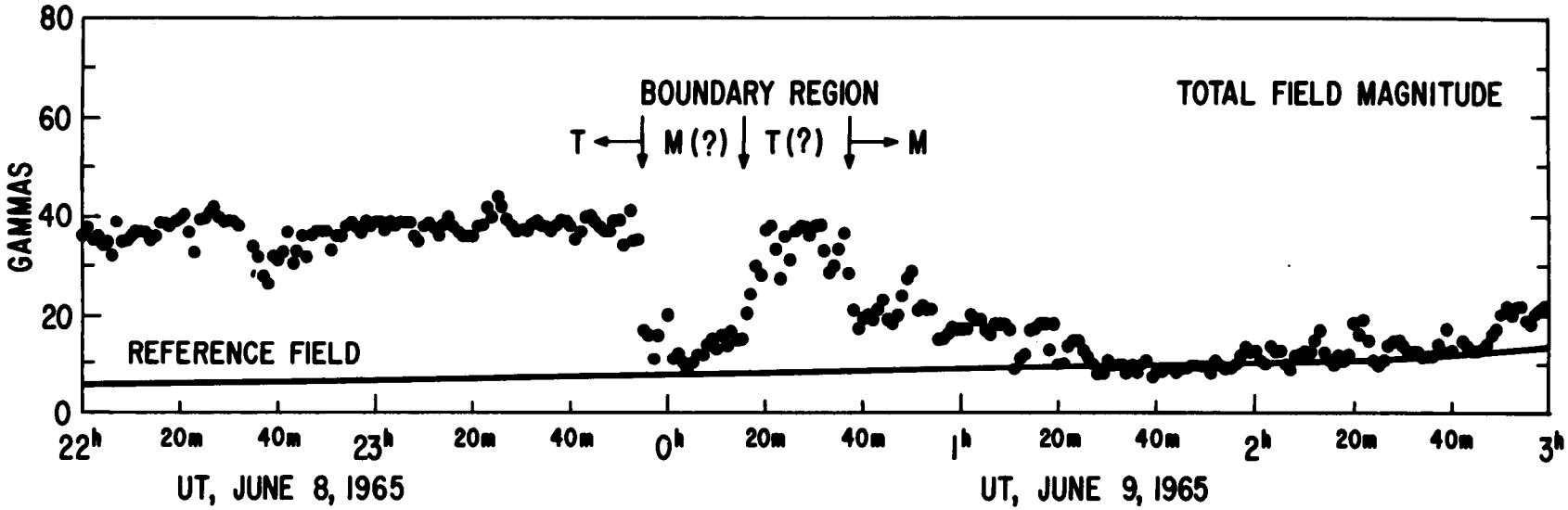
80
60
40
20
0
GAMMAS
BOUNDARY REGION
T
M(?)
T(?)
M
TOTAL FIELD MAGNITUDE
REFERENCE FIELD
22h
20m
40m
23h
20m
40m
0h
20m
40m
1h
20m
40m
2h
20m
40m
3h
UT, JUNE 8, 1965
UT, JUNE 9, 1965

Figure 43

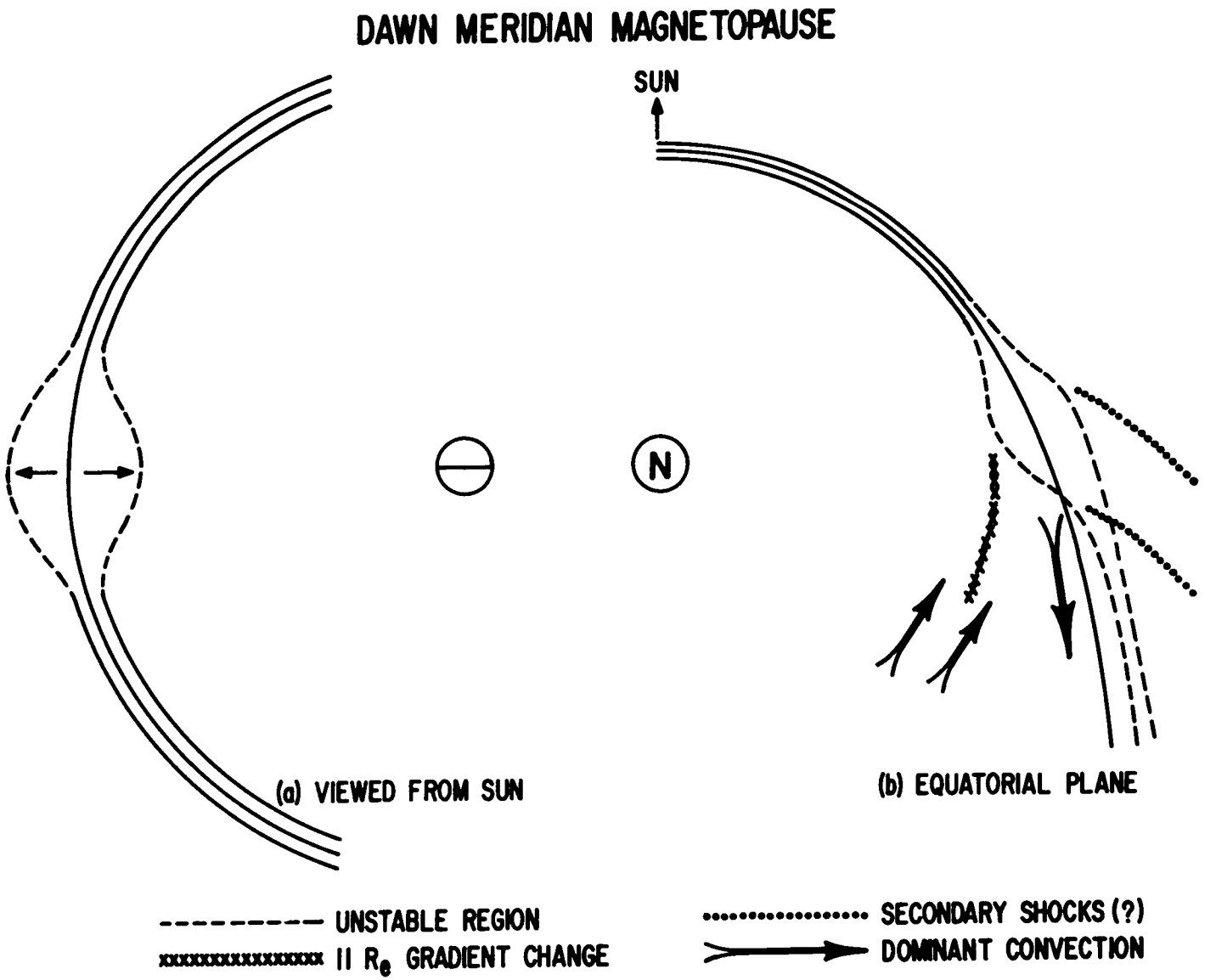
DAWN MERIDIAN MAGNETOPAUSE
SUN
N
(a) VIEWED FROM SUN
(b) EQUATORIAL PLANE
UNSTABLE REGION
11 R_e GRADIENT CHANGE
SECONDARY SHOCKS (?)
DOMINANT CONVECTION

Figure 44